Estimating Groundwater – Surface Water Interaction using Remote Sensing Techniques

Submitted by:
Aqua Strategies Inc.
In collaboration with
INTERA Inc.
and
GeoSystems Analysis Inc.

TEXAS WATER DEVELOPMENT BOARD

March 2025

AquaStrategies

GSA GeoSystems Analysis, Inc. Innovations in Hydrology

INTERA GEOSCIENCE & ENGINEERING SOLUTIONS

Estimating Groundwater – Surface Water Interaction using Remote Sensing

Prepared by:

Peter Zamora, PhD, PG
Mike Vielleux, PE
Barney Austin, PhD, PE
Aqua Strategies
Chad McKenna
Jonathan Tanis
GeoSystems Analysis
Guillermo Martinez, PhD, PE
Steve Young, PhD, PE, PG
INTERA Incorporated

Prepared for:

Texas Water Development Board
1700 North Congress Avenue,
Austin, TX 78701

March 2025

Geoscientist and Engineering Seals

This report documents the work of the following Licensed Texas Geoscientists and Engineers:

Dr. Barney Austin and Dr. Peter Zamora conducted fieldwork, analyses, and prepared documentation for Sections 1, 2, 4 , 5.1, 5.2 and 5.3 and provided editorial synthesis for Section 6.

[insert Barney and Peter's seals]

Dr. Guillermo Martinez supervised and conducted the analyses presented in Sections 3, 5.4, and 5.5.

[Insert Guillermo's seal]

Executive Summary

This study evaluated the utility of remote sensing data products from both satellite and aerial (drone) methods to support future Texas Water Development Board's (TWDB) Groundwater Modeling program development, with a specific focus on its application in understanding groundwater-surface water interactions along the Brazos River and its Alluvium Aquifer within the central portion of the Carrizo-Wilcox Aquifer groundwater availability model. The research highlights the potential of emerging technologies to enhance the characterization of hydrological systems while acknowledging the complexities of applying these tools in dynamic, heterogeneous environments.

Key Findings

1. **Groundwater Availability Modeling (GAM)**
    - Remote sensing can enhance groundwater availability models by providing spatially consistent and temporally extensive data.
    - This report documents an approach for improving how the Brazos River alluvium is represented in the central portion of the Carrizo-Wilcox Aquifer groundwater availability model using the types of data collected and described in this report.
    - Recommendations include incorporating intra-annual variability and leveraging MODFLOW 6 for refined spatial analysis. Groundwater availability model refinement in the vicinity of the river could be constructed to explore groundwater-surface water interactions at a finer scale during periods with high hydrologic variability and augmented datasets.
2. **Complexities of the Brazos River Alluvium Aquifer**
    - The aquifer spans approximately 350 miles, with varied hydraulic properties and saturated thicknesses up to 85 feet.
    - The aquifer's physical heterogeneity and significant temporal variabilities in surface water flow create complex groundwater-surface water interactions.
3. **Fieldwork Challenges**
    - Variable river flows (e.g. 128–52,000 cubic feet per second this past year) and sediment scouring and aggradation dynamics complicate equipment deployment and data collection.
    - Recommendations include the use of radar-based sensors on river bridges and dedicated monitoring of nearby groundwater levels. Include sufficient instrumentation for tributaries and other significant variations in flow.
4. **Remote Sensing Applications**
    - Technologies such as satellite imagery, aerial sensors, and thermal imaging are instrumental in helping to build a better-integrated aquifer and watershed water balance at finer temporal and spatial scales.
    - OpenET and SWOT satellite data, in particular, show promise for large-scale and seasonal monitoring but require integration with ground data for more appropriate scaling and calibration.

5. **Thermal Data Limitations**
    - Diurnal temperature variations and diffuse groundwater discharge hinder precise quantification of groundwater-surface water interaction.
    - Proposed improvements include the use of static thermal cameras, mid-column temperature readings, and advanced drone-based methods. This should be combined with improved surface water monitoring instrumentation to determine gain-loss.

By addressing the technological limitations associated with integrating remote sensing with field data, this research provides a pathway for advancing the representation of groundwater-surface interactions at a regional scale in complex settings like the Brazos River alluvium. Remote sensing datasets for quantifying groundwater pumping, aquifer recharge, and river stage can greatly enhance groundwater availability models by capturing intra-annual variability and providing critical insights into groundwater-surface water interactions. Combined with higher temporal resolution, and local grid refinements in MODFLOW 6 with standardized river gain-loss datasets, these improvements enable more precise simulations of seasonal changes. These can be achieved while maintaining feasible data requirements for groundwater availability model analyses, recognizing that earlier periods often lack detailed seasonal information and may not reflect current or future conditions.

Table of Contents

Table of Figures

List of Tables

1. Project Background

In 2022 the Texas Water Development Board (TWDB) sought an investigation into the use of remote sensing techniques to identify and quantify the interactions between groundwater and surface water bodies. While the interaction is known to occur in many parts of the state, accurate quantification of the exchange has proven to be difficult. TWDB currently uses MODFLOW software, developed by the US Geological Survey, for groundwater-flow modeling (groundwater availability models – GAMs) but aims to expand it to include interactions between groundwater and surface water. However, data to calibrate these interactions is limited, often restricted to sparse stream gage locations and brief measurements. The state's water availability models (WAMs) allow for gains and losses to rivers but have been crudely estimated, based strictly on differences between upstream and downstream streamgages over time.

Remote sensing technologies have improved over the past few years, offering better spatial, temporal, and spectral resolutions that can potentially quantify the characteristics of surface water and riparian zones, aiding in the estimation of groundwater-surface water interactions. The TWDB would like to identify where these interactions occur, particularly in regions where streams and rivers overlay significant aquifers. For this investigation, the collected and downloaded remote sensing data was required to be verified with existing ground-truth data, and a method is described for using these new data to improve the calibration of groundwater availability models.

The Aqua Strategies Inc. team was chosen to perform this work, bringing expertise in groundwater availability modeling from INTERA Inc. and remote sensing (drones and satellites) knowledge and skills from GeoSystems Analysis (GSA). The project describes extensive fieldwork, satellite data downloaded and processed from multiple sources, and a process for incorporating groundwater-surface water interaction knowledge to improve the groundwater availability models.

After some deliberation with staff at the TWDB, the Brazos River Basin was chosen as a case study (see Figure 1.1). The Brazos River Basin is one of the largest and most important river basins in Texas, covering approximately 45,000 square miles in the central part of the state. The river itself flows for over 800 miles from the northern part of the state near the Texas-Oklahoma border to the Gulf of Mexico.

Geographically, the Brazos River Basin stretches across a diverse range of landscapes, including the rugged terrain of the Central Texas Hill Country, the rolling plains of the Brazos Valley, and the flatter coastal plains in the southeast. It serves as a boundary for several ecological regions, including the East Texas Piney Woods, the Blackland Prairies, and the South Texas Brush Country, contributing to a diverse array of plant and animal life. The basin plays a crucial role in Texas' water supply system, as it supports agricultural irrigation, municipal water use, industrial processes, and recreational activities. The Brazos River and its tributaries provide water to a significant portion of the state, including areas that rely heavily on surface water for drinking, irrigation, and industrial needs. The Brazos River Basin also includes several reservoirs, which help regulate water flow, provide flood control, and support recreational activities like boating, fishing, and wildlife habitat.

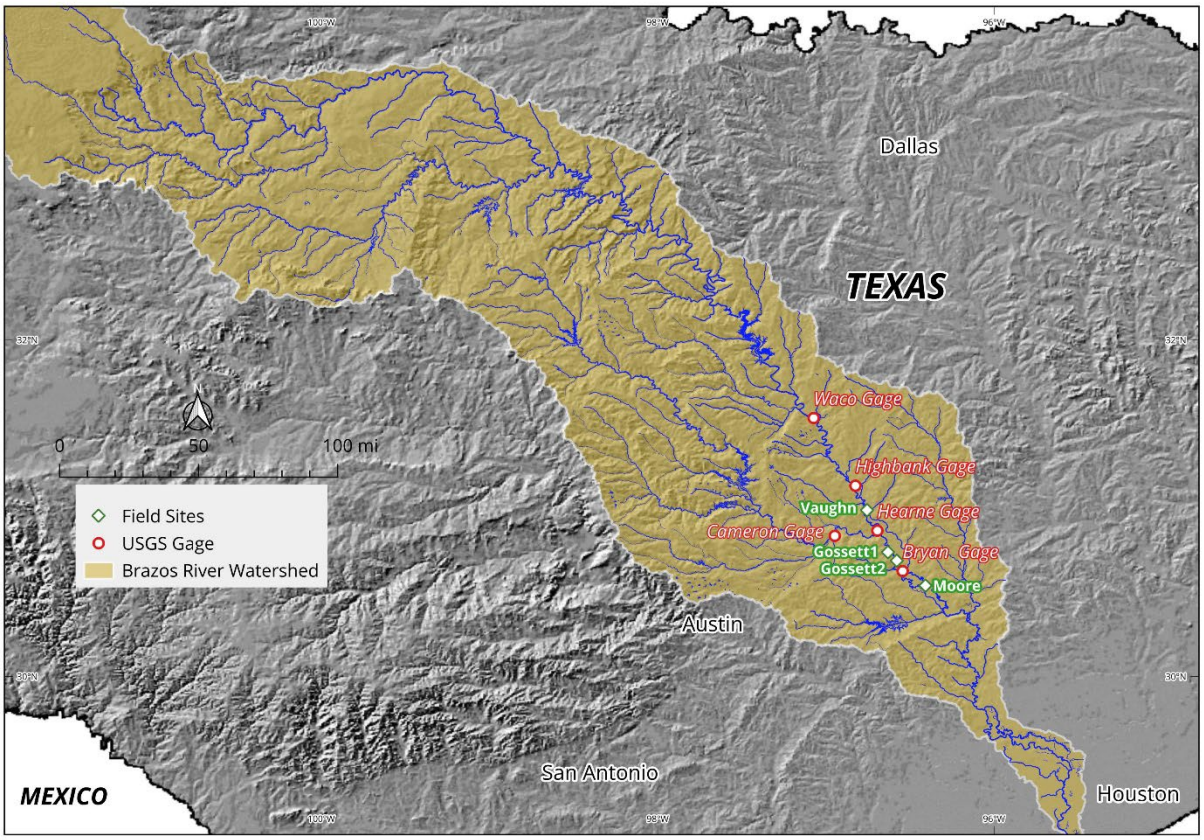

Figure 1.1 The Brazos River basin (from Brazos River Authority).

In order to study groundwater – surface water interaction, the stretch of the river that crosses the Brazos River Alluvial Aquifer was chosen (see Figure 1.2). This part of the river has many wells and there is known to be extensive movement of water (in both directions) between the river and the underlying aquifers. Field equipment was set up from the area above the Carrizo-Wilcox Aquifer outcrop to the area below.

Once the location for the study was selected, project staff visited the site with a Jon Boat and cameras to identify suitable places to launch the boat and set up equipment. An EarthViews camera was deployed, allowing project staff to capture 360-degree imagery for the entire river reach, with the stitched images being comparable to the Google Street View product, using a boat's vantage point instead. The images can be accessed here:

https://arcgis.earthviews.com/public/brazos-river-0523#90

There are two groundwater conservation districts covering the study reach: Post Oak Savannah Groundwater Conservation District (Milam and Burleson counties) and Brazos Valley Groundwater Conservation District (Brazos and Robertson counties). Because most of the alluvium is on the Brazos Valley Groundwater Conservation District side of the river for the reach selected, the team worked closely with the General Manager of Brazos Valley Groundwater Conservation District to identify landowners willing to provide access to the river and wells on their property. Mr. Alan Day was very helpful in making these connections.

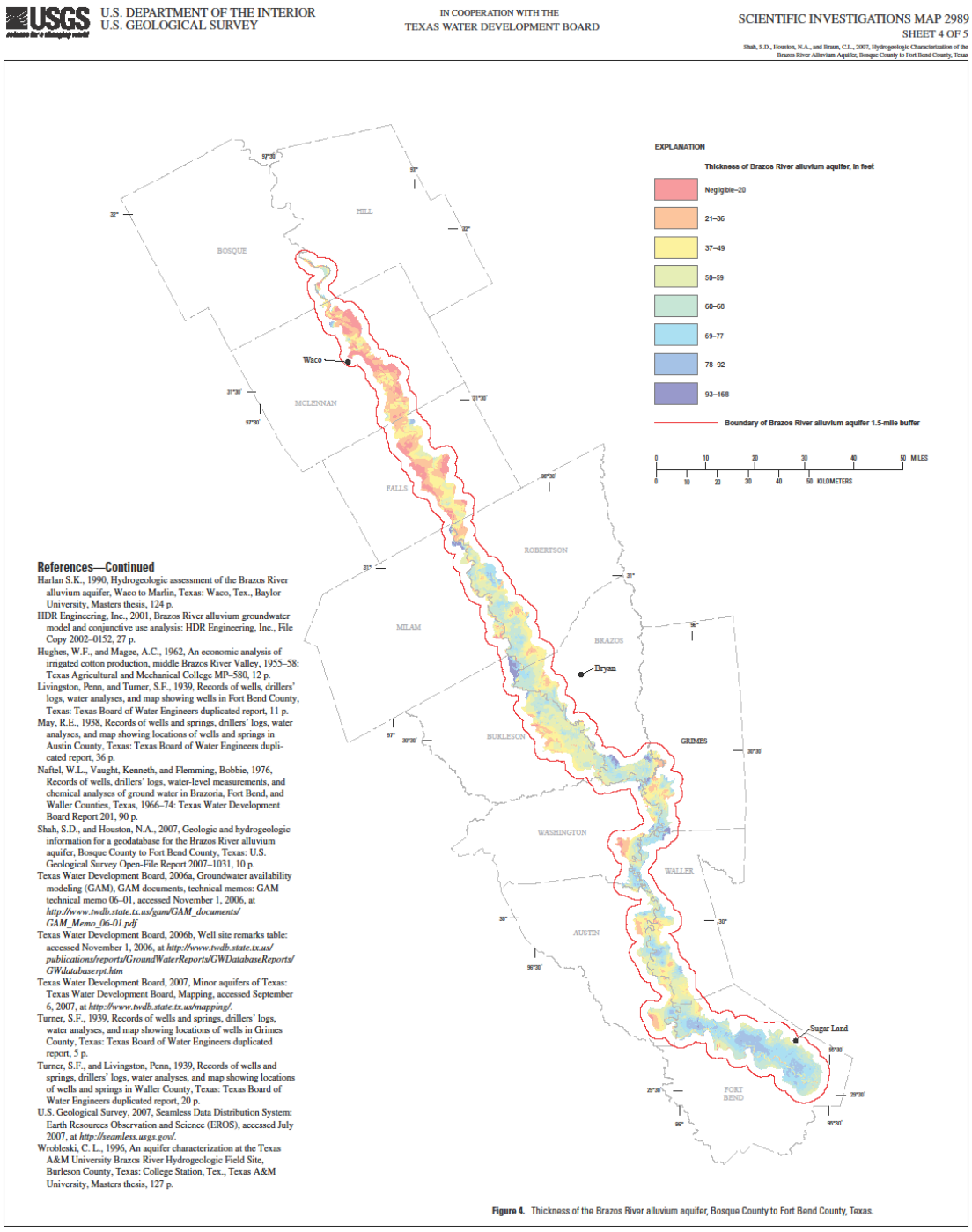

Figure 1.2 **Brazos River Alluvium Aquifer (from US Geological Survey). The study site is shown in the green box.**

2. Remote Sensing Applications in Water Resources

Remote sensing products have many applications for assessing hydrologic conditions and processes. Satellites track reservoir levels (Cooley and others, 2021), surface water extent in rivers at many scales (Huang and others, 2018), ocean levels (Ablain and others, 2017), water surface elevation in various types of water bodies (Nair and others, 2022), and evapotranspiration rates (Volk and others, 2024). More recently, remote sensing data have been used to predict stream discharge (Gejadze and others, 2022; Gleason and Durand, 2020). As technology advances, analytic capabilities increase and new satellites are deployed, the utility of remote sensing products continues to expand along with the accuracy and precision of derived variables. To better understand current and potential future remote sensing applications in hydrology, it is important to first grasp basic remote sensing concepts and definitions. This section defines and describes key remote sensing concepts with the greatest importance for remote sensing-based hydrologic analysis, plus puts these concepts into context with examples from the scientific literature.

2.1 Electromagnetic spectrum

The electromagnetic spectrum encompasses a wide range of wavelengths, from very short gamma rays to long-wavelength radio waves. In remote sensing, the electromagnetic spectrum is divided into specific bands based on wavelength ranges, each of which can be detected by different sensors on satellites, drones, or other platforms. These bands are crucial for observing and analyzing various features of the Earth's surface, as different materials (such as vegetation, water, or soil) reflect and absorb electromagnetic radiation at different wavelengths (see Figure 2.1).

Visible Light (0.4 to 0.7 microns): This range includes the wavelengths of light visible to the human eye. Remote sensing sensors detect the visible spectrum in red, green, and blue bands, which are commonly used in natural color imagery. These bands help in identifying land cover types like vegetation, water bodies, and urban areas.

Near-Infrared (0.7 to 1.5 microns): Beyond visible light, near-infrared (NIR) wavelengths are commonly used in remote sensing for vegetation analysis. Vegetation strongly reflects near-infrared light, making it highly useful for assessing plant health, biomass, and vegetation types. Conversely, surface water strongly absorbs near-infrared light, allowing for accurate identification and delineation. This band is essential for applications like crop monitoring, surface water delineation, and land use classification.

Shortwave Infrared (1.5 to 3 microns): This range helps in distinguishing between different types of vegetation and assessing water content in soil and plants. It is also useful for detecting mineral and rock types, as different materials absorb and reflect shortwave infrared radiation differently.

Thermal Infrared (3 to 15 microns): The thermal infrared region detects emitted heat from objects and surfaces, allowing for temperature measurements. This band is useful in environmental monitoring, such as detecting heat islands in urban areas, identifying water bodies, and assessing land surface temperature changes. Thermal infrared data can also be used to estimate actual evapotranspiration from riparian areas or agricultural fields.

Microwaves (1 mm to 1 meter): Microwave wavelengths are used in synthetic aperture radar (SAR) systems, which are sensitive to surface features like roughness and moisture content. These wavelengths can penetrate through clouds and vegetation, making them useful for all-weather, day-and-night remote sensing applications like soil moisture estimation, flood monitoring, and topographic mapping. Within the microwave spectrum, shorter wavelengths can measure surface elevations with more precision, while longer wavelengths penetrate further into soil and water. Measuring surface elevation with high precision often requires radar interferometry, a technique that analyzes phase differences between radar signals captured by two or more spatially separated antennas.

Remote sensing scientists can also utilize band ratioing techniques or band indices to compare the reflectance intensity of multiple bands to more efficiently and accurately detect various features on Earth. Satellite band indices are mathematical combinations of different spectral bands that help in analyzing specific features of the Earth's surface, particularly vegetation, water, and soil. More commonly used indices to identify the presence of water are discussed in other sections of this report.

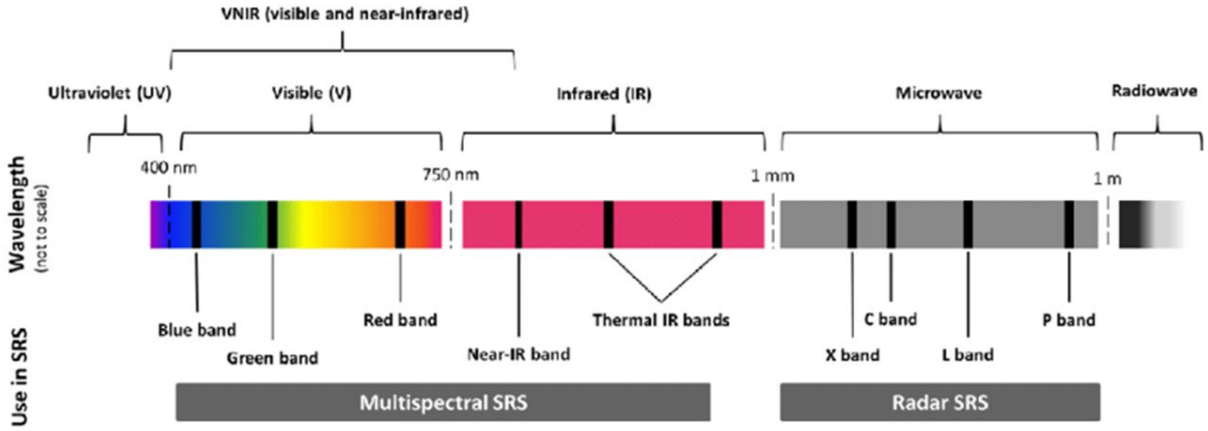

Figure 1.1 **Electromagnetic radiation spectrum with bands used in satellite remote sensing from Pettorelli and others (2018).**

2.2 Satellite data products

Until recently, regular monitoring of hydrologic variables like water surface extent was difficult and inaccurate in smaller rivers and streams because satellites with a more regular return interval collected relatively coarse resolution (e.g. 10 – 30 meter) data.

Satellite-based remote sensing platforms vary tremendously in terms of sensor types, return interval (the time between subsequent satellite passes), spatial resolution, area of coverage, data access and level of processing. There are often trade-offs involved – for instance achieving a higher spatial resolution may necessitate either a longer return interval or additional satellites in the constellation. In deciding which satellite platforms to incorporate into the study, key factors included:

- Medium to high spatial resolution (<30 meter)

- Regular return interval (< 2 weeks)
- Sensors capable of measuring water surface elevation and/or surface water extent (optical or radar)
- Publicly available data

These criteria narrowed the list of platforms down to three optical platforms (Sentinel-2, Landsat, Planet Scope) and one radar platform (SWOT). Sentinel-2 and Landsat are operated by the European Space Agency and National Aeronautics and Space Administration/US Geological Survey, respectively. Both have a long history of use for hydrology, agriculture, natural resource management, and many other disciplines. Planet Scope is an optical satellite constellation, known as "Doves," managed and operated by Planet Labs. Planet Scope imagery must be purchased, which may limit its suitability for broad-scale use in discharge measurements. However, the imagery is much higher resolution than that of Sentinel or Landsat and is collected daily across the globe. Planet Labs is able to accomplish this by operating a constellation of 130+ small "Doves" – whereas Sentinel-2 and Landsat only have 2-3 active satellites each. The high spatial and temporal resolution of Planet Scope imagery makes it particularly useful for assessing the accuracy of water surface elevation and water surface extent measurements from coarser resolution platforms. Other studies of water surface classification have also used Planet Scope imagery for this purpose (Ahmad and others, 2019). In contrast to optical satellites, the SWOT mission uses synthetic aperture radar (SAR) to measure both water surface elevation and water surface extent. Unlike passive optical sensors, synthetic aperture radar directly estimates elevations by sending out active radar signals and measuring the returns. Sentinel-1 is a second synthetic aperture radar satellite with applicability for water surface extent, although water surface extent data products were only made available at the end of 2024 and not included in the study. The C-band wavelength used by Sentinel-1 is less precise in measuring water surface elevation than the Ka-band used by SWOT, which was chosen specifically for the purpose of measuring surface water. See Table 2.1 for details.

Table 2.1 Details of the satellite data used.

Satellite	*Data Access*	*Sensor Type*	*Spectral Bands*	*Spatial Resolution*	*Temporal Resolution*	*Discharge Parameters Measured*
Sentinel-2	Free	Optical	12	10 m	5 days	DSWx
Landsat 8/9	Free	Optical	11	30 m	7-8 days	DSWx
SWOT	Free	Radar	Ka-band SAR	50 m	10-11 days	DSWx, WSE
Planet Scope	Paid	Optical	4 (Dove); 8 (Superdove)	~3.5 m	near-daily	DSWx
Sentinel-1	Free	Radar	C-band SAR	5x20 m	6 days	DSWx, WSE

Planet Scope Imagery
Planet Labs began deploying its Doves in 2014. These satellites capture near-daily images of the entire Earth's landmass at approximately 3.5-meter spatial resolution, allowing for more accurate and frequent monitoring of changes in the environment than previously possible.

Planet Scope currently operates a constellation of 130 satellites (Planet Labs, 2024). While three different sensors have been deployed since the initial launch, each Dove carries multispectral sensors that acquire data within at least four spectral bands: blue, green, red, and near-infrared. The most recent sensor iteration initially launched in 2020 acquires eight bands of data, adding red edge, yellow, a modified green band, and coastal blue. The latest Planet Scope sensor improves the capabilities for analysis and applications, particularly in areas like vegetation monitoring, hydrologic monitoring, and land cover classification.

Surface Water and Ocean Topography (SWOT)
Another key recent advancement in this area was the creation of the Surface Water and Ocean Topography (SWOT) satellite mission. SWOT is a collaborative initiative led by the National Aeronautics and Space Administration, the Canadian Space Agency, the UK Space Agency, and CNES (the French space agency) aimed at advancing understanding of Earth's water bodies and ocean dynamics (Neeck and others, 2012). SWOT's primary objective is to measure the elevation and lateral extent of water surfaces using advanced radar altimetry and interferometry to complement other satellite missions that collect data with more traditional optical sensors. SWOT data is distributed in both raster and vector format.

SWOT provides global coverage of rivers, lakes, and oceans, enabling comprehensive monitoring of the Earth's water resources. This benefits various fields, including hydrology, oceanography, climate science, and environmental management. SWOT is particularly useful for refining and calibrating hydraulic models as well as hydrologic monitoring because it measures surface water elevation and can be used to predict stream discharge. SWOT uses a radar interferometer to measure the water surface elevation over rivers and streams, with a reported vertical resolution of 6 centimeters (National Aeronautics and Space Administration, 2024). These measurements are then used to derive estimated streamflow. Despite its advantages, it is important to note that SWOT does have temporal limitations compared to traditional in-stream gages. While SWOT provides snapshots at approximately 10-day return intervals, changes in water levels cannot be monitored in near real-time due to the revisit frequency.

Sentinel-2 and Landsat Imagery
Both Sentinel-2 and Landsat are earth observation satellites operated by the European Space Agency and National Aeronautics and Space Administration/US Geological Survey respectively. The imagery collected from the two satellite constellations is similar in many ways – medium resolution, multispectral images acquired on an interval of approximately one week. Data products are publicly accessible, and both are widely used for water management, research in hydrology, and a multitude of uses in other disciplines. Imagery from the satellites includes both visible (red, green, blue) and multispectral (e.g. near-infrared, short wave infrared) bands that can be combined in different ways to classify water and land surfaces.

There are notable differences between the two satellite platforms as well. Sentinel-2 has a significantly higher spatial resolution and a somewhat higher temporal resolution compared to

Landsat. However, data is only available back to 2015-2017 (depending on geographic region) while Landsat has a continuous record dating back to 1972. In addition to multispectral bands, Landsat 8 and 9 also collect thermal imagery at a spatial resolution of 100 meters.

In addition to the multi-band imagery, there are also derived data products such as water surface extent water masks where surface water pixels have been classified. These products are created using an algorithm that combines various optical bands from Sentinel-2 or Landsat with existing data for land use and topography.

Google Earth Engine. (2024). USGS Landsat 8 Level 2, Collection 2, Tier 1. https://developers.google.com/earth-engine/datasets/catalog/LANDSAT_LC08_C02_T1_L2

Google Earth Engine. (2024). USGS Landsat 5 Level 2, Collection 2, Tier 1. https://developers.google.com/earth-engine/datasets/catalog/LANDSAT_LT05_C02_T1_L2

Google Earth Engine. (2024). Harmonized Sentinel-2 MSI: MultiSpectral Instrument, Level-2A (SR). https://developers.google.com/earth-engine/datasets/catalog/COPERNICUS_S2_SR_HARMONIZED

Sentinel-1

Sentinel-1 is another European Space Agency satellite platform that uses C-band synthetic aperture radar. This sensor functions similarly to the one on the newer SWOT satellite, but uses a C-band wavelength instead of the Ka-band on SWOT. While the Ka-band is specialized for measuring water elevations, C-band is a better general-purpose radar. It is used for measuring land use change, deforestation, flood extents, soil moisture and urban development. Sentinel-1 can measure water surface elevations, though not as precisely as SWOT. However, the better spatial resolution may offer advantages in measuring surface water extents.

Water surface extent products are also being created from Sentinel-1 data. These were only made available after September 2024 and therefore were not included in this study. The temporal resolution of Sentinel-1 has also been reduced since the technical failure of one of the two satellites in 2021. A third satellite was successfully launched in December 2024, and by 2025 the return interval will be reduced from 12 to 6 days.

Harmonized products

"Data fusion" and "data harmonization" are emerging, powerful techniques to leverage multiple datasets or platforms to create a more comprehensive, accurate analytic result. Harmonization involves processing different remote sensing datasets, often from various satellites or sensors, to create a unified dataset that can be analyzed consistently. The primary harmonized dataset used in this study is the Harmonized Landsat Sentinel (HLS) data, whereby the reflectance values from the two satellite platforms were calibrated. This allows the same water classification algorithm to be run on imagery from both Landsat and Sentinel-2, resulting in a water surface extent dataset with higher temporal resolution than either one individually. One downside of the HLS data is that the higher resolution (10 meter) Sentinel-2 imagery must first be downsampled to the 30-meter resolution of Landsat.

The process of data fusion may involve adjusting differences in spatial resolution and temporal frequency while combining spectral bands or radar data from multiple platforms. For instance, data

fusion might combine multispectral imagery or derivatives, like band ratios, with a sensor that captures radar data to better predict the extent of surface water. Data fusion techniques can serve to increase temporal resolution as well as overall accuracy of analysis, as different remote sensing sensors each have their own strengths and weaknesses that fusion approaches can account for. For instance, the SWOT sensor is very precise at measuring elevations, but the spatial resolution is relatively low (50 meter) compared to optical satellites like Sentinel-2 and Planet Scope.

2.3 Spatial and temporal resolution

In remote sensing, spatial and temporal "resolution" are most influential within hydrologic applications. Note that radiometric is another type of "resolution" within remote sensing products, but wasn't an analytic component for this project. Spatial resolution refers to the pixel size (or ground sample distance) in a grid dataset, including images, which substantially affects the level of discernible detail and size of identifiable objects. Finer (or "higher") spatial resolution provides greater detail and enhanced detectability of smaller objects on the earth's surface.

Temporal resolution refers to the frequency with which a satellite passes over and acquires data over the same location. Higher temporal resolution (or more frequent revisits) increases the ability to monitor changes over time and enables detailed tracking of dynamic processes such as vegetation growth or hydrologic processes.

Both spatial and temporal resolution are key considerations in determining the applicability of a specific remote sensing platform for a given objective. Due to data storage and transmission constraints, there are frequent trade-offs between the spatial and temporal resolutions - until recently, sensors with higher spatial resolutions typically had lower temporal resolutions and vice-versa.

The spatial and temporal resolution of remote sensing data play an important role in analyzing groundwater-surface water interactions. High spatial resolution products can be used to track fluctuations in the areal extent of river channels, wetlands, and groundwater discharge zones, enabling monitoring and mapping of surface water bodies. This detail is necessary for understanding localized interactions, such as the exchange of water between groundwater and surface water, and thus, can be potentially used to detect groundwater-caused variation in stream discharge. Temporal resolution is also important, as more frequent satellite observations allow for more monitoring over time, such as fluctuations in surface water levels, seasonal variations, and the impacts of climate events. With high temporal resolution, it becomes possible to track the potential influence of floods or droughts on groundwater interactions; conversely, it can reveal the impact on surface water extent or evapotranspiration when groundwater elevations decline due to pumping or other anthropogenic pressures. Accordingly, high spatial and temporal resolution data could enhance the predictive capability of groundwater-surface water interaction models, and inform water resource management, and environmental conservation efforts.

Higher-resolution remote sensing data products can be instrumental in assessing the accuracy of coarser-resolution remote sensing products by providing more detailed reference information that allows for the validation and calibration of the lower-resolution data. This process typically involves comparison of fine-scale data with the coarse-scale data to evaluate discrepancies, identify errors, and enhance the overall reliability of the coarse-resolution products. To assess groundwater-

surface water interactions, high resolution remote sensing satellite data or drone data are needed to assess the accuracy of coarser resolution remote sensing data.

Higher-resolution data can be directly compared with coarser-resolution products by overlaying the two datasets and assessing differences in feature boundaries, spatial patterns, or land cover classification accuracy. For example, finer-resolution satellite images can be used to validate the extent of water body boundaries identified in lower-resolution products. These comparisons highlight spatial misalignments or errors introduced by coarser pixel sizes, aiding in the refinement of classification algorithms used to analyze the coarse data. In the absence of field data for ground-truthing, high-resolution satellite imagery can act as a surrogate for detailed field measurements.

For this study, use of higher resolution data was primarily used to evaluate the accuracy of water extent detection indices from variously scaled remote sensing products.

2.4 Drone/Unmanned aerial vehicles data products

Drones, or unmanned aerial vehicles (UAVs), have become increasingly important and widely used tools due to their ability to collect very high-resolution data at specific locations and times. Unlike spaceborne satellite data, which often covers vast areas and provides global views, drones offer a more targeted approach to remote sensing data collection. However, each method has its own set of advantages and disadvantages, and the choice between drones and satellites depends on study objectives.

Drone data acquisition has a number of advantages compared to other forms of remote sensing. Image resolution is many times higher than satellite imagery, making it possible to resolve objects on the ground far more accurately. The highest resolution publicly available satellite data is Sentinel-2, with a resolution of 10 meters, while drone imagery is typically a few centimeters or less. Commercial satellite imagery such as Planet Scope has up to 3.3-meter resolution but can be costly and is still far coarser than imagery from a drone.

Another advantage of drone data is the level of control over the timing, location and flight parameters, whereas satellites have relatively fixed orbit paths. Drones can also be deployed quickly and used to capture data at specific times or during critical events (e.g., after precipitation, or during targeted runoff events). This high temporal resolution enables more responsive monitoring compared to satellites, which must be tasked to acquire data at a specific area and time. The flexibility of carrying a wide variety of swappable sensors also enables customized data collection tailored to specific research or monitoring needs. On cloudy days, drones are able to collect imagery of areas where satellite imagery would be obscured by cloud cover.

On the other hand, drone data collection requires physical travel to field sites by experienced and licensed pilots. Satellite imagery is often collected on a weekly or even daily basis, whereas this would be cost-prohibitive for drone imagery in most cases. Limitations in battery life, payload capacity and flight height make drone acquisition of large areas (>1,000 acres) quite labor intensive, while the satellite data products used in this study have a global coverage.

Satellite data is also relatively easy to download in bulk and is “analysis ready”, whereas drone data requires a lengthy processing step before it is usable. Drones are also highly sensitive to weather conditions, particularly strong winds, rain, or low visibility. This can limit their ability to collect data

in locations with adverse weather or during certain seasons. Drones are subject to regulatory limitations, such as no-fly zones and airspace restrictions.

Because of these considerations, drone data is most appropriate for particular use cases. Currently, available thermal data from satellites is too coarse a resolution (100 meters or greater) to assess surface temperature trends along a river reach. A drone-mounted thermal sensor proved better suited to the task, due to the higher resolution. For detecting groundwater seepage, continuous data collection is not essential. Furthermore, drone data can be collected in the early morning, when surface temperature patterns are easier to observe.

For measuring discharge parameters, drone data would not be an appropriate basis for continuous measurement of water surface elevation and water surface extent because of the cost and labor required. However, water surface elevation and water surface extent can be measured very accurately because of the high sensor resolution, and these drone-derived data are extremely useful in ground-truthing the accuracy of satellite platforms that collect imagery on a continuous basis.

2.5 Surface water discharge estimation

The following section describes the approaches used to estimate surface water discharge using remote sensing data.

2.5.1 Satellite data

Although approaches to estimating river discharge using satellite data are not new, technological advancement in terms of satellite sensors and data processing techniques have driven rapid development in the field over the past decade (Gleason and Durand, 2020). Accurate discharge estimates are essential for effective water management operations, and many river basins globally and in the United States are ungaged or sparsely gaged. Even in the better gaged basins, gages are typically spaced too far apart to effectively characterize or quantify groundwater-surface water interactions. Satellite measurements along an entire river are effectively instantaneous, allowing spatial variations in discharge to be observed for single moments in time. Once controlled for inflows and outflows, discharge variations could be primarily attributed to gaining and losing reaches.

Current research in the field is highly diverse, ranging from approaches where all flow parameters necessary to estimate discharge are directly measured by satellite, to those where only specific parameters are measured and then incorporated into hydrologic models. For this study, the team focused on the methods employed by the SWOT mission. The sensor on SWOT is a Ka-band synthetic aperture radar altimeter, which is well suited for both the classification of surface water and the measurement of water surface elevations.

There are multiple ways to calculate stream discharge, but for modeling and remote sensing the most appropriate is Manning's equation. Four key variables are needed in Manning's equation for the calculation of discharge: channel roughness, cross-sectional area, slope and channel width. Slope (derived from water surface elevations) and channel width (derived from water surface extent) are continuously measured, while roughness and area are assumed to be less dynamic and

only calculated periodically. Slope and channel width are categorized by the SWOT team as "time-variant", while roughness and cross-sectional area are "time-invariant". This is roughly comparable to how in-stream gages continually measure river stage, while rating-curves are updated less frequently.

Water surface elevation (WSE) and water surface extent (DSWx) are therefore the key variables to measure by satellite because they require continuous measurement, which is impractical to do at a large spatial or temporal scale through field or drone methods.

Water surface extent can be estimated by either optical or synthetic aperture radar satellite sensors. Optical sensors can collect both visible (red, green, blue) and multispectral (e.g. near infra-red) wavelengths of light, which are then used to classify water pixels. Many optical satellites have a higher spatial resolution than synthetic aperture radar sensors, but their usefulness can be limited in cloudy regions like the study area. Synthetic aperture radar sensors classify water pixels based on the intensity of radar returns, and the wavelengths typically used are not significantly affected by the presence of clouds. One limitation of the SWOT sensor is its 50-meter horizontal resolution, which can make measurement of channel widths relatively imprecise on narrower river reaches. SWOT discharge estimates are therefore calculated on a 10-kilometer reach scale, to average many width measurements together and reduce error. On the other hand, synthetic aperture radar sensors (especially the short wavelength Ka-band used by SWOT) can measure elevations very accurately. Optical satellites like Landsat and Sentinel-2 are not capable of measuring elevations except under very specific conditions, limiting satellite measurements of water surface elevation to radar-altimeters like SWOT. Although other synthetic aperture radar satellites are currently in orbit (e.g. Sentinel-1), the bands typically used (e.g. X, C and L bands) have longer wavelengths and therefore cannot measure water surface elevation with the same precision as the Ka-band.

While the SWOT mission does include methods for deriving time-invariant variables (roughness and cross-sectional area) from SWOT data alone, these parameters are likely to be more accurately estimated through other remote sensing and/or field methods. The same is likely true for channel width, at least on narrower rivers. SWOT discharge estimations will be made on a 10-kilometer reach scale, in part because the averaging of many channel width observations is necessary to reduce error within thresholds set by the SWOT mission. More accurate measurements of channel width could be made with optical satellites, other synthetic aperture radar satellites like Sentinel-1, or derived from SWOT elevations themselves if channel bathymetry is known. Downscaling the discharge estimations from 10 kilometer to shorter reaches would greatly increase the effectiveness of the data for characterizing GW-SW interactions.

2.5.2 Drone data

Drones are increasingly used to measure stream discharge because they offer a flexible, cost-effective, and safe method for collecting hydrological data in various environments, including remote or hazardous areas. The key techniques for measuring discharge using drones include QCam and velocimetry.

QCam uses a Doppler (velocity differential) radar, often integrated with an optical camera. Images are processed to estimate stream discharge based on changes in velocity, water stage, and surface area. The surface velocity is translated to a mean-channel (mean) velocity using the probability concept (PC), and discharge is computed using the probability concept-derived mean velocity and cross-sectional area. Factors including surface-scatterer quality, flight altitude, prop wash, wind drift, and sample duration may affect the radar returns and the subsequent computation of mean velocity and river discharge (Fulton and others, 2020).

Velocimetry (Particle Tracking or Surface Velocity Estimation) uses drone-captured video footage to measure surface water velocity. This is based on techniques like Large-Scale Particle Image Velocimetry (LSPIV) or Particle Tracking Velocimetry (pressure transducerV), which track the movement of natural (i.e. wood debris) or artificial tracers on the water surface. The process can be performed with thermal (Kinzel and Legleiter, 2019) or optical sensors (Duan and others, 2023). In essence, the drone records high-resolution video from a fixed position or along a transect over the stream channel. Then specialized software is used to analyze the video to measure the speed and trajectory of particles or patterns on the water surface. The surface velocity is combined with cross-sectional area measurements and correction factors (to account for depth-averaged velocity) to calculate discharge.

2.6 Sensors

Satellites measure surface water features using several remote sensing techniques, primarily involving optical, radar, and laser technologies.

Optical sensors passively capture reflections of light off surfaces. They are essentially analogous to everyday cameras, except that they often collect wavelengths of light outside the visible spectrum, such as near-infrared. Although optical satellites can be used to acquire elevation data, this involves expensive custom tasking of the satellites to collect images of the same location at slightly different angles. In the context of measuring discharge parameters, optical imagery is most useful for the derivation of water surface extent/channel widths. Planet Scope, Sentinel-2, and Landsat were the optical satellite platforms used in this study.

Radar from aircraft and satellites is typically a type called synthetic aperture radar (SAR) – meaning that the movement of the sensor itself is used to "synthetically" increase the length of the antenna, thereby increasing spatial resolution. Radar sensors are active, meaning they emit a radar signal and measure the return. Because of this, they can measure surface elevations based on the phase of the signal when it arrives back at the satellite. The amount of energy that is absorbed by the Earth's surface before it bounces back to the satellite is a second point of data. Water tends to absorb more of the radar energy than land, and so areas of surface water appear "dark" on radar images. Therefore, radar satellite data can be used for measuring both surface water elevations and extents.

Radar provides several advantages over optical sensors. The longer wavelengths are able to penetrate clouds, which is especially useful in humid regions. Also, the active sensor means that data can also be collected at night. However, radar data tends to be more difficult to work with than

optical data. Currently available optical imagery also generally has a higher spatial resolution than radar data.

2.7 Remote Sensing data indices

Indices are mathematical formulas that can be used to identify and extract characteristics from raw remote sensing data. These indices often leverage varying spectral responses across different discrete portions of the electromagnetic spectrum to highlight differences in surface properties, such as vegetation, water, soil, moisture, and more. For example, in the case of vegetation, indices can be used to compare the reflectance of near-infrared wavelengths (highly reflected by healthy vegetation) to red wavelengths (strongly absorbed by healthy vegetation) to characterize vegetation health and identify areas with more vegetation cover.

Other indices leverage the spectral reflectance characteristics of water, primarily using visible, near-infrared (NIR), and shortwave-infrared (SWIR) bands to optimize surface water identification from imagery. Below are the equations for commonly used indices for extracting surface water:

Normalized Difference Water Index (NDWI) = (Green + NIR) / (Green − NIR)

where Green is the green band and NIR is the near-infrared band. NDWI helps enhance the visibility of water features.

Modified NDWI (MNDWI) = (Green + SWIR) / (Green − SWIR)

where Green is the green band and SWIR is the short-wave infrared band. This is like NDWI but uses the shortwave infrared band instead of NIR to improve water detection under certain conditions.

Water Ratio Index (WRI) = (Green + Red) / (NIR + SWIR)

where Green is the green band reflectance, Red is the red band reflectance, NIR is near-infrared band reflectance, and SWIR is short-wave infrared band reflectance. The variety of bands used can help isolate water in certain environments.

Automated Water Extraction Index (AWEI) is an index that uses different shadow correction factors and ratios of green, short-wave infrared, and near-infrared bands.

3. Groundwater modeling approach

The Texas groundwater availability models are built as tools to develop reliable information on groundwater availability over long planning periods and coarse scales compared to the scales needed to describe the interaction between groundwater and surface water produced by climate variability (including precipitation and evapotranspiration) and human activity (i.e., agricultural pumping, diversions, river operations). Remote sensing methods provide powerful tools to augment ground-based data and increase spatial or temporal coverage which, in turn, can greatly increase the number of targets and calibration parameters in a groundwater model. Remote sensing also has the potential to help describe, in more detail, groundwater-surface water interactions.

One of the main limitations of remote sensing in this domain is that the acquired data often cannot be directly related to processes represented in the current groundwater availability models, and the precision or temporal scale of remotely sensed data does not match the scale of the groundwater availability models. The challenging task of improving the calibration of a groundwater availability model by better representation of groundwater-surface water (GW-SW) interaction can be addressed by incorporating relevant seasonal variability, but also by coupling the model directly or indirectly with other models and data that represent key aspects of the groundwater-surface water interactions.

In the current groundwater availability model packages and calibration processes, three groups of input variables drive much of the simulated groundwater-surface water flux within a given model cell:

- **Surface Water Geometry**: location, length, width, river bottom elevation, slope, and connection to other model cells.
- **Flow conditions** in the surface water and groundwater within the given time step: flow, discharge, and/or head in the surface water body, and groundwater levels in simulated and adjacent numerical cells.
- **Hydrologic/hydrogeologic characteristics**: bottom thickness, roughness coefficient, and vertical hydraulic conductivity/conductance of the bed.

The field-measured gain-loss within a section of the river reach provides us with the cumulative effect of all these input parameters. Because the distance between stream gages can be significant, the uncertainty of the aforementioned variables is high. The technical approach presented here involves the collection of field-based and remote sensing data within a selected river reach and the use of these data to:

- Improve estimates of the geometry of the surface water body.
- Measure the flow conditions in the river and the groundwater adjacent to the river.
- Improve estimates of groundwater pumping by incorporating actual evaporation estimates.
- Estimate the total gain-loss at different sections within the river reach.

There are a variety of remote sensing platforms that have been used or are under development to estimate surface water conditions and discharge rates, particularly in ungaged rivers. These include a LANDSAT-based Dynamic Surface Water Extent (DSWE) product that maps surface water extent from 1982 through the present and the use of satellite altimetry to predict river channel stage

levels and longitudinal slope with the development of stage-discharge curves from the remote sensing data (Birkinshaw and others, 2014; Paris and others, 2016). Other recent advancements include drone collected Large-Scale Particle Image Velocimetry (LSPIV) data (Duan and others, 2023). The SWOT mission provides radar-based measurements to observe surface water elevation and storage changes, discharge, and land surface water dynamics globally, further enhancing hydrologic understanding and prediction (Fu and others, 2024). Finally, remote sensing estimates of Actual Evapotranspiration (AET) can greatly enhance the quality of hydrological predictions regarding actual evapotranspiration, runoff, and groundwater recharge (Hendrickx and others, 2016). Specifically, accurate actual evapotranspiration information can inform the development of model stresses, such as seasonal variation of groundwater pumping for irrigation, and evaluate several components of the water balance. A detailed description of our technical approach is presented in the following sections.

3.1 Background

The Project Work Plan identified a segment of the Brazos River along the western boundary of Robertson County, Texas, which coincides with the outcrop of the Carrizo-Wilcox, Queen City, Sparta, and Yegua-Jackson aquifers. For analysis, the groundwater availability model selected is the one corresponding to the central portion of the Carrizo-Wilcox Aquifer. The model files and associated files are version 3.02 (Young and Kushnereit, 2020) and were obtained from the Texas Water Development Board (TWDB) groundwater availability model files download page.

3.1.1 Description of the central portion of the Carrizo-Wilcox Aquifer groundwater availability model

For this study, the interaction between the Brazos River and groundwater along the 30-mile-long study area will be modeled using the groundwater availability model for the central portion of the Sparta, Queen City, and Carrizo-Wilcox aquifers (Young and others, 2018a; Young and Kushnereit, 2020). The development of this groundwater availability model was partly funded by groundwater conservation districts in Groundwater Management Area 12, the Lower Colorado River Authority, and the Brazos River Authority to improve the representation of groundwater/surface water exchange compared to the previous groundwater availability model for the region (Kelley and others, 2004) by making the following enhancements:

- Added a separate model layer to represent the Brazos River Alluvium
- Added a thin model layer near the surface that represents and connected the shallow groundwater flow to surface water bodies including the Brazos River Alluvium
- Reduced the grid size from 1 square mile to 0.25 square mile across the Brazos River Alluvium

Figure 3.1 shows a conceptualization of the groundwater availability model layers and hydraulic processes presented in Section 3.5 of Young and others (2018a) for the central portion of the Carrizo-Wilcox Aquifer groundwater availability model. In the study area, the Brazos River Alluvium is represented by layer 1. Model layer 2 represents a shallow flow system that primarily includes the outcrops of the hydrogeologic units. This model layer serves to promote lateral flow among the different aquifers and between groundwater and surface water. The rationale and potential benefits

associated with incorporating a shallow groundwater flow layer into a groundwater availability model is explained by Young and others (2018b).

Model layers 3 through 10 represent the confined regions of the eight major hydrogeologic units that comprise the groundwater flow system. From youngest to oldest, these hydrogeological units are the: Sparta Aquifer, Weches Formation, Queen City Aquifer, Reklaw Formation, Carrizo Aquifer, and Wilcox Aquifer. The Wilcox Aquifer is comprised of the Calvert Bluff Formation, the Simsboro Formation, and the Hooper Formation. In the groundwater system, the Reklaw Formation represents a regional aquitard, and the Weches Formation consists of clayey deposits that often serve as a localized aquitard.

The top image in Figure 3.1 is a schematic of a vertical cross-section of the groundwater availability model layers. The figure shows that all aquifers include an outcrop that intersects the ground surface and a subcrop that dips downward and towards the Gulf of Mexico. Near the surface, layer 2 includes the outcrop of the aquifer and formations represented by layers 3 through 8. Where present, the Brazos River Alluvium occurs as layer 1. The bottom image in Figure 3.1 is a conceptualization of the flow processed controlling groundwater flow in the eight geologic units represented by layers 3 through 10 and the Brazos River Alluvium. The outcrop associated with each geologic unit is represented by the portion of each model layer where the alluvium exists, and where recharge and evapotranspiration occur.

3.1.2 MODFLOW-USG

The groundwater availability model is a MODFLOW-USG model (Panday and others, 2013) and MODFLOW packages are used to represent hydraulic boundary conditions, pumping, and groundwater-surface water interactions. The groundwater availability model simulates groundwater flow using annual time steps. The Brazos River Alluvium is represented using a variable hydraulic conductivity with an arithmetic mean of 322 feet/day and ranging between 27 and 1000 feet/day. The pumping distribution for the Brazos River Alluvium Aquifer was generated from the MODFLOW-USG files for the Brazos River Alluvium Aquifer groundwater availability model (Ewing and Jigmond, 2016). Recharge across the outcrops and the alluvium deposits were simulated using the MODFLOW Recharge package. Recharge rates vary spatially based on surface geology and vary temporally based on annual precipitation.

Across the entire model domain, the recharge rates vary temporally by at least a factor of two between the low and high precipitation years. Spatially, the rate of recharge increases from the south to the north. This trend occurs because both precipitation and the percentage of precipitation that becomes recharge increases from the south to the north. Annual recharge rates for the Brazos River Alluvium average around 6 percent of the annual precipitation.

3.1.3 Area of interest

Figure 3.2 shows the Area of Interest for the study. The study is about 30 miles long and 5 miles wide and occurs along the boundary of the Post Oak Savannah Groundwater Conservation District (POSGCD) and the Brazos Valley Groundwater Conservation District (BVGCD). The Brazos River Alluvium boundaries in Figure 3.2 are defined by the boundaries of the Brazos River Alluvium in the groundwater availability model. The total area is 96,960 acres, with 79% falling under the

jurisdiction of the Brazos Valley Groundwater Conservation District in Robertson and Brazos counties, and the majority of the area in the western portion of Robertson County with 75,360 acres. The remaining 21% are situated within Post Oak Savannah Groundwater Conservation District, covering Milam and Burleson counties.

3.2 Representation of Groundwater-Surface water exchange

The MODFLOW River (RIV) Package (McDonald and Harbaugh, 1988) was used to simulate groundwater exchange with the Brazos River and its tributaries in the area of interest. The RIV Package simulates the flow exchange based on the hydraulic head difference between the river and the groundwater system across the riverbed. The variables that need to be defined to use the River Package are river stage, river bottom, aquifer hydraulic head, and riverbed conductance. These variables are visually defined in Figure 3.3 and are described below.

- River bottom, B_{riv} , is the elevation of the bottom of the riverbed.
- River stage, H_{riv} , is the water level (or head) in the river/stream.
- Aquifer hydraulic head, h, is the hydraulic head of the aquifer grid cell.
- Riverbed Conductance, C_{riv}, is the factor that relates the difference in hydraulic head to the rate of flow between the river and the aquifer. C_{riv} is defined by the equation below.

$$C_{riv} = \frac{K \cdot L \cdot W}{T_{riv}}$$

where: K = hydraulic conductivity of riverbed
W = Width of riverbed
L = Length of riverbed
T_{riv} = Thickness of riverbed

When the aquifer hydraulic head in the cell is higher than the river stage, groundwater flows into the river. When river stage is higher than the aquifer hydraulic head in the cell is higher, river water flows into the aquifer. The rate of flow is determined by the following equation.

$$Q_{riv} = (h - H_{riv}) \cdot C_{riv}$$

where: Q_{riv} = flow rate between river and aquifer

The RIV package was employed to simulate groundwater exchanges with major rivers and perennial streams in the Brazos River. The initial locations of the river cells in the central portion of the Carrizo-Wilcox Aquifer groundwater availability model were adapted from Kelley and others (2004). Adjustments were made to river cell locations along the Brazos and Colorado Rivers to align with the refined numerical grid, which was developed using the US Geological Survey National Hydrograph Dataset of rivers and streams. These refinements are illustrated in Figure 3.4 of this report, which corresponds to Figure 4.5a in Young and others (2018a). Similarly, as shown in Figure 3.5 of this report (corresponding to Figure 5.7 in Young and others (2018a)), the model includes 5,560 river cells representing the interactions between the rivers and the aquifer system.

The attributes of each river cell, such as node number, river bottom elevation, river stage, and river conductance, were defined based on the refined numerical grid and are detailed in the electronic

deliverables accompanying this report. River conductance values in the model range from 1,000 to 58,000 square feet per day, reflecting variability in streambed properties and river-aquifer interactions.

The area of interest consists of 477 model grid cells with two different sizes thanks to the local grid refinement capabilities provided by MODFLOW-USG. Of these cells, 434 overlap with the existing hydrography network in the alluvium, each measuring 0.5 miles by 0.5 miles. The remaining 43 grid cells measure 1 mile by 1 mile. Figure 3.6 uses a red background to delineate the 311 cells where either the Brazos River or one of its tributaries crosses a grid cell. In this figure the 109 grid cells outlined in grey mark the Brazos River channel. In the following section, water budgets for the fluxes defined in the conceptual model are provided for three distinct control volumes: the entire layer 1, a subset of the area of interest excluding cells representing the Brazos River, and a separate budget for only the cells that intersect with the Brazos River.

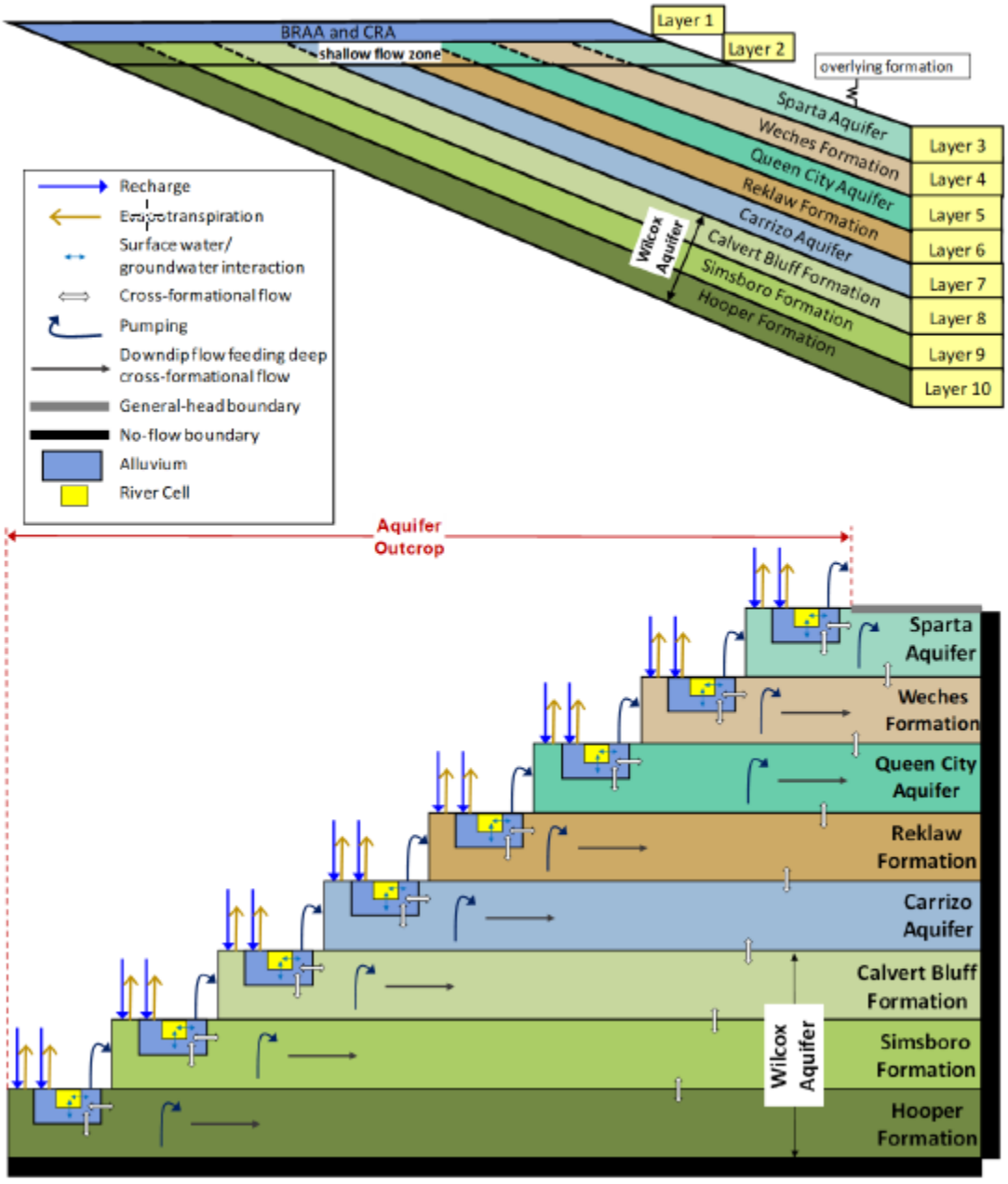

Source: Figure 3.5a, Young and others (2018a)

Figure 2.1 **Conceptual model for the central portion of the Carrizo-Wilcox, Queen City and Sparta aquifers groundwater availability model.**

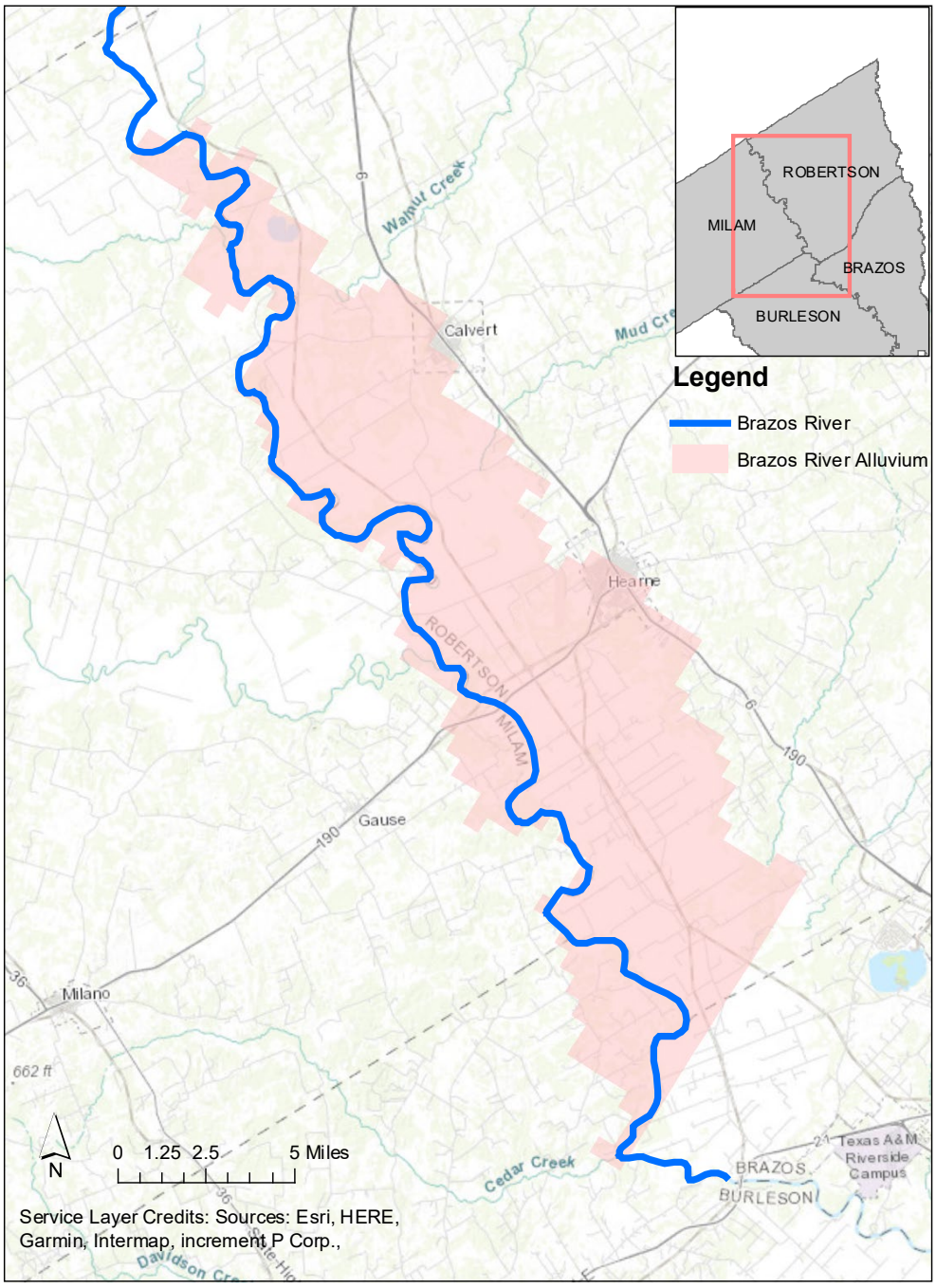

Figure 3.2 **Area of interest for sensitivity analysis.**

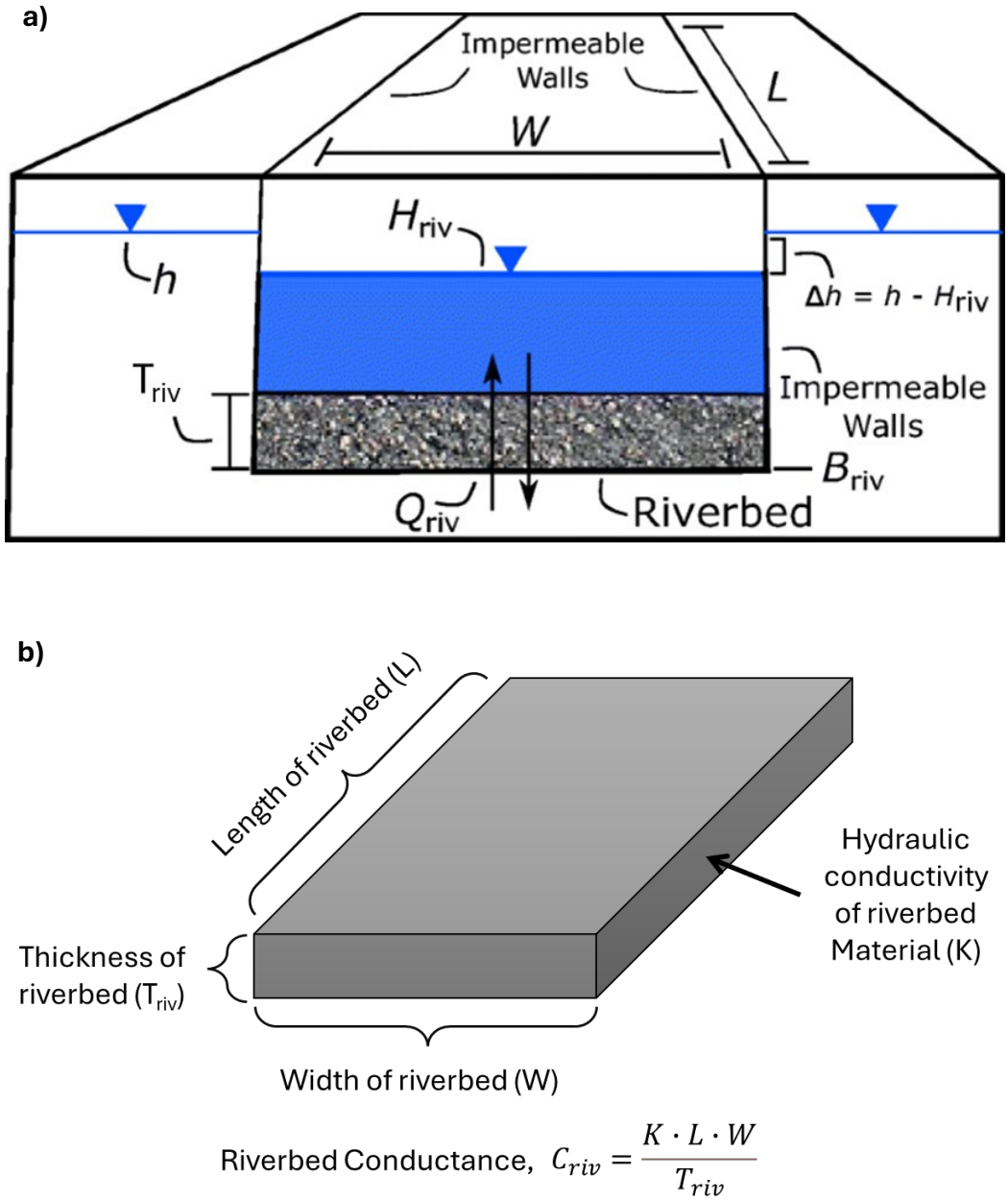

Modified from: Ghysels and others (2019) and McDonald and Harbaugh (1988)

Figure 3.3 **Visualization of the variables that are used to define the: a) MODFLOW River Package; and b) MODFLOW Riverbed Conductance.**

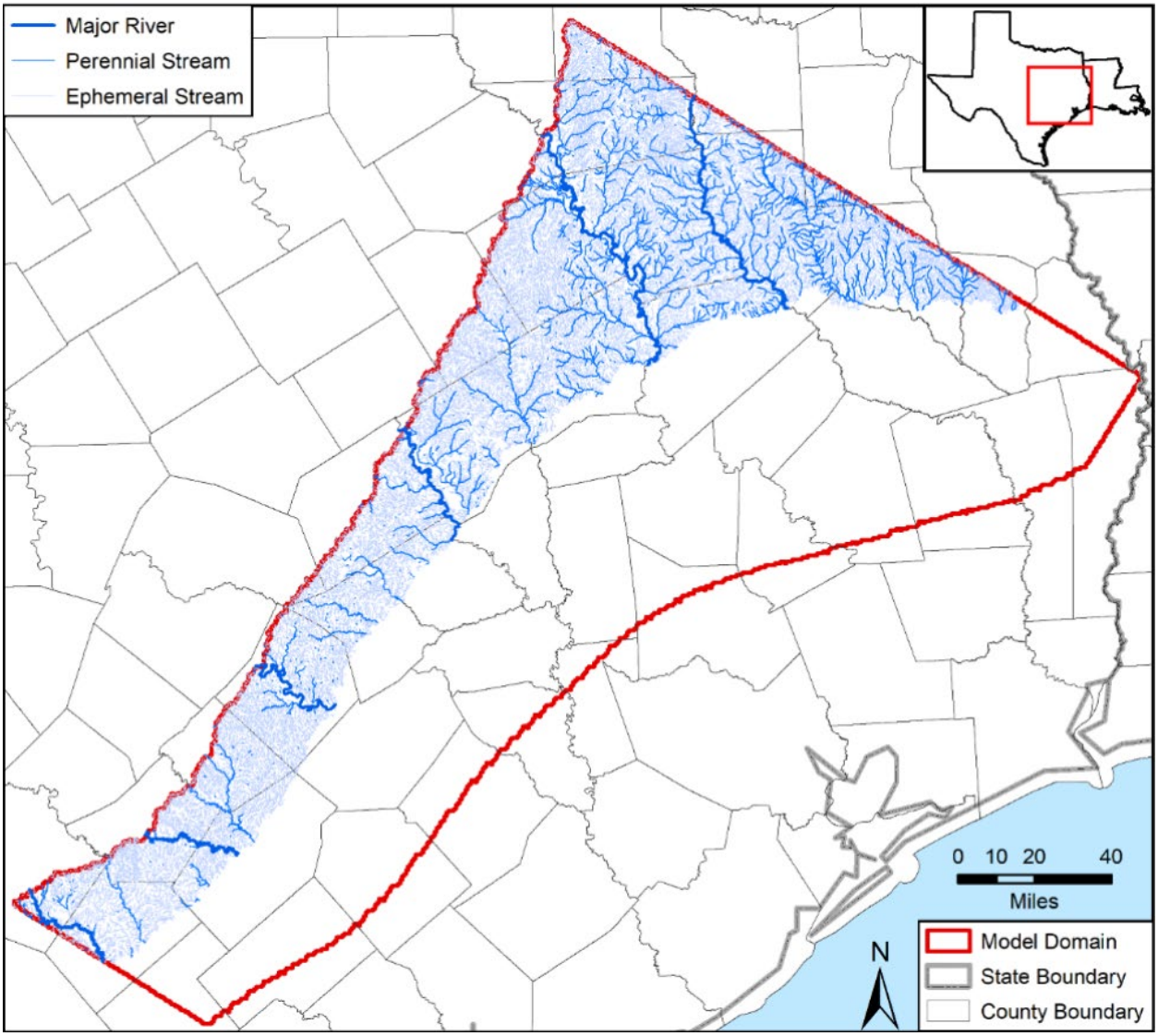

Source: Figure 4.5a, Young and others (2018a)

Figure 3.4 **Locations of major rivers and perennial and ephemeral streams in the outcrop areas based on United States Geological Survey national hydrograph data for the Carrizo-Wilcox Aquifer (central portion) groundwater availability model.**

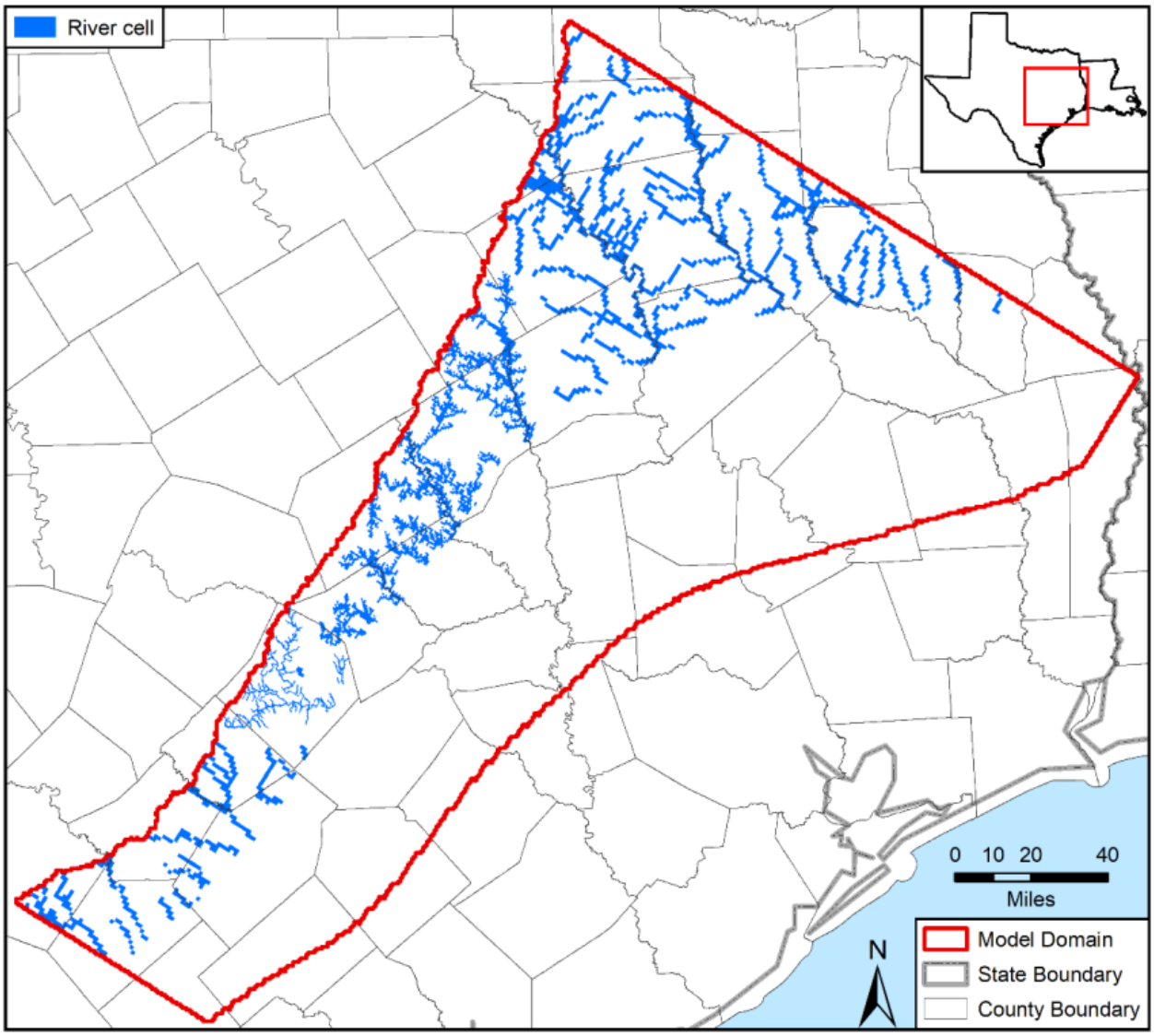

Source: Figure 4.8a, Young and others (2018a)

Figure 3.5 **Location of river cells in the Carrizo-Wilcox Aquifer (central portion) groundwater availability model.**

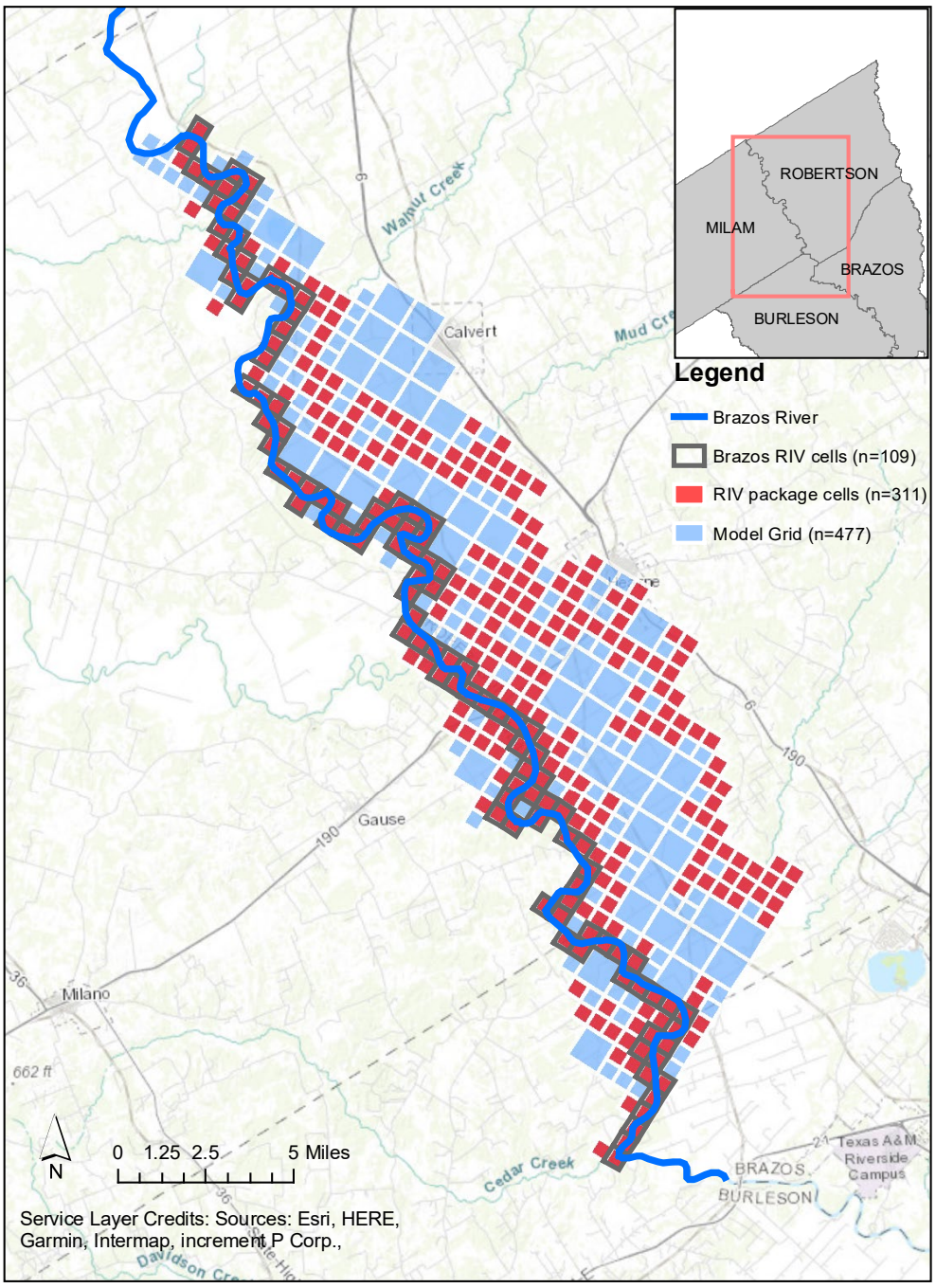

Figure 3.6 **Location of River (RIV) Package cells in the area of interest.**

3.3 Water budget for the central portion of the Carrizo-Wilcox Aquifer groundwater availability model

A Python script was developed to plot the components of the water budget for different sets of zones in the model. The zones can be defined by layer, aquifer, or a combination of criteria including the location of the Brazos River Alluvium hydrogeologic unit. Figure 3.7 presents the water

budget for layer 1 in the model which represents the Colorado and Brazos rivers alluvium. This figure matches the figure presented in Section 5.5 of Young and others (2018a) report. Incoming fluxes into the aquifer are positive while outgoing fluxes are negative. The main components of the water budget for layer 1 are river leakage representing the net exchange with the RIV package, wells representing pumping in the alluvial aquifer, recharge, and the exchange with layer 2 that represent the shallow groundwater flow associated to different hydrogeologic units. Fluxes from the groundwater ET package and the drain package used to simulate outflow from ephemeral streams, intermittent streams, and seeps are very small. The same Python script was used to compare the water budget for both the cells in the area of interest surrounding the Brazos River, and the cells representing the Brazos River, as shown in Figure 3.8 and Figure 3.9, respectively.

Figure 3.7 Water budget by layer number for layer 1 (Alluvium).

Model cells in the area of interest surrounding the Brazos River are labeled as Zone 20 while the RIV cells intersecting the Brazos River are labeled as Zone 21. For the 368 cells in Zone 20, shown in Figure 3.8, the flow with the largest magnitude is pumping while river leakage is relatively small. Fluxes to other units are small when compared to the magnitude of recharge, river leakage, and pumping. The trend in pumping is similar to the one shown for layer 1, with pumping increasing in the 1950s and peaking at the end of the 2000s. For the 109 cells in Zone 21, shown in Figure 3.9, the largest fluxes are river leakage, the exchange with the surrounding alluvial aquifer, pumping, and recharge. On an annual basis, the Brazos River alluvium is always contributing to the Brazos River, and this trend has decreased with time due to pumping. For the area of interest, the largest portion of river leakage occurs for model cells intersecting the Brazos River and that the main exchange between the Brazos River cells is with the surrounding alluvium. There is also significant pumping in the Brazos River cells starting in 1950s and following a trend similar to the pumping in layer 1.

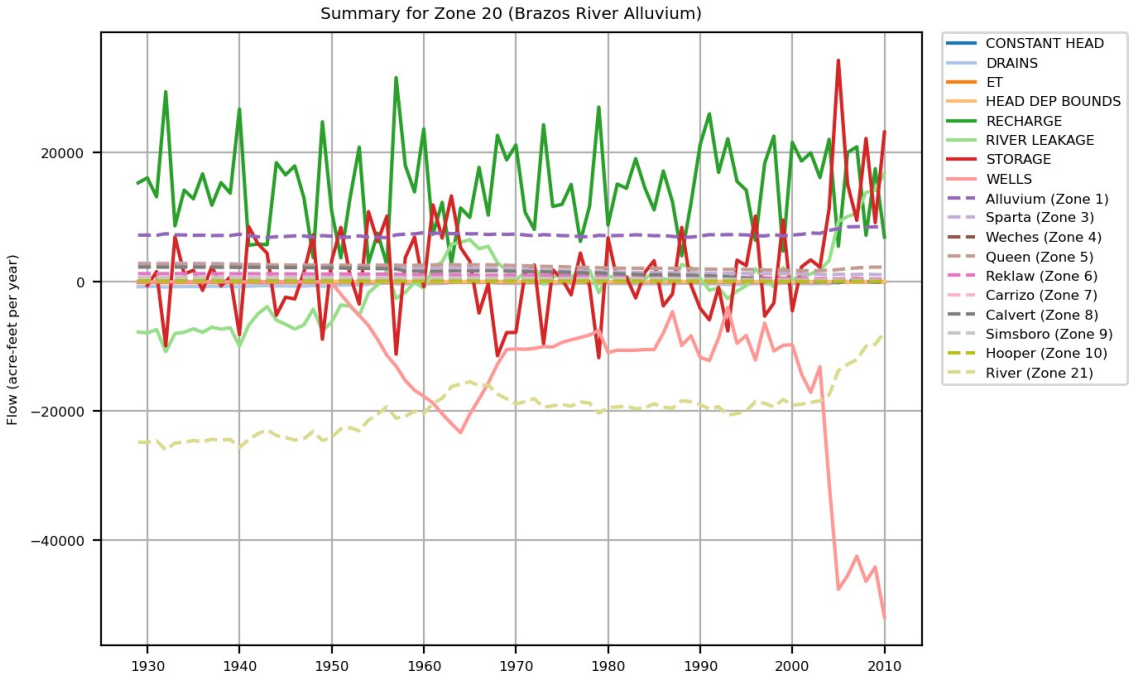

Figure 3.8 **Water budget by aquifer in the area of interest except for cells intercepting the Brazos River.**

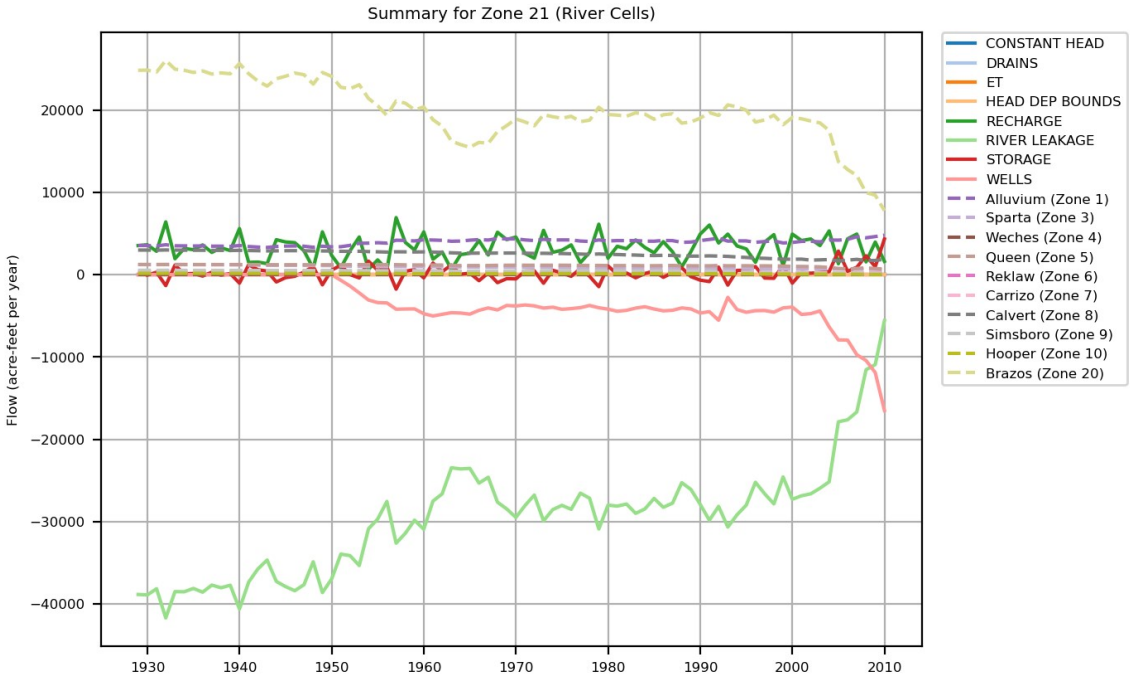

Figure 3.9 **Water budget by aquifer for RIV model cells intercepting the Brazos River.**

In order to rank the exchange between the river cells and the underlaying hydrogeologic units, Figure 3.10 presents only the fluxes between the cells representing the Brazos River and the underlying units in layer 2. The magnitude of the fluxes for the entire area of study is below 1,200

acre-feet per year (acre-ft/yr) or about 2 feet^3/second, except for the flow from Calvert Bluff formation (labeled as Calvert in Figure 3.10) ranging between 1,800 and 3,000 acre-feet/year (2 and 4 feet^3/second). The larger values for the Calvert Bluff formation and Queen City Aquifer (labeled as Queen) can be explained by the larger contact along the Brazos River with about 8 miles and 6 miles, respectively. Note that the magnitude of the fluxes is considerably smaller than the median annual flow at the US Geological Survey 08098290 Brazos River near Highbank, TX, which is about 2,300 feet^3/second.

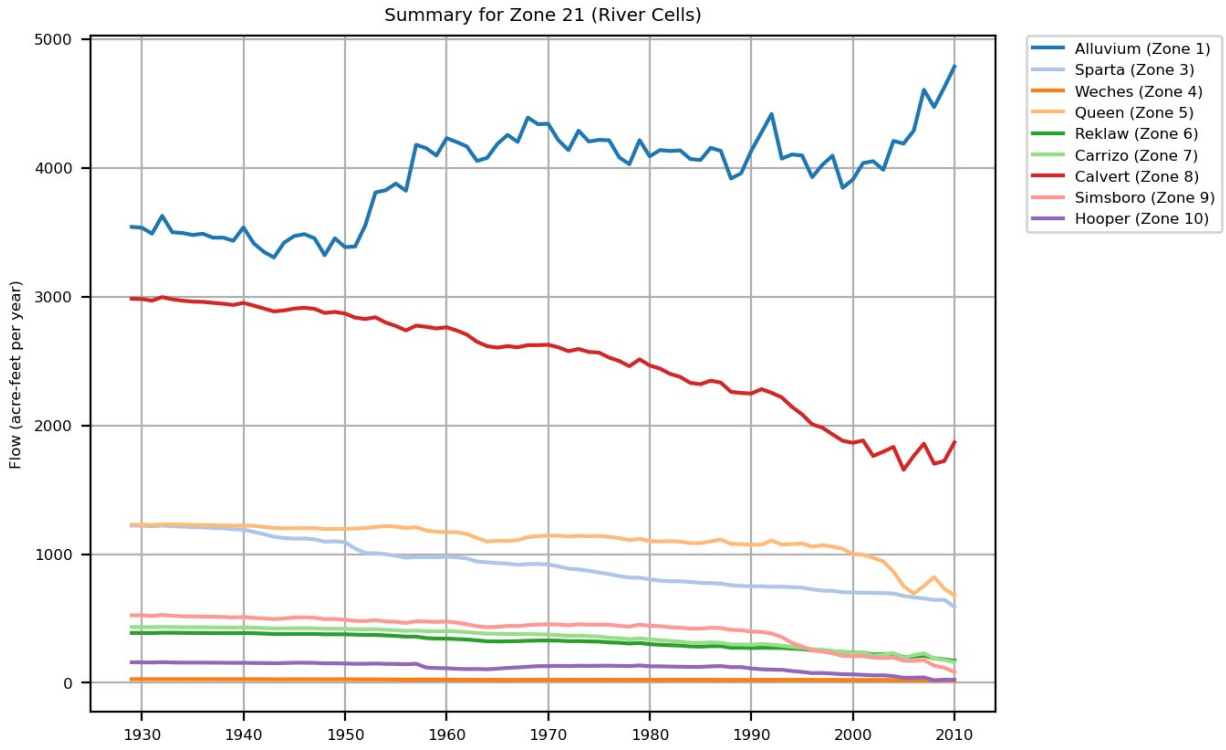

Figure 3.10 Flow between hydrogeologic and model cells intercepting the Brazos River.

Figure 3.11 presents the RIV package parametrization for the cells intercepting the Brazos River. The RIV package river stage (shown in orange) is assumed to be 3 feet above the riverbed bottom elevation, Rbot (green). Also shown are the top and bottom of the cells for the Brazos Alluvium. The Brazos River cells are organized in descending order by Rbot, which aligns well with the alignment downstream order of the cells, allowing for easier comparison of parameter and fluxes. The figure also includes the groundwater heads for the entire simulation, with gray lines representing groundwater heads from 1930 to 2010.

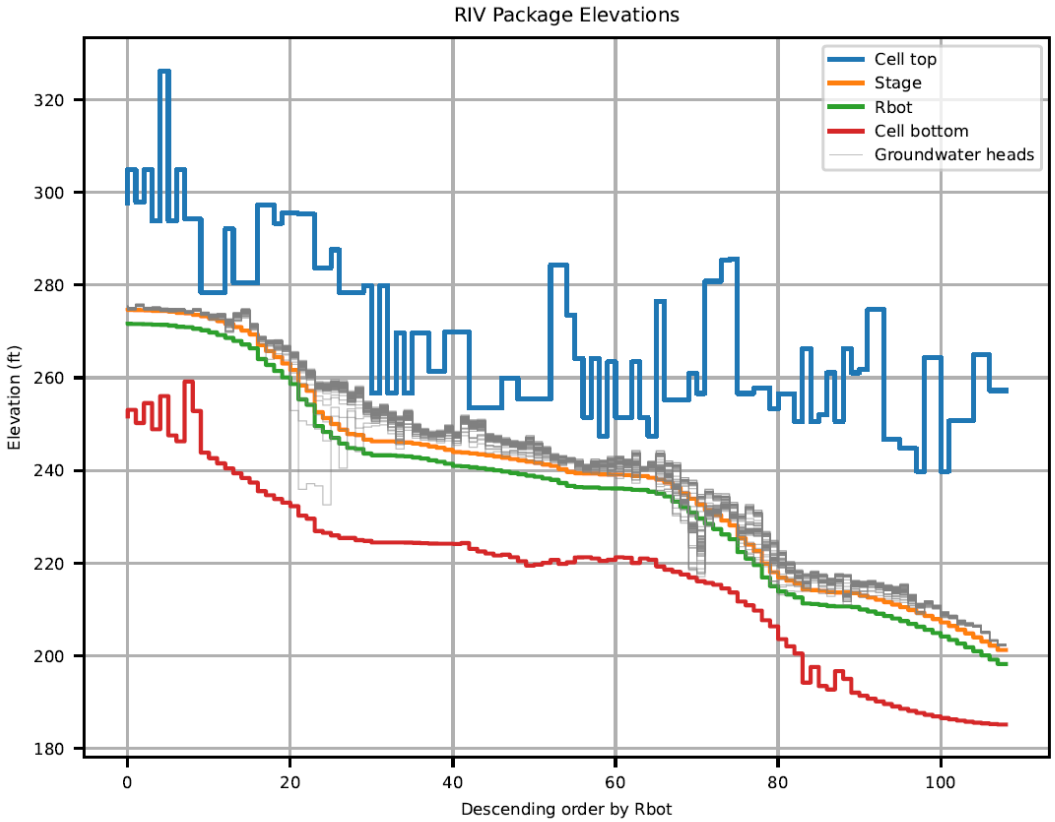

Figure 3.11 **RIV Package elevations and groundwater heads between 1930 and 2010 for model cells intercepting the Brazos River.**

Figure 3.12 presents the river conductance along the Brazos River ranging between 3,000 and 39,000 feet/day. Moving downstream, conductance first decreases from about 25,000 feet/day to 3,000 feet/day and then increases to 15,000 feet/day. Another low is observed around 5,000 feet/day, between cells 60 and 80, and then gradually increases to 39,000 feet/day. Figure 3.13 and Figure 3.14 present RIV package elevation information at the top subplot and RIV fluxes at the bottom subplot for years 1952 and 2010, respectively. The subplots at the bottom use the left axis to show fluxes at each individual cell, while the right axis shows the difference between river stage and groundwater head. The bottom subplots also include pumping from WEL package (WELLS flux), and an estimate of groundwater flow based solely on conductance and head difference. This estimate does not consider the bottom of the riverbed (Rbot) as a constraint for head difference and was used to check parametrization units.

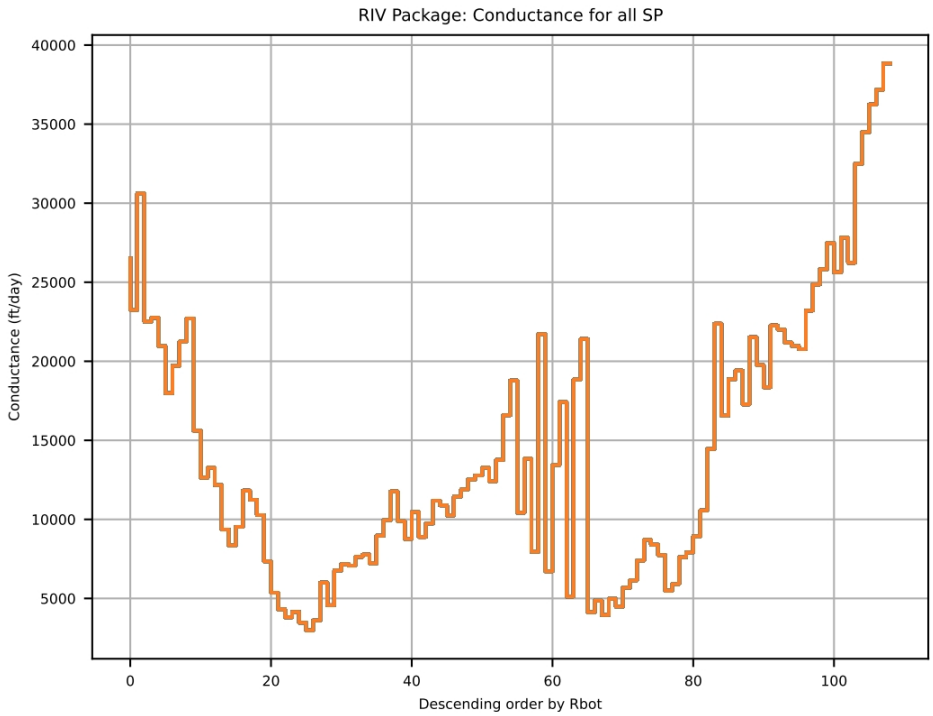

Figure 3.12 RIV Package conductance for model cells intercepting the Brazos River.

When groundwater heads are above river stage, the difference is negative, and the flow direction goes from the Brazos Alluvium to the Brazos River cells. On the other hand, when the difference between river stage and groundwater head is positive, the flow direction goes from the river to the underlying aquifer. Flow from aquifer to the river is predominant for most of the simulation (river cells gaining), except for the later years when there is an inversion of the flow at several segments (river cells losing). In year 2010, the location of these losing segments matches the location of cells where pumping flow is higher than 1 feet^3/second. Visual inspection of the location of pumping in the Brazos alluvium also suggests the impact of pumping on the location of losing segments.

Figure 3.15 provides a comparison of the RIV and WEL package fluxes within the alluvium for the year 2010. The two segments with losing river cells are indicated in orange, while the gaining cells are indicated in blue. Pumping in the alluvium is indicated with a green color scale. The majority of pumping occurs in the lower portion of the area of interest, where the alluvium is the widest and the largest losing segment is located on the western edge. In contrast, during the predevelopment steady-state stress period and the initial years in the groundwater availability model simulation (1930 to 1951), there is no pumping occurring in the alluvium and the RIV flow is always from the alluvium to the river for all Brazos River cells.

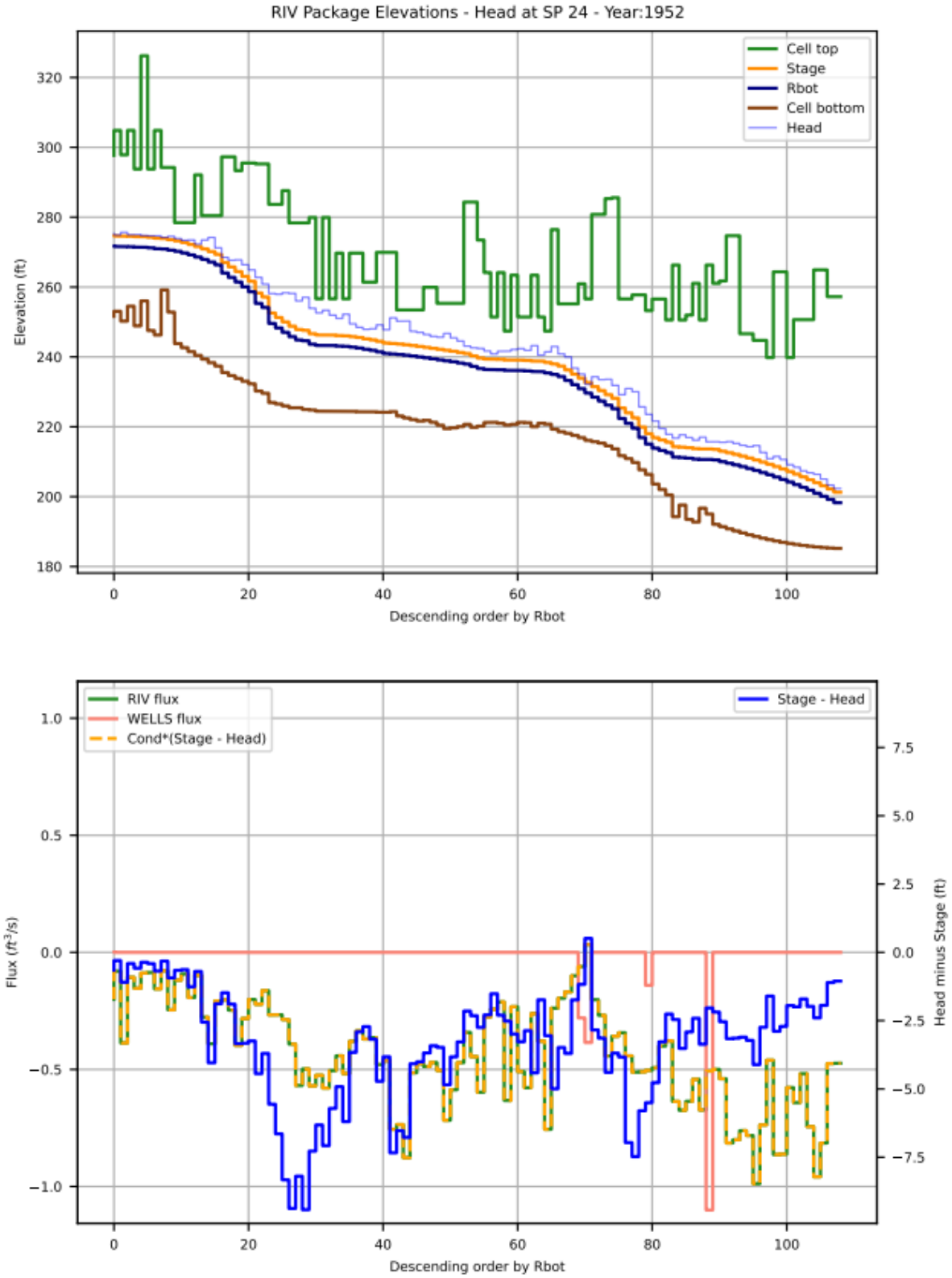

Figure 3.13 **RIV Package parametrization and groundwater heads and associated fluxes in year 1952 for model cells intercepting the Brazos River.**

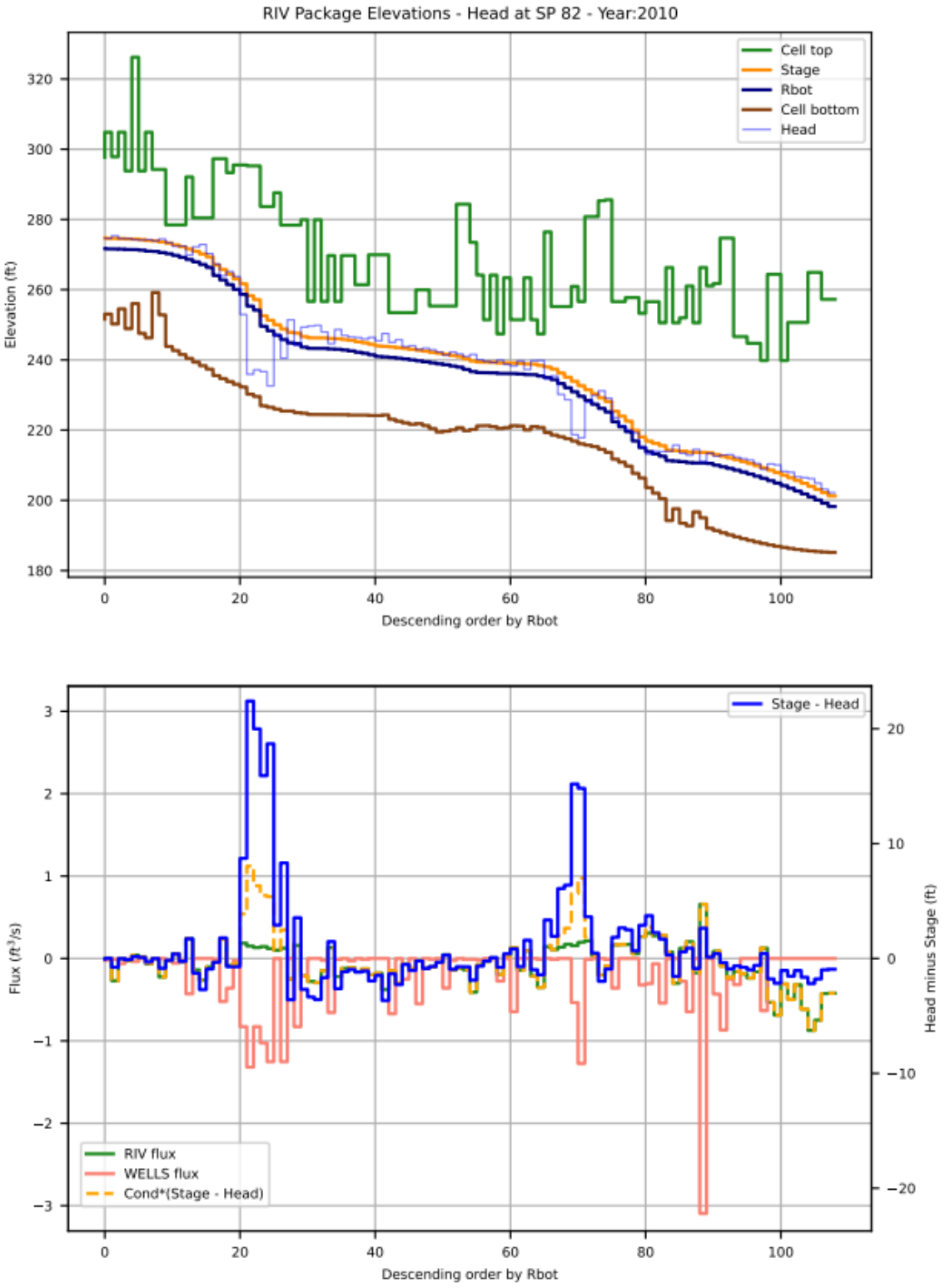

Figure 3.14 **RIV Package parametrization and groundwater heads and associated fluxes in year 2010 for model cells intercepting the Brazos River.**

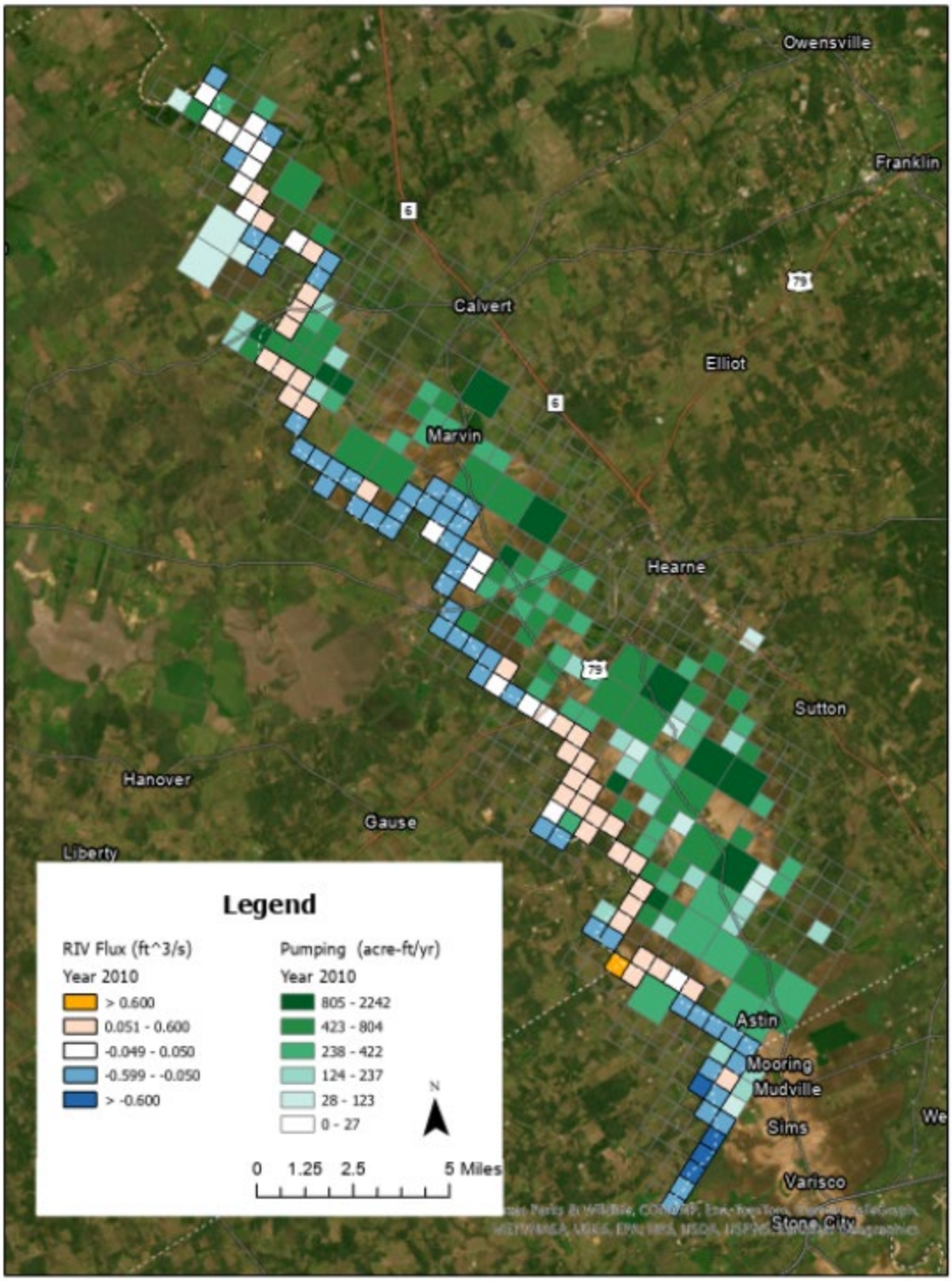

Figure 3.15 **RIV Package flow in the year 2010 for model cells intercepting the Brazos River.**

4. Data Collection and Processing

To support the refinement of the groundwater availability model, project staff downloaded remote sensing satellite data from April 2023 to November 2024, and conducted several field trips to the area of interest, deploying equipment to measure groundwater levels in the alluvium, surface water elevations, temperature profiles along the riverbank, river discharge (flow) rate, and channel bathymetry. The team also deployed two types of drones – fixed wing and quadcopter – to collect multi-spectral imagery. Details of the fieldwork and data collected are described in this chapter.

It should be noted that the team faced significant difficulty accessing the river for the fieldwork - when flows were below 500 cubic feet per second at the US Geological Survey gage (08108700) the propeller of the Jon boat was in regular contact with the bottom of the river, causing safety concerns and navigation challenges. Similarly, when flow in the river was above 8,000 cfs the velocity was sufficiently high to present deployment challenges and risk overturning the boat. See Figure 4.1 for the timeline of river flows through the course of the project.

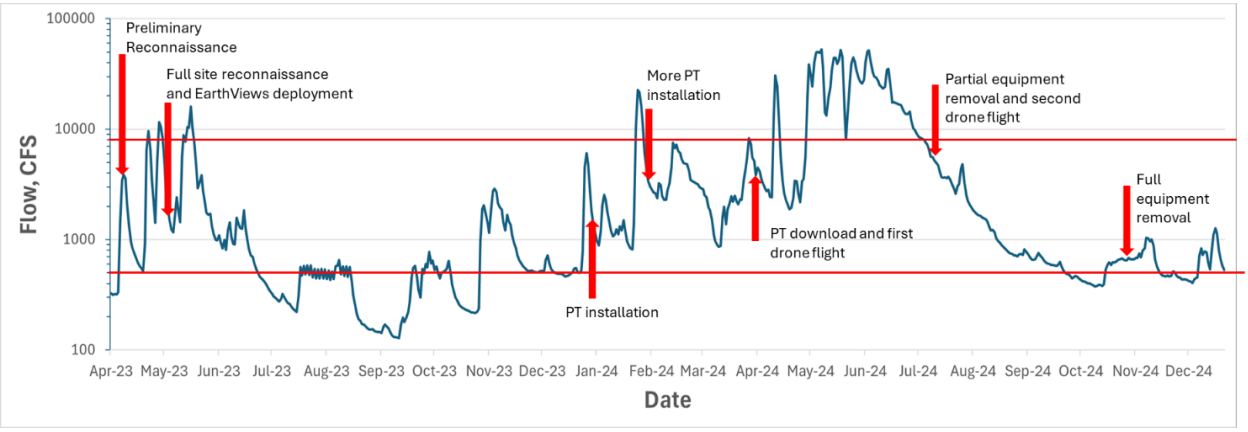

Figure 4.1 Timeline of field activities from US Geological Survey gage 08108700 (Bryan gage).

There are some interesting features of the hydrograph above that are worth mentioning. First, there is clearly a prolonged release of water from a reservoir in August 2023, probably for a downstream water user. Second, we were unlucky to not have dry winters with low interference of irrigation and precipitation. Dry winters are an ideal time to measure groundwater-surface water interaction as signals from irrigation and precipitation are non-existent. Our SWOT analysis shows quarter 3 as the lowest river-stage period, when heavy rainfall can often occur and heavy use of groundwater also occurs. This is an unfortunate situation with this site, for this particular period of time.

A compounding issue with data collection at high flow rates is that it is difficult to secure equipment and keep it safely recording through the full range of flows. We lost several of the river level monitoring pressure transducers from bank erosion around the fenceposts. Similarly, some pressure transducers were buried under several feet of sediment (see recovery efforts at one of the sites, below; Figure 4.2).

Although we anticipated periods of very low water as well as strong pulses from the Brazos River, we did not anticipate that *majority* of our deployment time (instrumentation) would be during these difficult field conditions. After our full equipment deployment in April 2023, we planned on

conducting 3 to 4 field surveys, mostly flow measurements over 2 to 3 week intervals, to develop local rating curves from the upstream and downstream end of our study reach. However, river flows remained high weeks after the April fieldwork and extended to late June. Flows went down substantially in July when we were able to go out and collect our field equipment and conduct a flow survey, but then remained too low for additional surveys for an extended period of time.

Figure 4.2 **Recovery of a pressure transducer following flooding on the Brazos River using a metal detector and a spade.**

The team was able to access wells near the river for deployment of groundwater level monitoring equipment thanks to the contacts provided by Alan Day (General Manager of the Brazos Valley Groundwater Conservation District). These landowners were kind enough to provide access to their wells, land, and in some instances also provided access to the river. Without their cooperation and consent, this project would have suffered from a lack of data.

4.1 Field data collection

Data collection was conducted to determine field-based measurements of potential groundwater-surface water exchange, determine the underlying hydrogeologic framework of the selected reaches, and acquire field data to support our remote-sensing-based analysis. Three study sites were selected representing areas where the Brazos River Alluvium Aquifer has potential connections to the Carrizo-Wilcox, Queen City, Sparta, and Yegua-Jackson aquifers (Figure 4.3). Furthermore, these sites are relatively accessible (with owners' permission) for the team to access the river with small boats. Fieldwork was conducted in January 2023, for both reconnaissance and initial deployment of instruments. Full deployment of instruments and field surveys was conducted in April 2023, whereas equipment removal took place in August 2024. Field activities included:

1) The deployment of pressure transducers for measuring water levels in both the Brazos River and groundwater wells adjacent to the selected river reaches to determine water levels (Figure 4.3).
2) Stream gaging using Acoustic Doppler Current Profiler (ADCP) upstream and downstream of the reaches.
3) Electrical resistivity surveys to assess the subsurface geology/geohydrology.
4) Temperature vertical profile loggers (thermocouples) were also installed adjacent to one of the river pressure transducers, however, the instruments were washed out by flood pulses two weeks after the installation.

4.1.1 Groundwater level and river stage measurements

Water levels were monitored along the study reaches (river stage) and in groundwater wells within a few hundred meters of the river shoreline to determine groundwater gradient trends and quantify potential groundwater-surface water exchange fluxes. The selection of wells close to the river increases the likelihood that hydrologic events occurring in the river can be measured/reflected in groundwater. This also allows for assessing hydraulic connectivity between groundwater and surface water. Pressure transducers were also installed in both the upstream and downstream end of the study reaches complemented with discrete river discharge measurements to develop rating curves. The goal is to monitor the differences in discharge between the upstream and downstream sections and relate gains or losses with potential groundwater-surface water exchange fluxes. Figure 4.3 shows the location of the installed pressure transducers deployed along the selected reaches and groundwater wells adjacent to these reaches. ONSET-HOBO U20 pressure and temperature loggers were installed in four wells that are within 200 meters of the closest bank/shoreline of the Brazos River channel. The same type of pressure transducers were installed upstream and downstream of the selected reaches using fence posts driven 2-3 feet into the riverbed. The pressure transducers were tied to the posts about a foot above the riverbed. A barometric pressure logger was deployed at the middle reach site (Gossett) and used as reference for correcting water levels measured using the pressure transducers. Depth-to-water (DTW) measurements from a reference point along the lip of the wells were measured noting the time of data collection to tie groundwater levels to river stage measurements. A Trimble R12 real-time kinematic (RTK) GPS was used to determine the reference point elevations and river stage at the study reaches.

The well (VGHN well) near Vaughn Reach, located in Calvert, Texas is about 1000 feet away from the closest shoreline and 1800 feet from the surface water gage (VGHN sw). The well is currently used for livestock and based on the well data trend is being pumped on a regular basis. VGHN gage1, was installed about a mile upstream of VGHN sw. The Gossett Reach wells in Mumford, Texas were constructed for irrigation but currently, GSST1 well is unused whereas GSST2 well is occasionally used based on the logged trends. The GSST1 well is about 560 feet from the closest river shoreline where GSST1 sw, a water level logger, was installed. GSST1 gage1 was installed 4000 river feet from GSST1 sw. GSST1 gage2, 2.25 miles downstream of GSST1 sw, served as both the downstream end of GSST1 and upstream end of GSST2. GSST2 well is about 580 feet from the closest river shoreline and about 2000 feet from GSST2 gage1 which was installed in the opposite bank. The Moore well in College Station, Texas (across the Texas A and M farm) is frequently used for irrigation on a regular basis and is about 510 feet from the closest river shoreline where Moore sw (pressure transducer) was installed. Moore gage1 and gage2 were installer 1.6 and 1.2 miles upstream and downstream of Moore sw respectively.

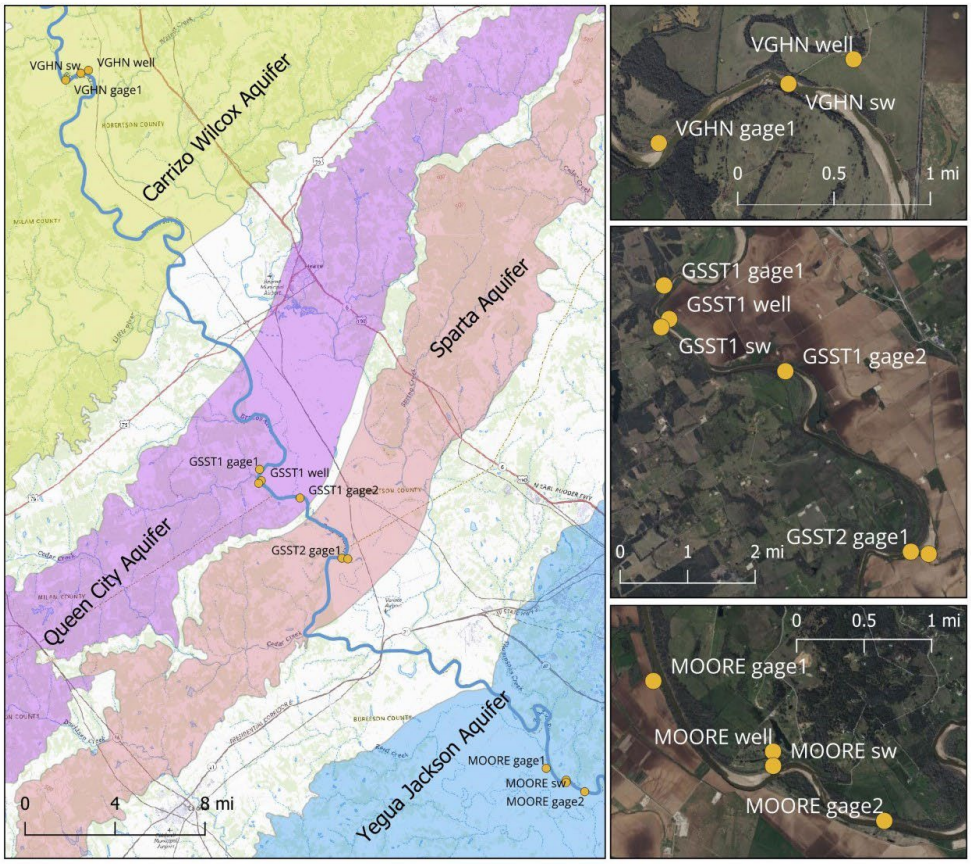

Figure 4.3 **Study reach locations and measurement sites for groundwater levels (well), river stage (sw and gage), and river discharge (gage).**

4.1.2 River discharge measurements

River discharge measurements were taken along cross sections upstream and downstream of the selected study reaches (Figure 4.4). A SonTek M9 acoustic Doppler current profiler (ADCP) was used to collect depth velocity profiles across the river sections (see example in Figure 4.4). Velocity measurements were repeated at least four times to assess measurement uncertainties. The mean of the four measurements was then taken as the estimated discharge value. Integration of the velocity profiles to generate net discharge values was done using the River Surveyor Live software (SonTek).

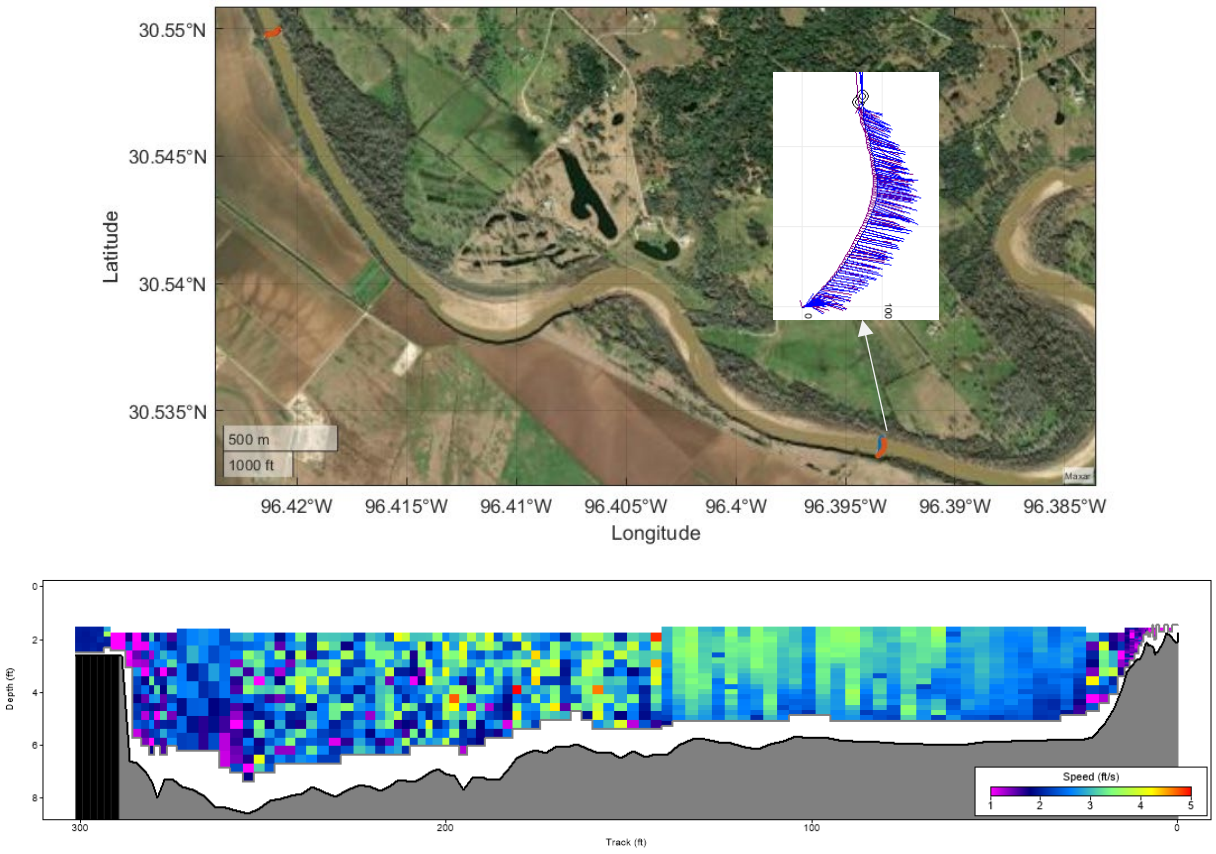

Figure 4.4 **Depth velocity profiles collected in April 2024 at the downstream end of Moore Reach. The inset image in the top panel shows the repeat measurements with velocities as vector lines.**

4.1.3 Electrical resistivity

Underwater electrical resistivity (ER) surveys were conducted along selected sections of the study reach to assess the hydrogeologic characteristics and estimate the thickness of the alluvium deposits where groundwater-surface water exchange is potentially occurring. A Super Sting R8 (AGIUSA) with a 56-electrode graphite cable was used to measure sub-river bottom resistivity. A dipole-dipole array setup was used for the surveys and resistivity inversions were conducted using R2 software (Binley, 2023) with ResIPy python graphic user interface (Blanchy and others, 2020). Our estimate of the depth of investigation is 6-7 meters (see Figures 5.1 through 5.3, in the next

chapter) which coincidentally appears to be a transition between lower resistivity to higher resistivity zones. The inversion mesh was refined by increasing discretization closer to the river bed. ER data were then re-inverted using data that were within -3 to 3 normalized inversion error.

4.1.4 Aquifer permeability estimation

Aquifer hydraulic conductivities (K_{sat}) were estimated from well specific capacity (SC) which are calculated by dividing the pumping rate by the net drawdown. Aquifer transmissivity (T) was first calculated following Driscoll (1986) with the saturated hydraulic conductivity calculated by:

$$T = 1500 * SC$$

$$K_{sat} = \frac{T}{b}$$

where b represents the saturated thickness of the aquifer (Table 5.1). Well specific capacities were calculated from the drawdown and pumping rate reported in the well drillers' report (TWDB Submitted Drillers Reports Database, 2024). All wells used in estimating permeability for the specific study reaches are either the monitored wells or wells closest to the study sites.

-https://www.twdb.texas.gov/groundwater/data/GWDBDownload.zip

-Date accessed: 12/27/2024

4.1.5 Groundwater exchange calculation

Groundwater fluxes (q) were estimated using Darcy's Law given by the equation below:

$$q = K_{sat} \frac{H_{GW} - H_{SW}}{d}$$

where the groundwater flux is the product of the saturated hydraulic conductivity (K_{sat}) and the hydraulic gradient. The hydraulic gradient is the difference between the groundwater head (H_{GW}) and surface water head or stage (H_{SW}) divided by the distance (d) between the well and the river shoreline. The distances and elevations were measured from the well to the closest river shoreline using the latest satellite imagery.

4.1.6 Other relevant information used

The team communicated with Professor Joe Yelderman from Baylor University and his graduate student Mark Nickels who is working on his master's research on the interactions between the Brazos River in the vicinity of our fieldwork and the Brazos River Alluvium Aquifer. They are using both historical hydrologic gradient determination and chemical techniques to evaluate the groundwater-surface water exchange. They report their preliminary results of historical analysis of US Geological Survey gage data and groundwater gradients to be consistent with previous work where the generalized hydrogeologic gradient is from the Brazos River Alluvium Aquifer to the Brazos River with limited temporary reversals during periods of high river discharge and higher channel water levels. Our team also observed these trends from our data although within a shorter instrument deployment but at a higher temporal resolution. This suggests that, at least for the sites that we studied, the timing of potential exchange reversals is consistent with reported historical trends.

4.2 Drone and satellite data

Remote sensing data along the study reach of the Brazos River were collected, processed and analyzed with two primary purposes in mind: 1) determining the suitability of currently available remote sensing platforms for directly estimating groundwater-surface water interactions, and whether those estimates could be used to calibrate and parameterize existing groundwater availability models, and; 2) exploring various other ways in which remote sensing products might be used to improve representation of groundwater-surface water interactions. This section details the use of both drone and satellite remote sensing data towards those ends.

Two approaches were employed for direct estimations of groundwater-surface water interactions: thermal signatures and discharge variation. Gaining reaches may display unexpectedly cool water temperatures as plumes of groundwater enter the river. These thermal signals tend to be stronger during periods of lower flows, as higher volumes of water dilute their impact. GSA has demonstrated this using similar drone-mounted thermal imagery in an area with known seepage on the Rio Grande in New Mexico (Figure 4.5). However, this was during a period of very low flow, and it was unclear whether the same methods would be effective on the Brazos River.

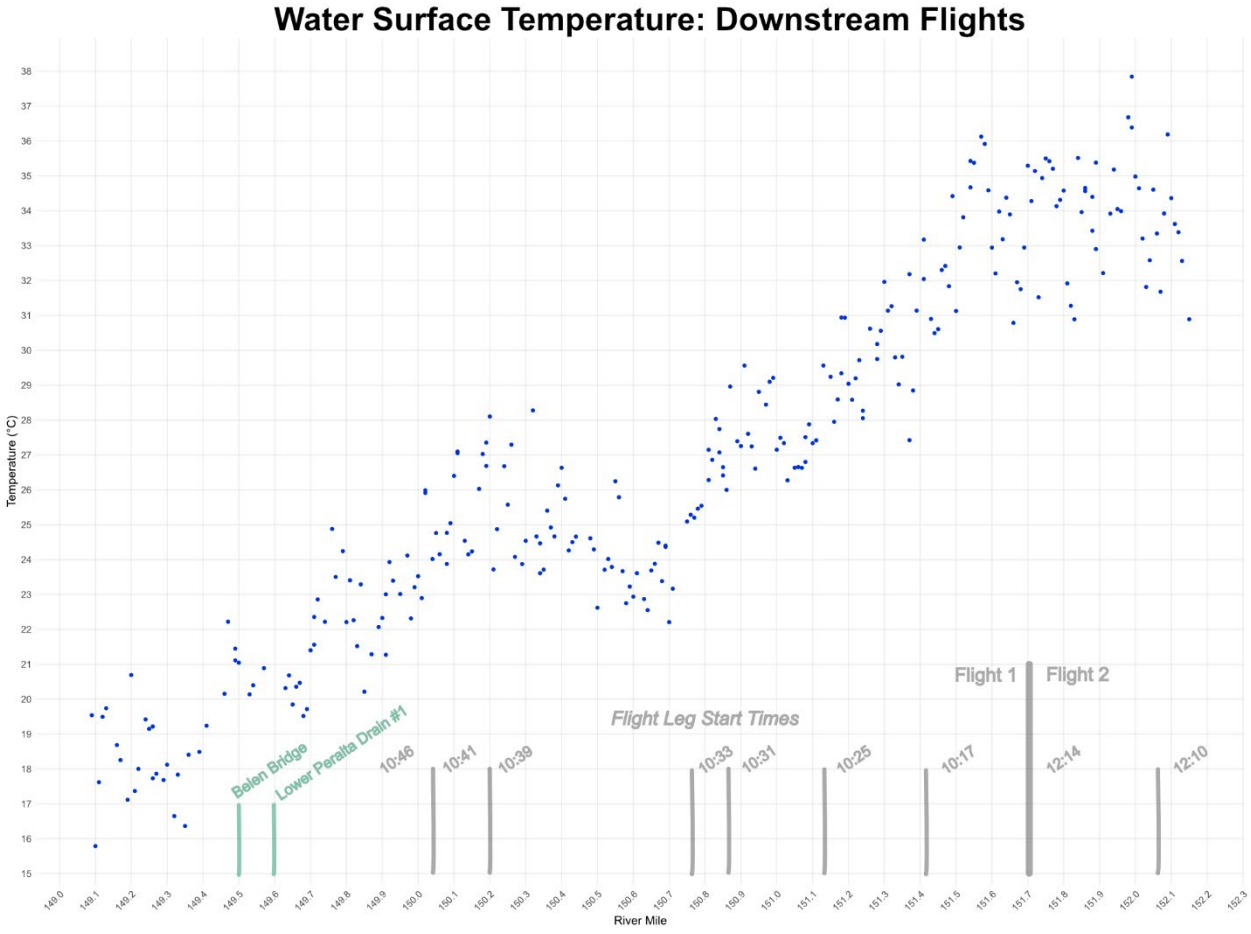

Figure 4.5 **Surface water temperatures drop significantly from upstream (right) to downstream (left) at a location of known seepage.**

Even under ideal conditions, the ability to detect groundwater thermal signatures is dependent on the temperature difference between surface water and groundwater, and can only indicate gaining reaches (there is no groundwater input into losing reaches). These temperature differences are affected by seasonal and even daily surface water temperature variations. Furthermore, methods to quantify the actual volume of water exchange are still being developed (Liu and others, 2016). As such, the bulk of the remote sensing analyses focused on remotely sensed estimations of stream discharge, with the assumption that variations in discharge can be attributed to groundwater interactions once other factors have been controlled for. Current approaches to remote sensing of discharge (Durand and others, 2023) divide the variables for discharge calculation into "time-invariant" and "time variant" variables. Although all variables do change over time, an assumption is made that the time-invariant variables, channel roughness and channel dimension, change relatively slowly compared to the time-variant variables: water elevation/slope and channel width which are then used to calculate cross-sectional area.

The most feasible scenario to approximate continuous remotely sensed discharge is one in which water elevation and extent (i.e. slope and channel width) are regularly measured by satellite (on a daily to weekly basis), while roughness and channel dimensions determined from bathymetry are periodically measured using a combination of field and drone-based methods. Our analysis therefore assesses the accuracy of various satellite sensors which measure water elevations and extents.

Aside from discharge estimations, we also explored other ways in which remote sensing data could be applied to improve how the groundwater availability model represents groundwater-surface water interactions. First, satellite imagery was used to reassign RIV (river) cells in the model to the locations that actually intersect the river. Decades of satellite imagery from Landsat and Sentinel were run through a script developed in Google Earth Engine to classify surface water and aggregate the results, resulting in a dataset that indicates the probability of surface water occurrence. Assigning RIV cells empirically instead of relying on outdated maps helps the groundwater availability model more accurately represent the hydrologic landscape.

Additionally, satellite-based estimations of actual evapotranspiration from OpenET (2024) were used to improve the estimates and the seasonality of agricultural groundwater pumping in the area of interest. When splitting the temporal scale of the groundwater availability model from 12 months to 6 months, these data allow the split to be made based on seasonal patterns of pumping – which is the single most significant driver of groundwater flux. More detail on how these inputs are incorporated into the groundwater availability model is provided in Section 5.2.

4.2.1 Drone Data Collection

In this study, drone data were primarily used for thermal analysis and for extraction of high-resolution water surface extents. Thermal data was used to assess temperature as proxy to determine gaining or losing river sections. Water surface extents from optical imagery were used to assess the accuracy of satellite-derived water surface extent and used for deriving channel geometry in the calculation of conductance.

There are other ways drone data could be potentially incorporated into remote sensing of groundwater-surface water interactions. Under very low flow and/or low-turbidity conditions, drone

imagery can be a method of quickly collecting high-resolution bathymetry data (see Legleiter and Harrison, 2024), which could significantly increase the accuracy of satellite estimations of discharge. However, conditions were not conducive during either of the field visits for mapping of bathymetry, and rarely are on the Brazos River due to typically high turbidity.

4.2.1.1 Drone Data Collection

Drone/unmanned aerial vehicle imagery was acquired on two separate field visits, one during 3/31/2024 – 4/3/2024 and a second during 7/31/2024 – 8/2/2024. On both visits, all three field sites (Vaughn, Gossett, Moore) were flown using two separate drone/sensor packages. At each Acoustic Doppler Current Profiler transect, high resolution imagery was collected concurrently with the field discharge measurements. This imagery was collected with a DJI Phantom 4 Pro V2 quadcopter flown at low elevation, using multiple Post-processing kinematic-enabled ground control points for accurate derivations of topography and water surface extent. Post-processing kinematic (PPK) ground control ties points in the imagery to survey-grade GPS measurements. The high resolution was limited to several hundred meters upstream and downstream of the transect. Multispectral and thermal imagery was also acquired using a fixed-wing Wingtra One Gen II mounted with a Micasense Altum sensor (see Figure 4.6 showing images of the two drones). Because the primary purpose of this imagery was detection of thermal trends, these missions were flown at a higher altitude and covered between 5 and 10 river miles per site. Table 4.1 provides further details on flight parameters. Side overlap refers to the degree to which images from adjacent flight paths overlap each other, while front overlap is the overlap between consecutive images on the same flight path. Higher overlap values tend to make image processing easier and can improve the quality of derived elevation data. However, high side overlap values also increase flight times, and front overlap values are limited by camera shutter speed and the flight speed of the drone:

Table 4.1 Details of drone flights.

	Phantom4 Pro V2	*Wingtra One*
Flight Height Above Ground Level (AGL)	150ft	400ft
Side Overlap	80%	75%
Front Overlap	80%	75%
Corridor Width	N/A	400ft
Imagery Bands	Red, Green, Blue	Red, Green, Blue, Near IR, Red Edge, Thermal
Imagery Coverage	300-500m upstream and downstream of ADCP transects	3-6 miles upstream and downstream of each site
Ground Sample Distance (pixel size)	~ 2cm	~5cm

Figure 4.6 Wingtra fixed wing (left) and DJI quadcopter (right) drones used on this project.

4.2.1.2 Data processing

All drone imagery was processed using Agisoft Metashape photogrammetry software. Photogrammetry is the process of generating a three-dimensional point cloud from a set of overlapping images, which can then be used to create digital elevation models (DEMs), 3D models, and ortho-rectified mosaic imagery. Digital elevation models and orthomosaics were exported for each of the high-resolution Phantom 4 flights, for the purpose of extracting water surface elevations and extents.

Orthomosaics were also generated for the fixed-wing imagery. However, a technical problem with the thermal sensor led to a significant striping effect, where alternating flight paths showed differences of up to 15 degrees Fahrenheit. By comparing the raw temperature values to calibration data collected in the field using a handheld FLIR thermal camera, GSA determined that the striping was a result of outliers in the corner of each drone image. Because Metashape averages all overlapping images at each pixel location, the presence of these erroneous values resulted in alternating lines of overly high and overly low temperatures.

A script was developed by GSA using the ArcPy and NumPy python packages to detect bad data values and average the remainder. With the 75% overlap parameters, each pixel generally had 10-20 overlapping images. After removing outliers most pixels still had 7 or more data points, and any pixels with less than 5 were not used in the analysis. Running this script over the entire flight extent proved too computationally expensive, so analysis of the thermal data was conducted by generating a set of sample points and extracting thermal values at just those locations. All surface temperature analysis presented in the report is based on data that had been processed using these methods.

4.2.2 Satellite data collection

Satellite data were acquired and analyzed to assess their suitability for both estimation of stream discharge and incorporation into the groundwater availability model as discussed above. For discharge estimations, measurements of water surface elevation and water surface extent from several satellite platforms were assessed for accuracy as these are the two key variables that need to be measured continuously. water surface elevation measurements from the SWOT mission were also incorporated into the groundwater availability model sensitivity analysis. Other derived satellite products such as actual evapotranspiration and surface water occurrence were also investigated for potential fine-tuning of groundwater availability model parameters.

4.2.2.1 Data collection

In order to compare various remote sensing platforms, it was first necessary to find dates when multiple image acquisitions overlap. Drone imagery was only collected twice for each field site, and the satellite platforms in question all have different return intervals. Planet Scope imagery is technically collected on a daily basis, however clouds obscured the Brazos River channel on many of those images. This is a limitation with any optical satellite, including Sentinel-2 and Landsat. Depending on the wavelength, synthetic aperture radar sensors are generally not greatly impacted by cloudy conditions and do not require filtering.

A table was created for the period of April – September 2024 with dates of all cloud-free satellite passes over the area of interest, along with dates of drone acquisitions from the field. Table 4.2 summarizes the number of days with usable imagery. Note that SWOT is not affected by clouds, and therefore all SWOT passes were considered "cloud free". Dates when drone and Planet Scope overlapped were used for verifying the use of Planet Scope as a workable ground-truth for other satellites. Dates when Planet Scope overlapped with Sentinel-2/Landsat/SWOT were used to compare water surface elevation and water surface extent measurements from those platforms. Because data were collected at different times of the day, gage data from the US Geological Survey gage at SH21 near Bryan was used to determine the range in discharge during those days (see Table 4.3). For example, differences in water surface extent between Planet Scope and Sentinel-2 imagery from the same day may be attributable to either sensor capabilities or to an actual change in water surface extent between the acquisition times.

Table 4.2 Cloud coverage at the field site.

Satellite	*Cloud Free Days*	*Percent of Total Days (Apr – Sept 2024)*
Sentinel-2	24	14%
Landsat	10	6%
SWOT	17	10%
Planet Scope	58	34%

Table 4.3 **Dates with data overlap. PS = Planet Scope, S-2 = Sentinel-2, LS = Landsat. When only 1 or 2 field sites were cloud-free in the imagery, those sites are indicated.**

Date	*Overlap*	*Discharge Range (cfs)*
4/2/2024	PS, Drone (Gossett)	450
4/5/2024	PS, S-2	280
4/10/2024	PS (Gossett/Moore), S-2	24930
5/10/2024	PS (Gossett/Vaughn), S-2, LS,	2800
5/15/2024	PS(Vaughn), S-2	4300
5/18/2024	PS (Gossett/Vaughn), SWOT, LS	5200
5/29/2024	PS (Vaughn/Moore), SWOT	1600
7/4/2024	PS (Moore), S-2	270
7/9/2024	PS (Moore), S-2	200
7/31/2024	Drone (Gossett); SWOT	100
8/1/2024	PS (Vaughn/Moore), Drone (Moore)	100
8/8/2024	PS, S-2	40
8/21/2024	PS (Vaughn), SWOT	31
9/7/2024	PS, S-2, LS	27

Because Planet Labs requires an expensive subscription to access imagery, individual Planet Scope images were purchased through Skywatch (Skywatch, 2024), a satellite imagery re-seller. As water extents needed to be digitized by hand from the imagery, the imagery was limited to the Brazos River corridor near the three field sites, rather than the entire area of interest. Because commercial satellite imagery is priced by the square kilometer, this also helped to reduce the cost of purchasing imagery. SWOT data was downloaded through Earthdata (National Aeronautics and Space Administration, 2024), an open access data platform managed by the National Aeronautics and Space Administration.

Sentinel and Landsat data were downloaded in two formats: (1) water surface extent where water pixels have already been classified and made available through the National Aeronautics and Space Administration/US Geological Survey, and (2) the original, unclassified imagery. Water surface extent data products are currently only available at a 30-meter resolution, which is the native resolution of Landsat. However, the 10-meter native resolution of Sentinel-2 imagery is significantly higher, so Sentinel-2 water surface extent was downsampled to match the Landsat outputs. These unclassified Sentinel-2 images were also acquired and classified by GSA using a Modified Normalized Difference Water Index threshold to see if the increased resolution had an impact on water surface extent accuracy.

The analysis of evapotranspiration and river extent (water occurrence) required combining many years of satellite data. For these tasks, most of the processing was done through Google Earth Engine, a cloud-based platform where users can access the entire period of record for Landsat and Sentinel imagery). Earth Engine greatly reduces the labor, storage and processing power required to analyze very large geospatial datasets. Details of the processing steps for both Earth Engine and other satellite data are outlined in the following Analytical Methods section.

4.2.2.2 Analytical methods

Water Surface Elevation (WSE)

To assess the accuracy of water surface elevation measurements from SWOT, they were compared to the pressure transducer data collected at the three field sites, along with reported river stage from the two US Geological Survey stream gages present in the area of interest (Brazos River at FM485 near Hearne, and Brazos River at SH21 near Bryan). Although SWOT data has been compared to other satellite measurements of water surface elevation (Normandin and others, 2024), there are no published studies comparing SWOT data to in situ field measurements.

SWOT data is aggregated first to the "node" level, which are points spaced every 200 meters along the river centerlines. The elevation assigned to a node is the average of all nearby pixels classified as surface water. Therefore, when flows are higher and water extents wider, node elevations are based on a larger sample size of pixels. For each pass, every node observation is also assigned a quality indicator, ranging from 0 (highest quality) to 3 (lowest quality). For this analysis, only observations assigned a quality indicator of 0 or 1 were used.

After downloading all SWOT node data for the study period in shapefile format, a python script was used to exact elevation and quality values into tabular format and filter out low quality observations. SWOT elevations are relative to the EGM2008 geoid, while all other measurements used in the study were relative to the NAVD88 datum. The offset in the area of interest ranges from 0.2 to 0.3 meters, and all SWOT elevation data was converted into NAVD88. This dataset was then shared with INTERA for integration into the groundwater availability model sensitivity analysis.

Pressure transducer and gage data were compared with both the elevations from the single closest node to the pressure transducer/gage, as well as the four closest nodes. SWOT nodes are spaced 200 meters apart, so the nodes assessed ranged from approximately 800 meters upstream to 800 meters downstream of the field measurements. Field measurements were made in 15-minute intervals, and the 4 measurements closest in time to the SWOT fly-over were averaged. Exact SWOT fly-over times were extracted from the metadata and converted from UTC to Central time.

The surface water pressure transducers were deployed at field sites for varying lengths of time, although all three were in place from at least 4/1/2024 through 8/18/2024. This period overlapped with 13-15 SWOT passes at each site after bad quality nodes were removed. The two US Geological Survey stream gages had continuous measurements for the entire SWOT period of record (November 2023 through September 2024), with 13 SWOT passes at the Hearne gage and 24 at Bryan.

At each of the five locations (three temporary pressure transducers installed by the team and two US Geological Survey gages), Root Mean Square Error (RMSE) and Bias were calculated, along with standard deviation of the error. RMSE quantifies the average error, while Bias indicates whether SWOT elevations are consistently over- or underestimating the field measurements.

Water Surface Extent (DSWx)

Water surface extents (DSWx) were available from several data sources: field collected drone imagery, high resolution Planet Scope imagery, medium resolution Sentinel-2 and Landsat imagery, and SWOT node data. Unlike water surface elevations where field data was collected continuously, drone imagery of water extents was only collected during the two field visits. Furthermore, satellite

data of the area of interest vary temporally by platform, from near-daily for Planet Scope to every 10-11 days for SWOT. A large percentage of the optical satellite imagery was not usable due to cloud cover. Because of these factors, it was not possible to directly compare field and satellite datasets as in the case of water surface elevation. Instead, the following approach was developed whereby higher resolution data was used to assess the accuracy of lower resolution data.

In practice, this amounted to first using drone imagery to assess Planet Scope, then using Planet Scope imagery to assess Sentinel-2, Landsat, and SWOT. Aside from a single day with both drone and SWOT data, all dates with data overlap involved Planet Scope coinciding with other data sources (Table 4.4). Fortunately, the relatively high spatial resolution of Planet Scope imagery makes it an appropriate basis for cross-comparison.

Water surface extent was compared in two formats: polygons of water extent and length of channel width. For datasets where polygons were available or digitizable, the entire area of surface water was compared. Only channel widths are available from SWOT vector data, so when comparing SWOT to Planet Scope or drone imagery, channel widths were used instead of area. Channel widths were also estimated for Sentinel-2, to more directly compare optical satellite data with SWOT. It should be noted that water surface extent area and channel width are somewhat interchangeable: widths can easily be extracted from a polygon of water extent, and if widths are spaced close together, they begin to approximate the water surface extent area.

Table 4.4 summarizes the various comparisons made between water surface extent datasets, and the number of data points available for comparison.

Table 4.4 Channel geometry estimates by data collection type.

Dataset 1	*Dataset 2*	*Geometry Compared*	*Samples*
Drone	Planet Scope	DSWx polygon	2
Planet Scope	HLS-DSWx	DSWx polygon	20
Planet Scope	Sentinel-2 MNDWI	DSWx polygon	14
Planet Scope	SWOT	Channel Width	4
Planet Scope	Sentinel-2 MNDWI	Channel Width	14
Drone	SWOT	Channel Width	2

Water surface extent was digitized by hand in GIS software for drone imagery and Planet Scope data. The water surface extent for Sentinel-2 and Landsat (HLS-DSWx) already has surface water classified and required no additional processing other than clipping the area to Planet Scope imagery boundaries. Because the HLS-DSWx data products are provided at a 30-meter resolution, 10-meter resolution Sentinel-2 imagery was also classified using the Modified Normalized Difference Water Index spectral-index to see if it offered an improvement over the 30-meter data. Modified Normalized Difference Water Index uses the difference between Green and Short Wave Infra-Red bands to classify water pixels. Pixels with a Modified Normalized Difference Water Index value over a certain threshold were classified as surface water. Water surface extent polygons were generated using both the default threshold of 0, and a manually identified threshold of -0.2.

For SWOT vector data, channel widths are included as an attribute value of each node. No additional processing was required other than filtering out low quality data. As with the water surface elevations, observations with a 2 or 3 quality indicator were excluded. Channel widths for other data sources were extracted from the water surface extent polygons.

To quantify the error when comparing water surface extent polygons, the Intersect over Union (IoU) metric is commonly used (Mukherjee and others, 2024). Intersect refers to the area where the two polygons overlap, while Union refers to the total area of both polygons combined (see Figure 4.7). Dividing Intersect by Union gives a value between 0 and 1, representing the degree to which the two polygons overlap. Intersect over Union is especially useful when the size of the areas being compared vary in each instance.

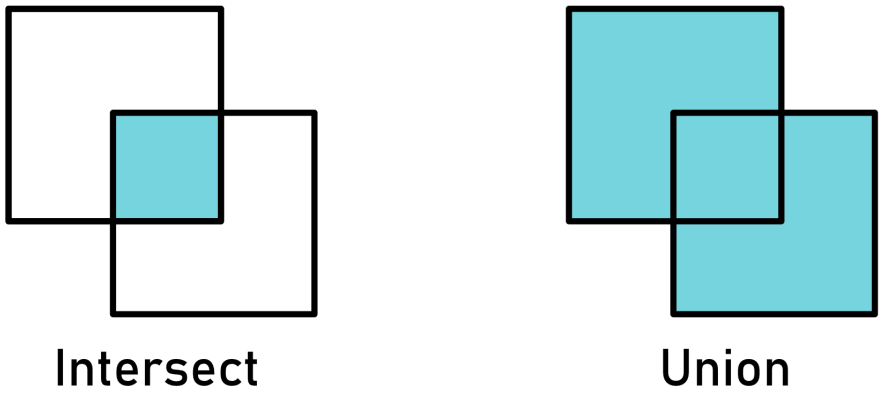

Figure 4.7 Schematic of intersecting and union polygons of the Intersect over Union calculation.

Root mean square error (RMSE), Bias, and standard deviations were generated for channel width comparisons. Average channel width was also compared at each site, as sensors like SWOT rely on spatial averaging to arrive at usable data.

Thermal

Water surface temperature measurements from the drone-mounted thermal sensor were analyzed to find potential gaining reaches. The river centerlines at all three sites were first digitized as line features, based on the visible spectrum orthomosaics from those same flights. River Mile points were then generated at every hundredth of a mile along the centerlines. Temperature values were extracted at each of these points for both spring and summer field visits, then plotted longitudinally from upstream to downstream.

Because the typical increase and accumulation of solar radiation is a confounding factor for surface temperatures, a table was created of flight times and integrated into the temperature plots. The effect of time is especially important for longer study reaches like Gossett, which involved 5+ flights over approximately 7 hours.

Ultimately, the assessment of potential gaining reaches was qualitative, due to several subjective factors, including the difficulty in controlling the effect of time and high levels of noise in the data. Regions of lower surface temperatures were seen as more likely to be representative of seepage if those patterns were present during both field visits, and if temperatures decreased later in the day.

Note that the indicated reaches are *potentially* gaining, and that the data collected were insufficient to make stronger claims or quantify flux.

OpenET

To estimate quarterly groundwater pumping demand volume factors, the eeMETRIC, Google Earth Engine implementation of the Mapping Evapotranspiration at high Resolution with Internalized Calibration algorithm from OpenET, was used to disaggregate annual pumping estimates. This approach calculates the difference between the estimated actual evapotranspiration (AET) and effective precipitation (P_{eff}), where the difference is satisfied by groundwater pumping for irrigation. Effective precipitation is the amount of precipitation that infiltrates into the soil and is available to plants. The OpenET eeMETRIC algorithm relies on Landsat satellite imagery to provide monthly actual evapotranspiration estimates at a 30-by-30-meter resolution. Although this calculation was performed at a monthly time step, eeMETRIC data and interpolation techniques can support daily estimates, which are expected to improve over time as additional remote sensing information becomes available.

Precipitation data were derived from the 4-by-4-kilometer gridMET product; however, finer spatial resolution datasets (e.g., PRISM at 800-by-800 meters and NEXRAD at 1-by-1 kilometer) can also be incorporated to enhance accuracy. The actual evapotranspiration calculations focused on agricultural pixels identified annually through the USDA cropland dataset. For each month, the average actual evapotranspiration (AE) and precipitation over the area of interest were estimated in inches. As a simplified estimate, effective precipitation was assumed to be 80% of total precipitation following the approach of Morrison (2023) based on observations in Utah, instead of conducting a more detailed soil water balance approach. This assumption may be refined based on local irrigation data and efficiency estimates.

In months where actual evapotranspiration was greater than effective precipitation the irrigation deficit was then calculated as the difference between actual evapotranspiration and P_{eff}. When monthly effective precipitation exceeded actual evapotranspiration, the irrigation deficit was assigned a value of zero. Currently, OpenET data are available from 2014 onward, gridMET data since 1980, and cropland data since 2008. Thus, the analyses here cover the period from 2014 to the present, as summarized in Figure 4.8 which shows the monthly estimated actual evapotranspiration and effective precipitation for the area of interest and the resulting estimated irrigation deficit for each month.

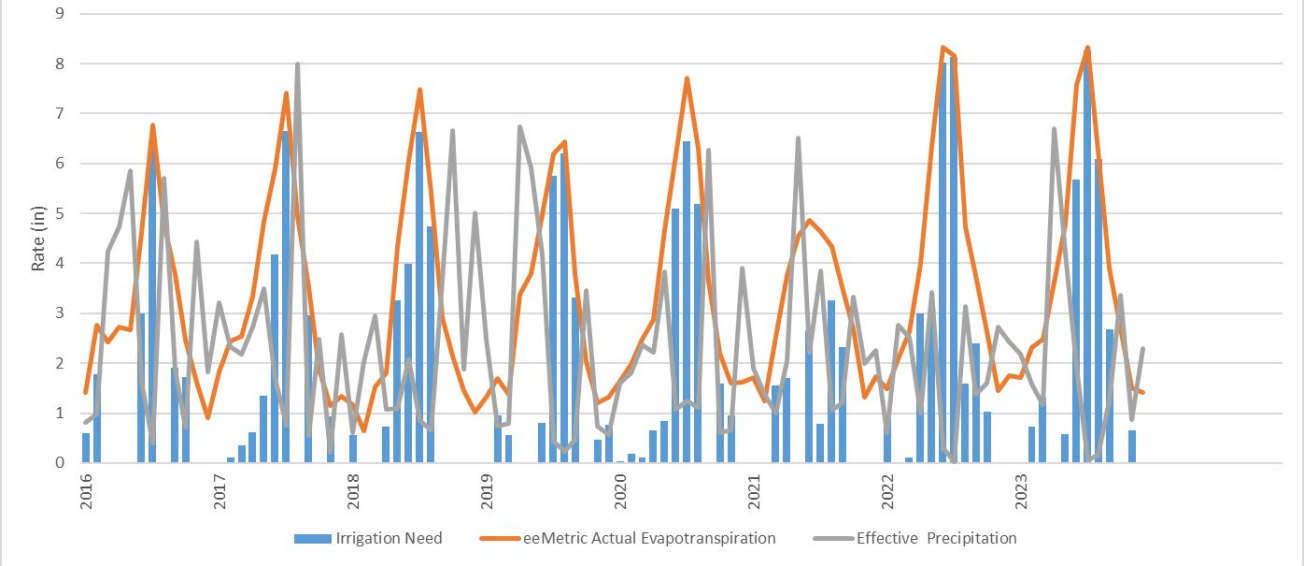

Figure 4.8 **Summary of OpenET and gridMET data used for estimating seasonal pumping factors in the area of interest.**

River Location/Water Occurrence

RIV cells in the groundwater availability model are supposed to be assigned according to intersection with the Brazos River channel. However, due to either inaccurate or out-of-date maps, they do not always correspond to the actual location of the river. Publicly available remote sensing imagery from Sentinel-2 and Landsat provide a rapid means of aligning RIV cells with areas of consistent surface water. Water occurrence maps were generated from both satellite datasets in order to demonstrate a possible workflow to improve the groundwater availability model.

Within Google Earth Engine, a dataset of available imagery was filtered to the Brazos River area of interest. Sentinel-2 imagery is only consistently available from January 2017. Landsat data was used from 1985 onwards, using imagery from both Landsat 5 and Landsat 8 satellites. Apart from the time period, the workflow was the same for both Sentinel-2 and Landsat images. Cloudy pixels were masked out, then a water mask generated for each individual image using the Modified Normalized Difference Water Index. All pixels with a Modified Normalized Difference Water Index over -0.2 were classified as water, as this threshold was found to work consistently in the region. The entire "stack" of water mask images was added together, creating a single image where the value of each pixel corresponds to the total number of times there was surface water present at the pixel. In the case of Sentinel-2 this number ranged from 0 (water never present) to 400 (water almost always present). For Landsat the values ranged from 0 to almost 900, due to the longer time period. Lastly, each pixel was divided by the total number of images, to give a final value between 0 and 100% for the percentage of time surface water is present.

In a number of locations, RIV cell assignment was found to deviate from locations with a high percentage of water occurrence. Figure 4.9 shows one such location, comparing RIV cells with the Sentinel-2 water occurrence data.

Figure 4.9 **RIV cells with the Sentinel-2 water occurrence data overlain.**

5. Results

The analysis of the field data, assessment of the remote sensing data, and how they are used to refine the central portion of the Carrizo-Wilcox Aquifer groundwater availability model are presented in this Chapter.

5.1 Hydraulic characteristics of the study sites

Although this study focuses generally on the Brazos River Alluvium Aquifer our site-specific work is on the fluvial alluvium part of the Brazos River Alluvium Aquifer which generally underlies the Brazos River and its current floodplain. As with any alluvial deposit, the Brazos River Alluvium Aquifer is generally heterogenous with fine-coarse deposits of sand, gravel, silt, and clay (Shah and Houston, 2007). However, it has been reported that its hydraulic characteristics are more leaning towards typically sandy-gravelly systems. Electrical resistivity surveys conducted during the field campaign show an electrical resistivity range of 7-30 Ωmeters within the depth of investigation similar to shales-sandstone considering the water-saturated fluvial depositional setting of the study site. Electrical resistivity inversion results also show a consistent boundary between lower to higher resistivity zones between 2 to 25 feet relative to the river-bed surface. These values are well within the reported thickness (Cronin and Wilson, 1967) of the Brazos River Alluvium Aquifer. The electrical resistivity transitional zone appears to be shallower in the Vaughn site suggesting thinner alluvium sediment packages. This is expected as the surveyed section at Vaugn is near the outcrop of the Carrizo-Wilcox Aquifer. See Figures 5.1 through 5.3.

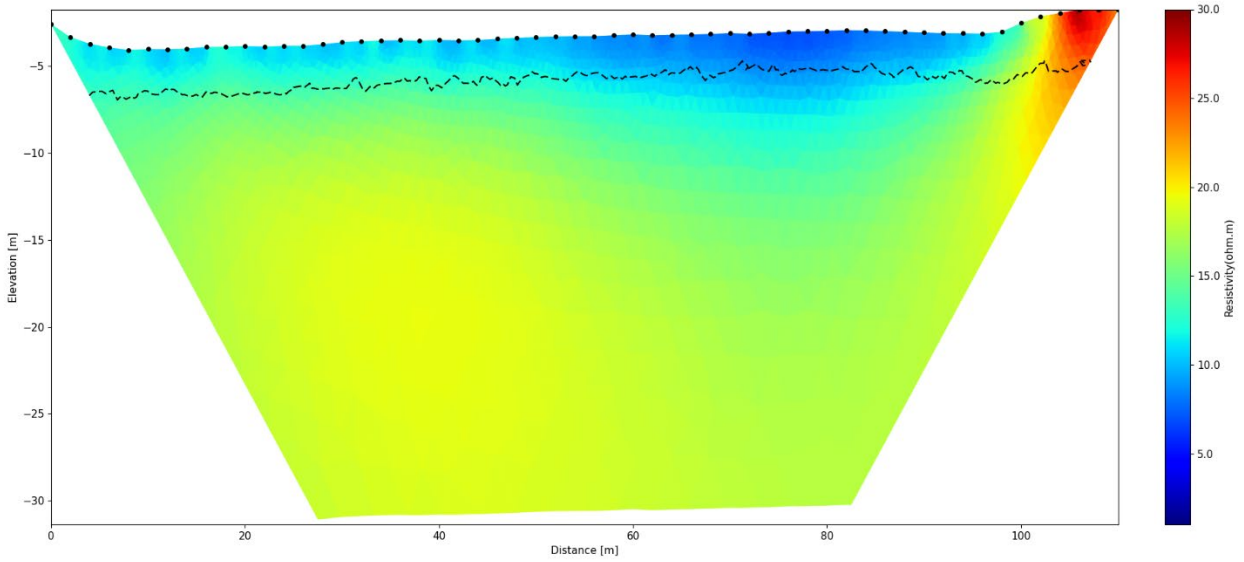

Figure 5.1 Inverted electrical resistivity profile for Gossett1 Reach showing depth of investigation.

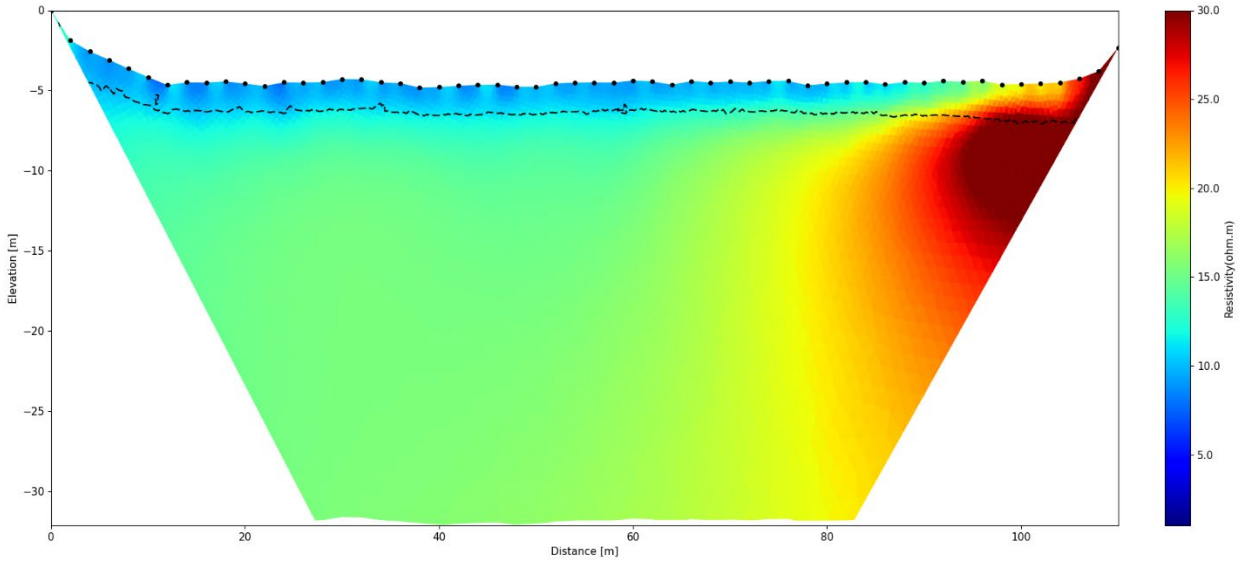

Figure 5.2 **Inverted electrical resistivity profile between Gossett1 and Gossett2 Reach showing depth of investigation (DOI). The ER section is located along GSST1 gage2.**

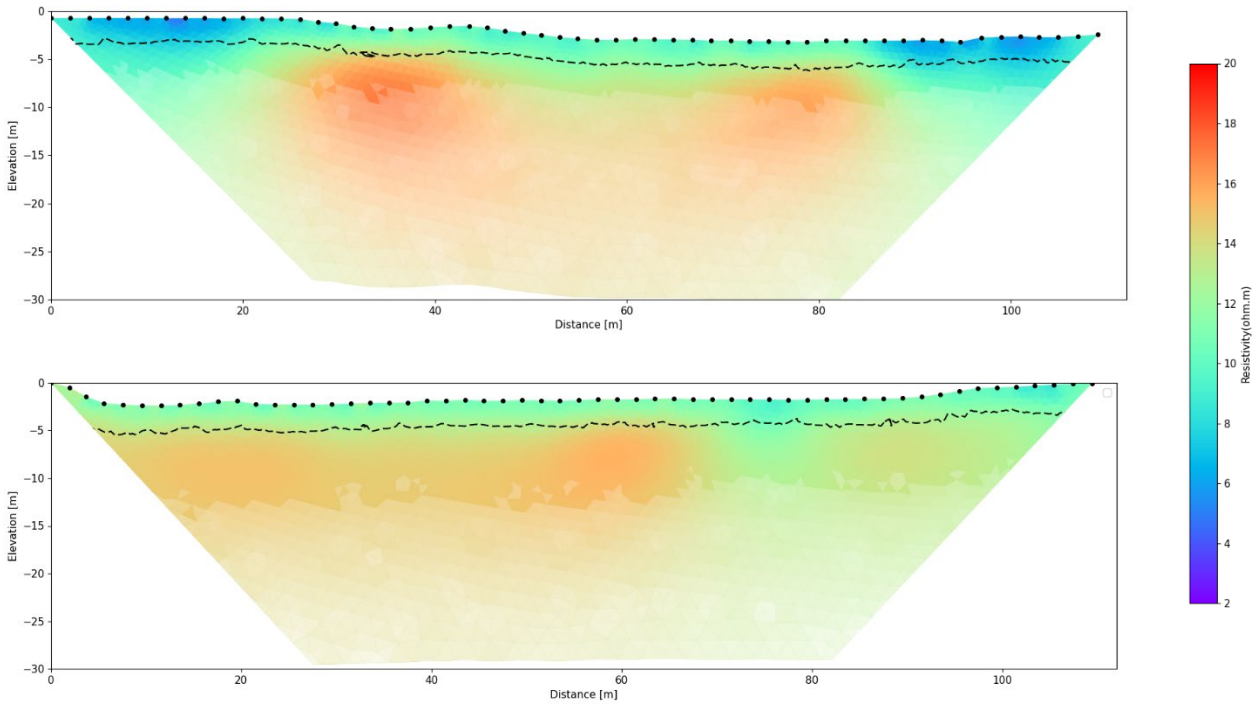

Figure 5.3 **Inverted electrical resistivity profiles for a) Vaughn and b) Moore Reach showing approximate depths of investigation (DOI).**

The well hydraulic conductivities calculated from the specific capacities are well within the range of estimates from other studies (O'Rourke, 2006; Shah and others, 2007) for the Brazos River Alluvium Aquifer (see Table 5.1). Permeabilities calculated from wells within the aquifer also showed a similar range, from 70 to 1600 feet/day. Other studies report ranges of less than a foot to 2,500 feet/day from samples using laboratory techniques (O'Rourke, 2006) and 179 to 447 feet/day from the analysis of groundwater well yields (Shah and others, 2007) similar to this work. Estimated hydraulic conductivities are summarized in the table below. Although the hydraulic conductivities calculated for the sites are well within the expected range, we recognize that there are uncertainties in these permeability estimates as these were taken from reported values with no quality assurance on the method of collection.

Table 5.1 **Estimated hydraulic conductivities of the Brazos River Alluvium from wells used in the study. Units are in gallons per minute (gpm), feet (ft), meters (m) and days (d).**

	Pumping Rate [gpm]	*Drawdown [ft]*	*DTW at pumping [ft]*	*Saturated Thickness [ft]*	*Specific Capacity [gpm/ft]*	*Hydraulic Conductivity [ft/d]*	*Hydraulic Conductivity [m/d]*
Vaughn*	600	20	17	44	30	137	42
Gossett1*	800	3	57	20	267	2674	815
Gossett2	75	11	37	10	7	137	41
Moore	800	5	50	16	160	2005	611

* Nearby well

5.2 Gain-loss patterns in the Brazos River

5.2.1 Gain-loss by site

The Gossett reaches 1 and 2, track changes in head and stage more closely compared to the Vaughn and Moore reaches water levels (see Figure 5.4). This suggests stronger connectivity between surface and groundwater (stronger groundwater-surface water interactions) at the Gossett reaches relative to the Moore and Vaughn sites. Groundwater is lower at the Vaughn reach suggesting a losing reach whereas it is more dynamic at the Gossett and Moore reaches. The estimated groundwater flux losses and gains are summarized in Table 5.2. The higher fluxes in Gossett1 and Moore sites are likely associated with higher estimated permeabilities compared to the Gossett2 and Vaughn sites.

The lower permeability at the Vaughn site is evident from the relatively large difference between groundwater level and stage despite the Vaughn well site being adjacent to the Brazos River. Despite the consistent extraction of groundwater, shown as consistent daily groundwater level fluctuations in the groundwater head, the drawdown does not appear to be significant suggesting a good connectivity to a replenishing groundwater source, which is likely the Brazos River. Hence, the Vaughn site can be considered a consistently pumped area with lower permeability (relative to other Brazos River Alluvium Aquifer sites) but well connected to the Brazos River.

The contrast in flux rates between Gossett1 and Gosset2 despite being closer together speaks of the heterogeneity in the hydraulic characteristic of the Brazos River Alluvium Aquifer. Although Gossett1 yielded a higher hydraulic conductivity relative to Gossett2, groundwater levels track the

fluctuations in the Brazos River stage showing as much as 50% of the amplitude of fluctuation of the change in river stage. The amplitude of fluctuations between the sites is also very similar despite Gossett2 having a lower permeability. This suggests robust connectivity between the Brazos River Alluvium Aquifer and the Brazos River along the Gossett reaches. The numbers presented in Table 5.2 assume a 60-mile stretch (our study reach) of river where discharge is occurring with an effective river depth of 10 feet (net depth for both banks), thus the contributing area to groundwater-surface water exchange is 73 acres.

The Moore site yielded highest fluxes owing to the higher estimated permeability and potentially strong connectivity to the Brazos River. Although the tracking of the river stage by the groundwater head is more muted on this site compared to the Gossett reaches, the response of the groundwater head to the net amplitude change is also close to 50%. Hence, the Moore site represents a river section with high permeability and connectivity to the Brazos River.

Table 5.2 **Summary of groundwater-surface water exchange in the different study reaches. Units are in feet per day (ft/d) specific discharge and acre-feet per year (acre-ft/yr), assuming 73 acres of discharge area.**

	Vaughn [ft/d]	*Gossett1 [ft/d]*	*Gossett2 [ft/d]*	*Moore [ft/d]*	*Average [acre-ft/yr]*
GW Recharge					
Max	1.8	67.1	8.7	93.4	1,138,830
Median	0.8	9.7	4.2	25.2	266,161
Min	0.2	0.001	0.001	0.011	1,157
Mean	0.8	16.8	4.2	33.4	367,913
Std	0.3	19.4	2.8	24.3	311,770
GW Discharge					
Max		15.3	2.4	17.7	315,104
Median		1.2	1.2	9.9	109,363
Min		0.004	0.002	0.018	215
Mean		3.3	1.1	9.2	120,958
Std		4.1	0.5	4.5	81,196

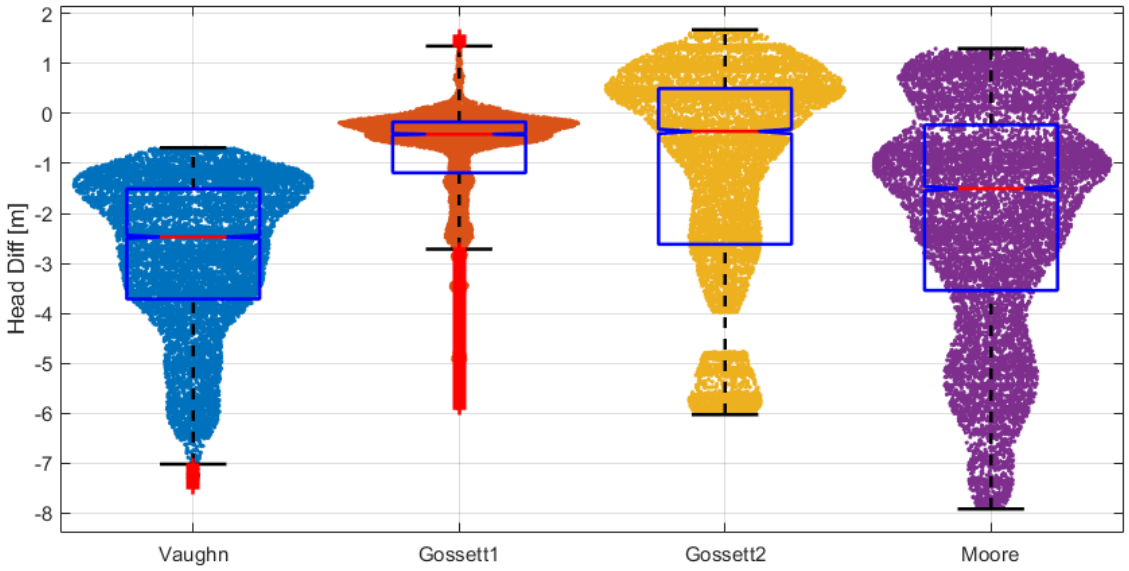

Figure 5.4 **Box and whisker plots of head differences between groundwater and river stage for the selected study reaches. Background scatter/swarm chart shows the distribution of measurements for each site.**

Site-by-site comparison of fluxes and groundwater levels suggests a high variability of fluxes across sites and its dynamic nature (discussed in the next section). This variability is expected considering the heterogeneous nature of the Brazos River Alluvium Aquifer. Assuming a 60-mile stretch of river with a conservative effective river depth of 10 feet the contributing area to groundwater-surface water exchange is 73 acres which gives an average recharge (loss) of 368,000 acre-feet/year and 121,000 acre-feet/year discharge (gain) using the near-instantaneous values as summarized in Table 5.3. These values are in the same order of magnitude as the gain-loss averages, based on the analysis of US Geological Survey discharge data which are roughly 258,000 and 601,000 acre-feet/year, loss and gain respectively. This similarity in magnitude speaks of the importance of accounting for groundwater-surface water exchange in groundwater models that include the Brazos Alluvium.

Table 5.3 **Estimated gains and losses between Highbank + Cameron US Geological Survey gage and Bryan gage. Units are in acre-feet per day (acre-ft/d) and acre-feet per year (acre-ft/yr).**

	Losses [acre-ft/d]	*Gains [acre-ft/d]*	*Annual Losses [acre-ft/yr]*	*Annual Gains [acre-ft/yr]*
Max	-11,569	37,949	-4,222,685	13,851,385
Median	-305	492	-111,387	179,544
Min	-0.09	1.42	-31	517
Mean	-708	1,649	-258,401	601,885
Std	1,314	3,358	479,501	1,225,707

5.2.2 Temporal gain-loss patterns

Time series plots of groundwater heads and river stage (Figure 5.5) generally follow similar trends in all sites. Groundwater recharge into the aquifer based on head difference (losing stream conditions) is generally dominant during flood pulses whereas gaining conditions (groundwater discharge) are more dominant between pulses and at lower river stages at the Gossett and Moore sites. The river stage is always at a higher elevation at the Vaugn site indicating a losing condition throughout the time series. Plots of the difference between the groundwater head and river stage are generally in the negative which indicates potentially losing conditions within the deployment period (Figure 5.5). A report by Turco and others (2007) suggests that the Brazos River is predominantly gaining especially in the section where it crosses outcrops of the Carrizo-Wilcox, Queen City, Sparta, and Yegua-Jackson aquifers which is in contrast with our head difference measurements. The previous report used data from 1966-2005, hence two decades have passed since the analysis was done. One possible reason for this contrast is that groundwater levels may have substantially changed. Alternatively, it is also possible that conditions within our period of study is just predominated by the high river stage, which drove the gradient more towards the Brazos River alluvium (losing). The gaining events observed from Gossett and Moore sites after flood pulses are likely associated with the slow decline of groundwater levels after strong recharge (strong losing) conditions.

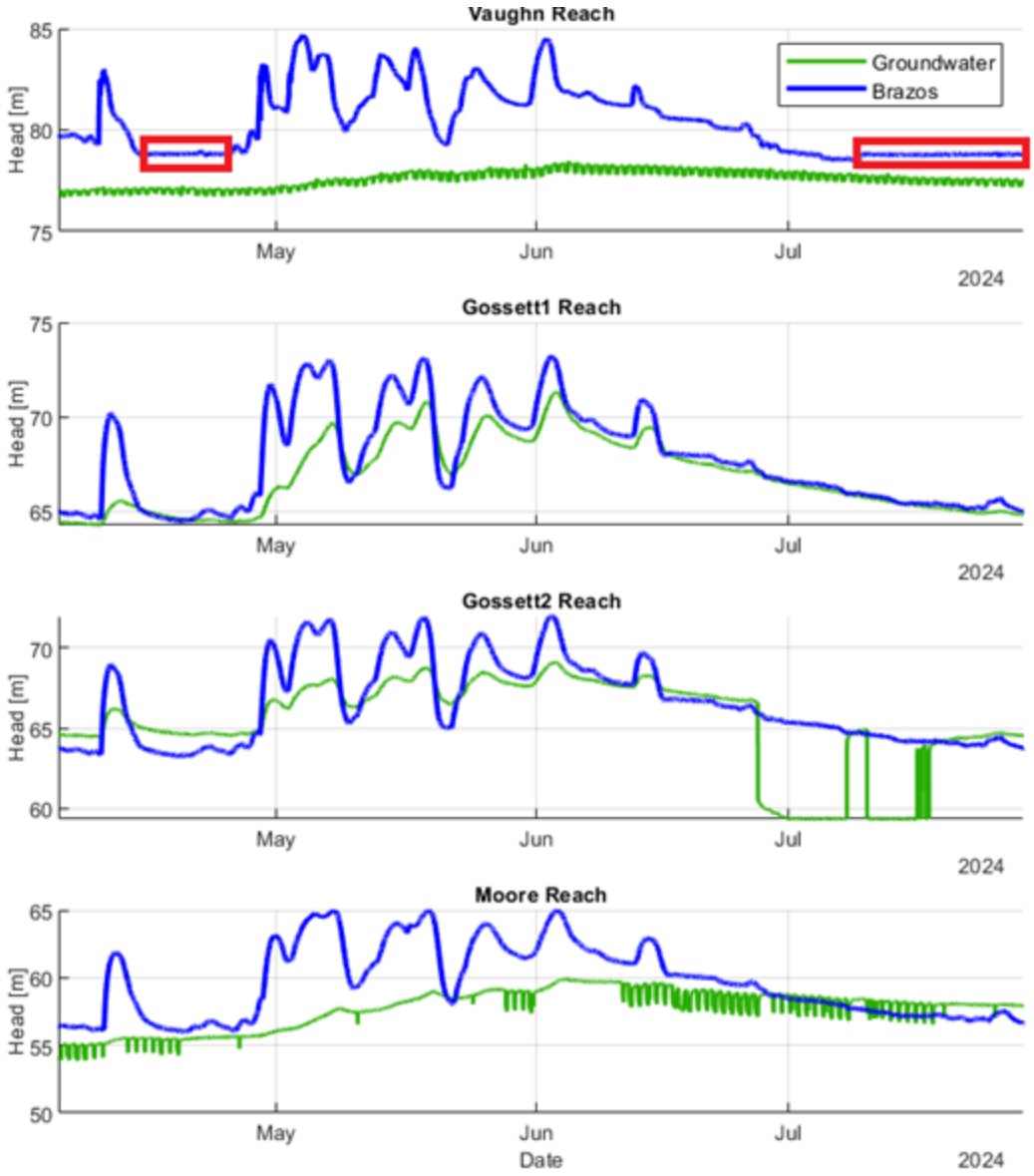

Figure 5.5 **Groundwater heads and river stage in winter-summer 2024 at selected study reaches along the Brazos River. Red boxes in Vaughn plot indicate period where the pressure transducer may have been in a pond due to sediments impounding the instrumented section of the bank.**

Monthly averaged depth to water trend of groundwater wells from the Brazos Valley Groundwater Conservation District database generally fall between 20 to 40 feet (see Figure 5.6). This is about the range of the water level change in the Brazos River relative to the floodplain which could indicate connectivity between the wells tapping the Brazos River Alluvium Aquifer and the Brazos River. Some high drawdown wells show a lowering of water levels between 60 to 120 feet below the ground surface. These high drawdown wells indicate either a high pumping rate or low connectivity to the Brazos River. Higher drawdown in these wells appears to increase from June to October, or the late 2nd quarter to the 3rd quarter of the year. This suggests potentially higher pumping rates likely for irrigation during this period associated with lower rainfall during this period (Figure 5.6).

Majority of the drawdowns do not appear to behave similarly to the wells with higher drawdowns which suggests a good connectivity with the Brazos River.

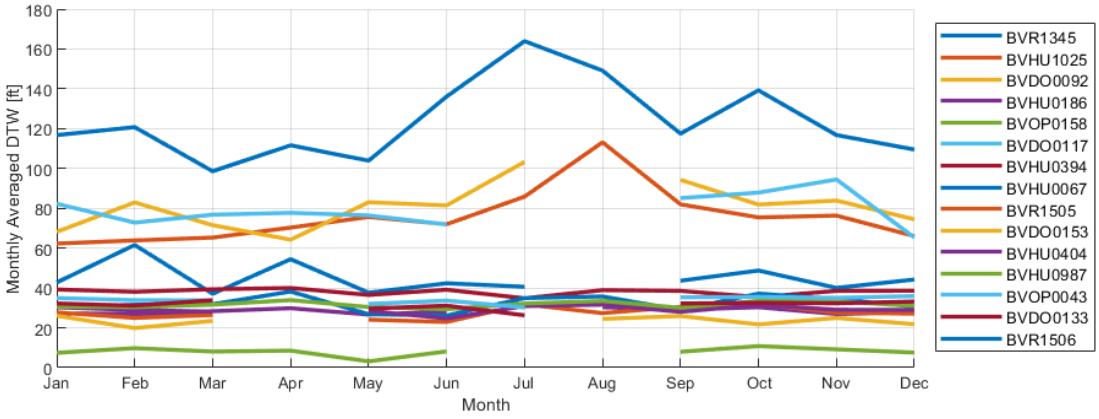

Figure 5.6 **Monthly averaged depth to water from the Brazos Valley Groundwater Conservation District (BVGCD) database.**

River discharge measurements along sections are plotted in Figure 5.7. Discharge was much higher in April 2024 during the full deployment of the pressure transducers - between 4,000 and 6,000 cfs – whereas it was around 600-1,600 cfs in August 2023 (see Figure 4.1 from the previous chapter). These measurements are close to the reported discharges in US Geological Survey gages between Highbank and Bryan which lends confidence to reported US Geological Survey discharge estimates. Because of limitations on the number of collected discharge measurements in the upstream and downstream end of the study reaches, as well as the measurement uncertainties, we are unable to estimate upstream and downstream flow differences. However, we can use the US Geological Survey streamgages to get an overall value for the 60-mile stretch between Highbank and Bryan gage. On average, it takes a day for a flow pulse to travel from the Highbank gage location to the Bryan gage location, hence time averaging the data using a weekly interval can spread this lag and allow us to do weekly comparisons. We consider the flows coming from the Little River, a tributary of the Brazos River, to be represented by the Cameron gage. Input flows towards the Bryan Gage are assumed to be the sum of the Highbank flows and the Little River, hence, the difference between the Bryan Gage flows and the sum of the upstream sites represents gains or losses from overland and small tributary flows or groundwater inputs or outputs. To tease out average temporal trends we grouped the weekly differences into monthly bins.

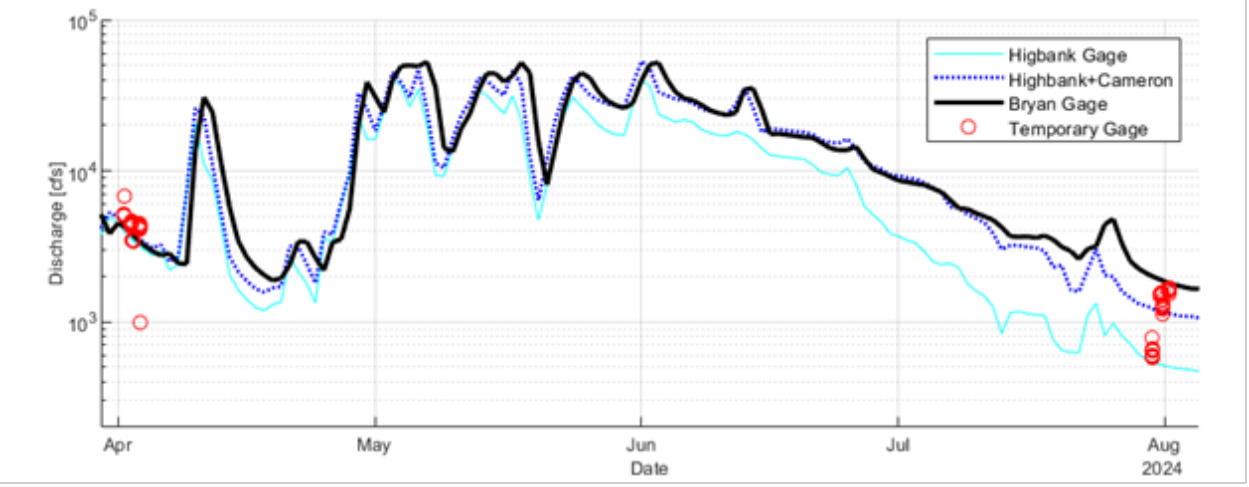

Figure 5.7 **River discharge field measurements along sections of selected reach (red dots).**

The monthly trend in the weekly mean discharge difference shows a dip in July through October. This period coincides with the 3rd quarter (Q3) and early 4th quarter (Q4) of the year (Table 5.4). Boxplots of this monthly time series also indicate well-constrained values which are predominantly in periods where river discharge (Bryan gage) is low. The generally low discharge caused by relatively low rainfall in this period is likely driving smaller differences in flows. This period also presents a time where potential gains or losses due to groundwater inputs or outputs may represent a significant part of the discharge considering the potentially diffused nature of groundwater fluxes in alluvium aquifers. Table 5.4 shows the summary statistics for 3rd quarter weekly discharge differences.

Table 5.4 **Summary statistics for the 3rd Quarter of the weekly discharge difference between Bryan and Highbank+Cameron gage. Units are in acre-feet per day (acre-ft/d) and acre-feet per year (acre-ft/yr).**

	Losses [acre-ft/d]	*Gains [acre-ft/d]*	*Losses [acre-ft/yr]*	*Gains [acre-ft/yr]*
Max	-8,033	21,206	-2,931,972	7,740,190
Median	-232	328	-84,771	119,879
Min	-0.09	3.68	-31	1,345
Mean	-386	894	-140,747	326,491
Std	767	1,882	279,864	686,967

Mean gains potentially coming from groundwater discharge based on 3rd quarter values is approximately 326,000 acre-feet/year and mean potential losses due to groundwater recharge assuming 3rd quarter values represent mainly groundwater exchange is 141,000 acre-feet/year. Ewing and Jigmond (2016) reported losses by perennial streams, mainly to the Brazos River, around 68,000 acre-feet/year at the end of their 2012 simulation for river leakage which is 2 times lower than the calculated 3rd quarter value. This US Geological Survey differential gaging loss value is also just slightly more than half of the estimate using Darcy's law (Table 5.2). The gain value at 3rd quarter is 2.5 and 3.5 times higher that our Dracy's law estimate, and groundwater availability model results

from Ewing and Jigmond (2016). Considering differences in approach and the inherent uncertainties in the methods used to estimate groundwater-surface water exchange, these values are relatively close. Our estimates of the net fluxes losses on the Brazos River segments of study are generally much higher than previously estimated from groundwater availability models but of the same order of magnitude. Our study results indicate predominantly losing conditions whereas gains in the Brazos River primarily occur during low water stage, especially when preceded by flood pulses.

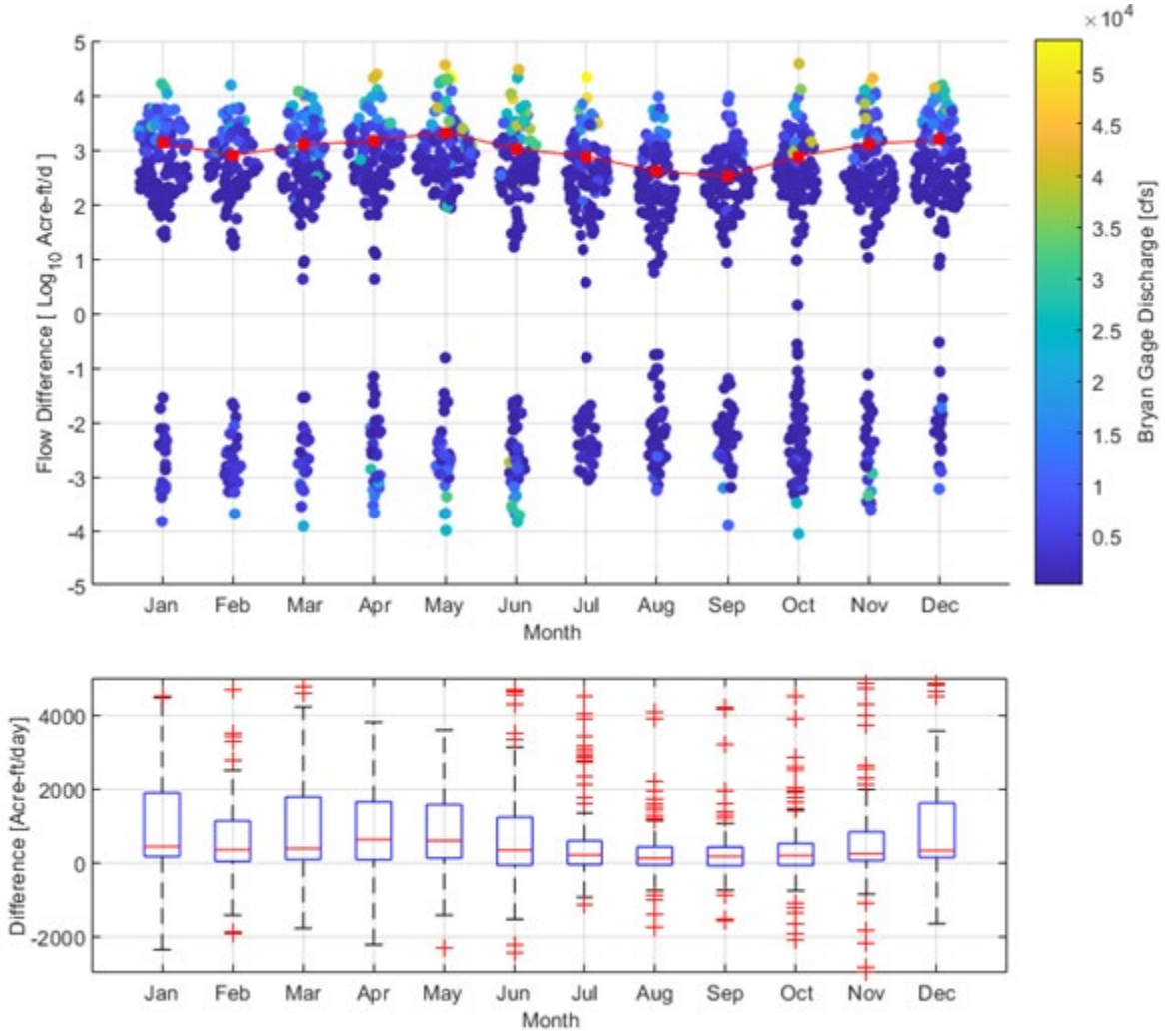

Figure 5.8 **Weekly averaged flow differences grouped by month in the last 3 decades between Highbank + Cameron and the Bryan US Geological Survey gage. Top panel: colored circles indicate the weekly differences colored by the discharge value at the Bryan Gage, red square represents the monthly mean. Bottom panel: red line and red plus symbols indicate the median and outliers respectively.**

5.3 Remote sensing analysis

Satellite remote sensing of river discharge involves the measurement of water surface extents and elevations. Extents from various platforms and classification techniques along with elevations from SWOT were compared to field or other ground truth data to assess their accuracy. Although the

measurements obtained from newer satellite-based sensors represent a significant advancement over previously available data, the level of error is likely still too high to estimate discharge accurately enough to quantify groundwater-surface water interactions. However, these discharge estimates could be adequate for other water management purposes, especially if constrained by existing stream gages and calibrated by additional field measurements. Much of the error was found to be systemic, rather than random. Because of this, there is a possibility to improve extent and elevation measurements and develop more accurate local models of discharge using the same data sources.

5.3.1 Measurement of discharge parameters

5.3.1.1 Surface Water Extent

Water surface extents from Sentinel-2 and Landsat were compared against Planet Scope imagery, using Intersection over Union values. Intersection over Union describes the extent to which two spatial datasets overlap, and is described in more detail in Chapter 4. Three sets of extracted water surface extent polygons were assessed:

HLS-DSWx – The Harmonized Landsat Sentinel water surface extent products are produced by NASA-JPL, and add Sentinel-2 imagery to the Landsat water surface extent data products which have been available for many years. They are provided at a 30-meter resolution, at a temporal resolution of <5 days. The exact temporal resolution varies due to differences in Landsat and Sentinel orbit cycles. Water pixels are classified using a complex algorithm that incorporates several visible and multispectral bands, land cover data, and elevation models.

S-2 MNDWI – Water pixels were also classified for Sentinel-2 imagery using the Modified Normalized Difference Water Index, which compares the difference between the Green and Short Range Infra-Red (SWIR) bands. This approach is less sophisticated than that of the HLS-DSWx products but is output at a higher resolution (10-meter vs 30-meter). For the initial test, the default threshold of 0 was used – where pixels with Modified Normalized Difference Water Index values over 0 are classified as water.

S-2 MNDWI Adjusted – Modified Normalized Difference Water Index thresholds were also manually adjusted to find a value that worked better for imagery from this region. The results presented here used a threshold value of -0.2, where any pixels above this value were classed as water. This approach is less generalizable to other regions but may provide better results at a local level.

The following table (Table 5.5) presents Intersect over Union values for the three approaches. For each date, water surface extent for each site is presented individually.

Table 5.5 Intersect over Union value for each of three approaches.

Date	*Site*	*Satellite*	*IoU HLS-DSWx*	*IoU S-2 MNDWI*	*IoU S-2 MNDWI Adjusted*
4/5/2024	Vaughn	Sentinel-2	76.2%	79%	83%
4/5/2024	Gossett	Sentinel-2	77.1%	80%	83%
4/5/2024	Moore	Sentinel-2	77.4%	77%	83%
4/10/2024	Gossett	Sentinel-2	80.1%	86%	88%
4/10/2024	Moore	Sentinel-2	73.9%	83%	87%
5/10/2024	Gossett	Sentinel-2	80.8%	83%	86%
5/10/2024	Vaughn	Sentinel-2	67.1%	85%	88%
5/15/2024	Vaughn	Sentinel-2	80.7%		
5/18/2024	Vaughn	Landsat	78.0%		
5/18/2024	Gossett	Landsat	82.1%		
7/9/2024	Moore	Sentinel-2	78.3%	78%	83%
8/8/2024	Vaughn	Sentinel-2	71.0%	57%	70%
8/8/2024	Gossett	Sentinel-2	70.6%	67%	76%
8/8/2024	Moore	Sentinel-2	68.6%	63%	73%
9/7/2024	Vaughn	Sentinel-2	69.7%	59%	71%
9/7/2024	Gossett	Sentinel-2	68.6%	65%	75%
9/7/2024	Moore	Sentinel-2	71.2%	64%	75%
9/7/2024	Vaughn	Landsat	67.7%		
9/7/2024	Gossett	Landsat	70.3%		
9/7/2024	Moore	Landsat	71.1%		
Vaughn Average			72.9%	70%	78%
Gossett Average			66.2%	76%	82%
Moore Average			73.4%	73%	80%
Total Average			74.0%	73%	80%

The Adjusted Modified Normalized Difference Water Index extents performed better than the other two in almost every case. The unadjusted Modified Normalized Difference Water Index actually performed slightly worse than the coarser resolution HLS-DSWx, although it did significantly better at the Gossett site.

In order to better understand the nature of the error, Omission and Commission Error metrics were also calculated (see Table 5.6). Omission Error (OE) indicates how much of the control dataset (here the digitized Planet Scope extents) was "missed" by the classification and incorrectly classified as not water. It is calculated by dividing the Intersection area of the two datasets by the total area of the Planet Scope dataset. Commission Error (CE) refers to how much area *outside* the Planet Scope extents was incorrectly identified as water by the classification and is calculated by dividing the intersection area by the classified extent.

Table 5.6 Omission and Commission errors.

Method	*Omission Error*	*Commission Error*
HLS-DSWx	0.12	0.20
S-2 MNDWI	0.25	0.03
S-2 MNDWI Adjusted	0.15	0.07

The HLS-DSWx product has higher Commission Error than Omission Error, meaning that it tended to overestimate the water extent by classifying areas outside the channel as surface water. The unadjusted Modified Normalized Difference Water Index had much higher Omission Error than Commission Error, meaning that it rarely classified land as water, but was overly conservative in identifying surface water that was actually present. As would be expected, the lower threshold used for the Adjusted Modified Normalized Difference Water Index reduced the Omission Error. It is still somewhat high, indicating that an even lower threshold may have performed even better.

Intersect over Union values for all three methods were also compared to reported discharge from the Bryan US Geological Survey Gage at SH21. For all three methods, higher accuracy was correlated with higher flows. This is, unsurprisingly, because when the channel is wider misclassifications of pixels around the edges of banks, islands or point bars have less of an impact on the total error. The predominance of edge errors is another marker for the importance of spatial resolution in measuring water extent (see Table 5.7).

Table 5.7 Mean cubic feet per second (CFS) correlation for Intersect over Union values.

Method	*Mean CFS Correlation*
HLS-DSWx	0.63
S-2 MNDWI	0.81
S-2 MNDWI Adjusted	0.83

Lastly, Root Mean Square Error and Bias were compared using the total water extent area. Unlike Intersection and Union, these metrics do not consider the extents' actual geospatial position – only the area – and so are less useful when taken on their own. However, they do provide additional insight in combination with the Intersect over Union analysis. For instance, the HLS-DSWx has a much lower Root Mean Square Error than S-2 Modified Normalized Difference Water Index, despite them having similar average values for Intersect over Union. This could indicate that the HLS-DSWx algorithm is performing better at classifying water pixels, but the large pixel size is resulting in "jagged" edges to the extent polygons. The pixelated geometry creates many small areas of over- and under-counting of water pixels, leading to higher omission and commission errors but canceling out to reduce the Root Mean Square Error. This would indicate that running the HLS-DSWx algorithm on 10-meter Sentinel-2 imagery may provide even better results than the three methods assessed here. The HLS-DSWx code repository is made freely available by NASA-JPL and likely could be modified slightly to work with the higher resolution imagery.

Table 5.8 **Root Mean Square Error and Bias for total water extent.**

Method	*RMSE*	*Bias*
HLS-DSWx	29.82	24.54
S-2 MNDWI	59.94	-59.94
S-2 MNDWI Adjusted	24.02	-22.60

For SWOT data, channel widths at each node are available instead of polygons of water extent. These were compared against width values derived from the Planet Scope water surface extent polygons. Of the period-of-record, only three points of comparison were available due to the lack of overlapping satellite passes and cloudy days (Table 5.9).

Table 5.9 **Comparison of SWOT channel widths and values derived from Planet Scope polygons. The Nodes column refers to how many SWOT nodes were included in the compared reaches. Nodes are spaced 200 meters apart. Units for all values are in meters.**

Site	*Date*	*RMSE*	*Bias*	*Nodes*	*Relative Error*
Gossett	5/18/2024	77.90	-1.42	63	59.29%
Moore	5/29/2024	92.71	-83.55	51	79.28%
Vaughn	5/29/2024	71.53	-15.90	28	66.97%

Average errors were very high at all three sites, especially compared with channel width averages of 100-130 meters. Unlike water elevations - where errors seemed to be biased in a systematic way – the errors at Gossett and Vaughn are mostly random. This is seen in the fact that bias values are much closer to zero than the root mean square error values, indicating that channel width is being over- and under-estimated to a roughly equal degree. At Moore, however, channel width is being consistently underestimated.

SWOT channel widths are intended to be averaged over 10-kilometer reach lengths in order to reduce error. When comparing average channel widths from Planet Scope and SWOT, the error is drastically reduced for the Gossett and Vaughn sites. The Gossett site is especially close to the Planet Scope average. However, the Moore site error is only marginally improved (see Table 5.10).

Table 5.10 **Estimated width of channel from Planet Scope (PS) and SWOT.**

Site	*Date*	*Avg Width PS*	*Avg Width SWOT*	*Relative Error*	*Reach Length (km)*
Gossett	5/18/2024	131.38	129.96	1.08%	12.6
Moore	5/29/2024	116.95	33.39	71.45%	10.2
Vaughn	5/29/2024	106.82	90.92	14.89%	5.6

Comparing root mean square error from rolling averages instead of individual nodes reduces error, as the number of nodes included in the rolling average increases. The Moore site is again an outlier, as root mean square error is lowest when using a 5-node window (see Table 5.11).

Table 5.11 Comparison of root mean square error (RMSE) based on number of nodes.

Site	Date	RMSE (5 node window)	RMSE (10 node window)	RMSE (25 node window)
Gossett	5/18/2024	49.36	37.18	28.91
Moore	5/29/2024	59.30	88.74	88.14
Vaughn	5/29/2024	55.01	38.83	25.26

It is unclear why channel width is consistently underestimated so drastically at the Moore site. A larger sample size would help understand the source of error. One possible explanation was the difference in time between the Planet Scope and SWOT passes, and whether the surface extent could have changed significantly between the acquisitions. A significant difference in time was observed, however there was little change in reported river stage during this period, and the same time difference also took place at the Vaughn site (see Table 5.12).

Table 5.12 Difference in time and stage between PlanetScope and SWOT passes at each of the sites (meters).

Site	Date	Time Difference	Stage Difference (m)
Gossett	5/18/2024	2:27	0.06
Moore	5/29/2024	10:47	0.09
Vaughn	5/29/2024	10:47	0.07

Channel widths were also compared between Planet Scope and widths derived from the adjusted Modified Normalized Difference Water Index Sentinel-2 water surface extent polygons so that Sentinel-2 and SWOT could be directly compared (see Table 5.13).

Table 5.13 Channel width comparison between Planet Scope and Sentinel.

Site	Date	RMSE	Bias	Relative Error
Gossett	4/5/2024	9.29	-3.18	10.6%
Gossett	4/10/2024	8.27	-2.14	7.8%
Gossett	5/10/2024	15.56	-8.77	14.9%
Gossett	8/8/2024	16.59	-11.91	22.1%
Moore	4/5/2024	13.74	-10.80	16.3%
Moore	4/10/2024	8.76	-0.61	11.5%
Moore	7/9/2024	23.78	-15.63	23.8%
Moore	8/8/2024	17.14	-14.09	26.4%
Vaughn	4/5/2024	10.44	-3.02	12.5%
Vaughn	5/10/2024	11.37	-4.42	10.5%
Vaughn	8/8/2024	21.68	-11.71	33.2%
Gossett	9/7/2024	11.56	-7.48	16.7%
Moore	9/7/2024	18.67	-15.59	26.6%
Vaughn	9/7/2024	13.71	-10.67	22.5%
Total		**14.33**	**-8.57**	**18.2%**

Errors at the individual node level are significantly less than with SWOT, with an average root mean square error of 14.33 meters versus 80.71 meters. While Sentinel-2 error is also improved by averaging to the reach, the observed improvement is much less than with SWOT (see Table 5.14).

Table 5.14 Comparison of widths (in meters) at individual nodes for the Planet Scope and Sentinel-2 datasets.

Site	*Date*	*Average PS (m)*	*Average S-2 (m)*	*Relative Error*
Gossett	4/5/2024	87.44	84.26	4%
Gossett	4/10/2024	105.67	103.53	2%
Gossett	5/10/2024	104.36	95.59	8%
Gossett	8/8/2024	75.23	63.32	16%
Moore	4/5/2024	84.09	73.29	13%
Moore	4/10/2024	76.53	75.92	1%
Moore	7/9/2024	99.72	84.09	16%
Moore	8/8/2024	64.91	50.82	22%
Vaughn	4/5/2024	83.46	80.44	4%
Vaughn	5/10/2024	108.64	104.21	4%
Vaughn	8/8/2024	65.27	53.56	18%
Gossett	9/7/2024	69.34	61.86	11%
Moore	9/7/2024	70.14	54.56	22%
Vaughn	9/7/2024	61.01	50.35	17%
Total				**11%**

5.3.1.2 Water surface elevation

Water Surface Elevation measurements from SWOT were compared to pressure transducer measurements at the three field sites and reported river stage at the two nearby gages. Error statistics were calculated using the SWOT node closest to the instrument location, along with average elevations from multiple nodes. Table 5.15 summarizes the findings. The "1 Node" column presents results for the single closest node, "3 Nodes" also uses values from one node upstream and one node downstream, and so on. For the Hearne gage, SWOT elevations were consistently 16-17 meters higher than the reported water surface elevation from the gage – leading us to suspect that the reported gage altitude on the US Geological Survey page is incorrect. Those results are therefore not presented here.

Table 5.15 **Comparison of water surface elevation measurements from SWOT and field surveys. All units are meters.**

		9 nodes	*7 nodes*	*5 nodes*	*3 nodes*	*1 node*
Moore	RMSE	0.49	0.47	0.48	0.66	0.64
	Bias	-0.30	-0.24	-0.27	-0.43	-0.45
	SD	0.26	0.27	0.26	0.28	0.34
Vaughn	RMSE	1.12	1.12	1.11	1.12	1.07
	Bias	0.96	0.97	0.97	0.97	0.91
	SD	0.59	0.58	0.58	0.58	0.58
Gossett	RMSE	0.45	0.45	0.46	0.53	0.53
	Bias	0.32	0.31	0.35	0.36	0.36
	SD	0.31	0.31	0.31	0.39	0.38
Bryan Gage	RMSE	0.41	0.27	0.28	0.29	0.57
	Bias	0.17	0.11	0.22	0.14	0.30
	SD	0.35	0.21	0.05	0.21	0.43
Total	RMSE	0.62	0.58	0.58	0.65	0.70
	Bias	0.29	0.28	0.32	0.26	0.28
	SD	0.38	0.34	0.30	0.36	0.43

Although the magnitude of error was higher than expected, and consistently higher than the SWOT mission goal of <10 centimeters – this is at least in part driven by systematic versus random error. SWOT elevations were consistently higher than measurements. Error also remained relatively consistent throughout the cluster of nodes around each site.

Comparisons were also grouped by date and then correlated with both mean daily discharge and daily discharge range. The Vaughn and Bryan Gage sites showed moderate to strong correlations between error and daily discharge range – meaning that higher errors occurred when discharge fluctuated more throughout the day - while there was little to no correlation for the other sites. None of the sites showed a correlation between error and mean daily discharge (see Table 5.16).

Table 5.16 **Comparison mean daily, and daily discharge range from SWOT. RMSE = Root Mean Square Error.**

SITE	*Bias Correlation*	*RMSE Correlation*
Vaughn	0.58	0.58
Gossett	0.062	0.086
Moore	0.13	0.16
Bryan Gage	0.77	0.73

In some cases, averaging multiple nodes reduced the magnitude of error, although this too was site-dependent. An average of 5 or 7 nodes tended to produce the most accurate values. Error values were also aggregated at the level of individual nodes, and certain nodes had average errors significantly lower than the average. Here, average values include the nearest node to the site, plus four nodes upstream and four nodes downstream. Distance refers to how many nodes away from the site the best node was. Notably, the best node was never the one closest to the site, and in two of four sites was one of the farthest (see Table 5.17).

Table 5.17 **Comparison of water surface elevation. RMSE = Root Mean Square Error.**

Site	Average RMSE	Average Bias	Best RMSE	Best Bias	Distance
Vaughn	1.14	1.00	0.94	0.76	4
Gossett	0.45	0.36	0.17	0.14	2
Moore	0.66	-0.57	0.45	-0.4	4
Bryan Gage	0.35	0.23	0.17	0.13	1

The following plots (Figures 5.9 through 5.12) show a time series of field water surface elevation measurements along with SWOT node elevations. For each SWOT pass, elevation points are shown for the 9 nearest nodes. Node position refers to the distance from the measurement site: 0 is the closest node, -1 is one node upstream, 1 is one node downstream, and so on. These are symbolized by color, as shown in the plot legends.

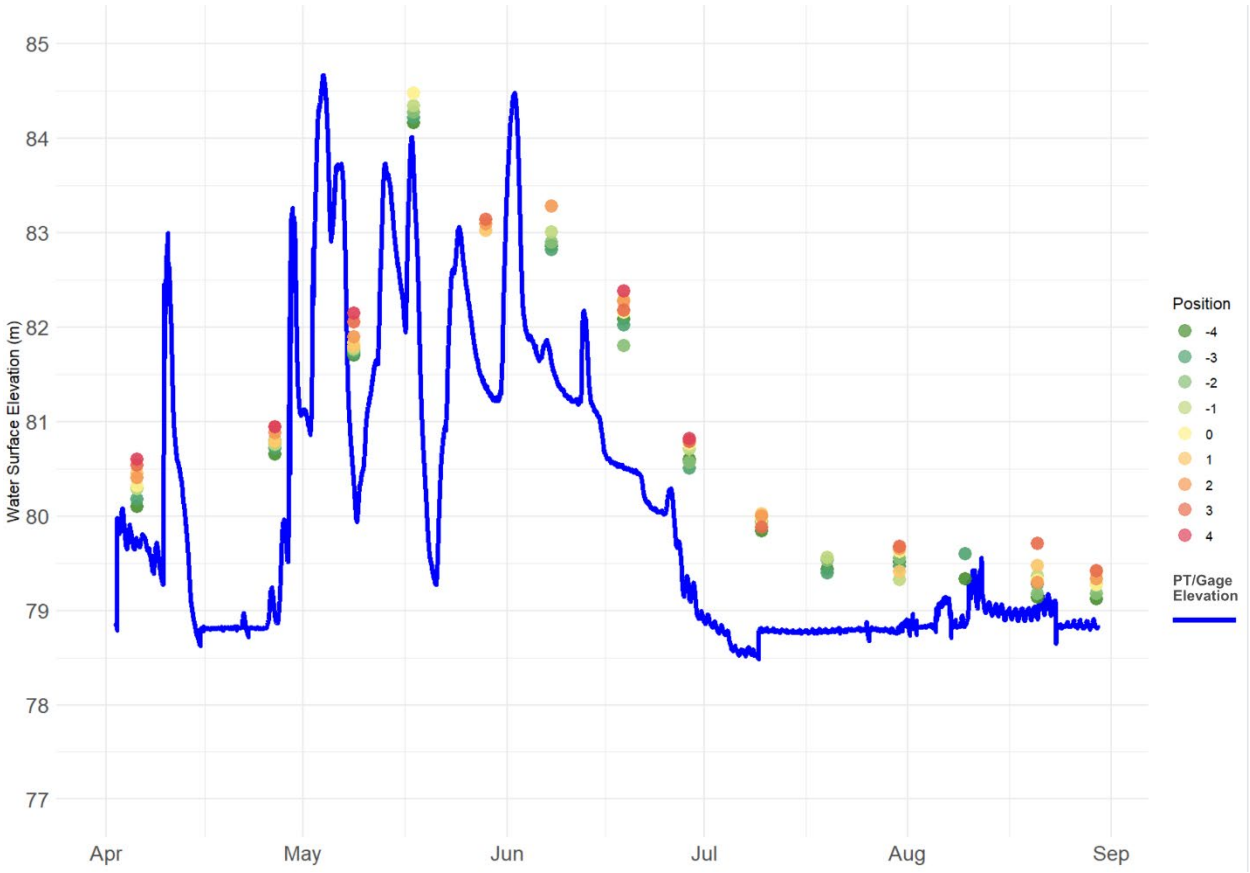

Figure 5.9 Vaughn Site pressure transducer and SWOT elevations. Units are meters.

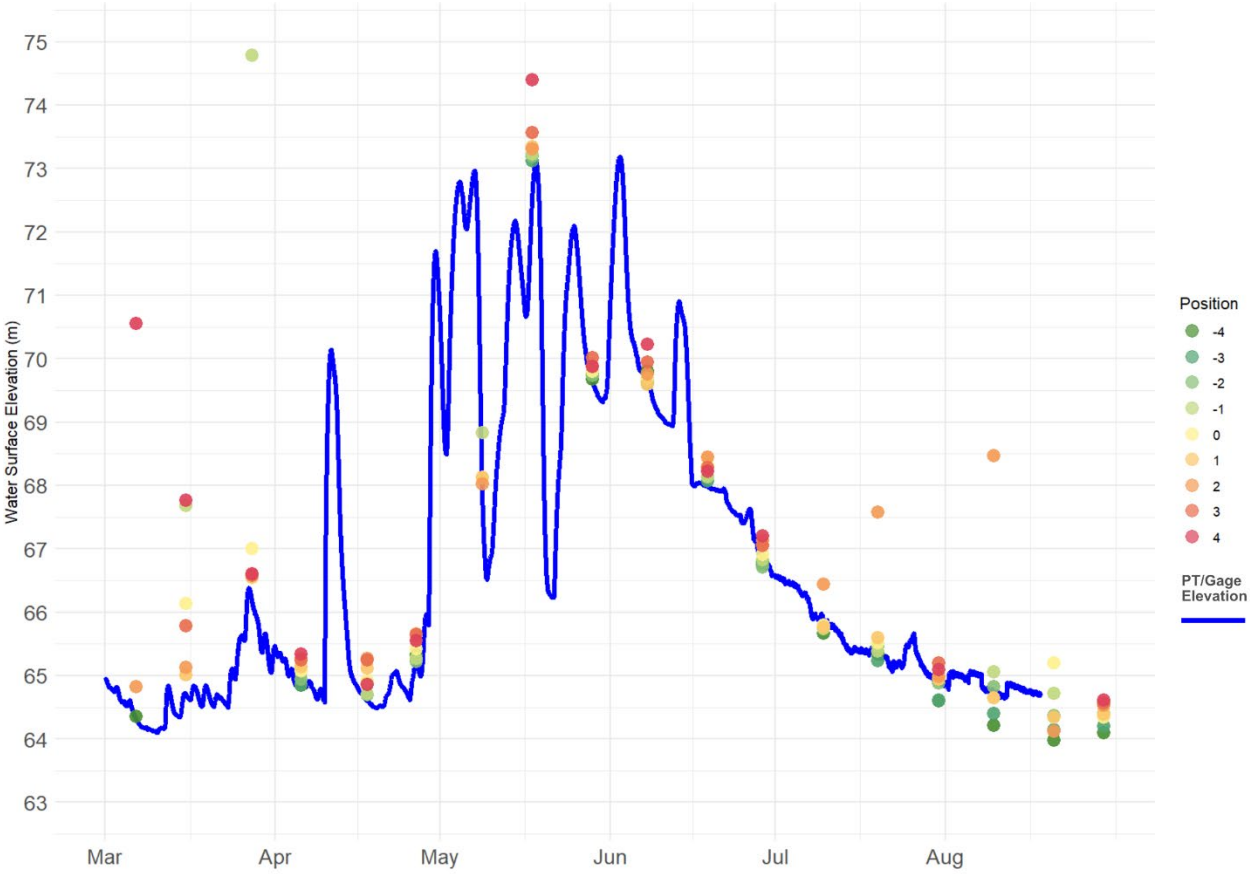

Figure 5.10 Gossett Site SWOT and pressure transducer elevations. Units are meters.

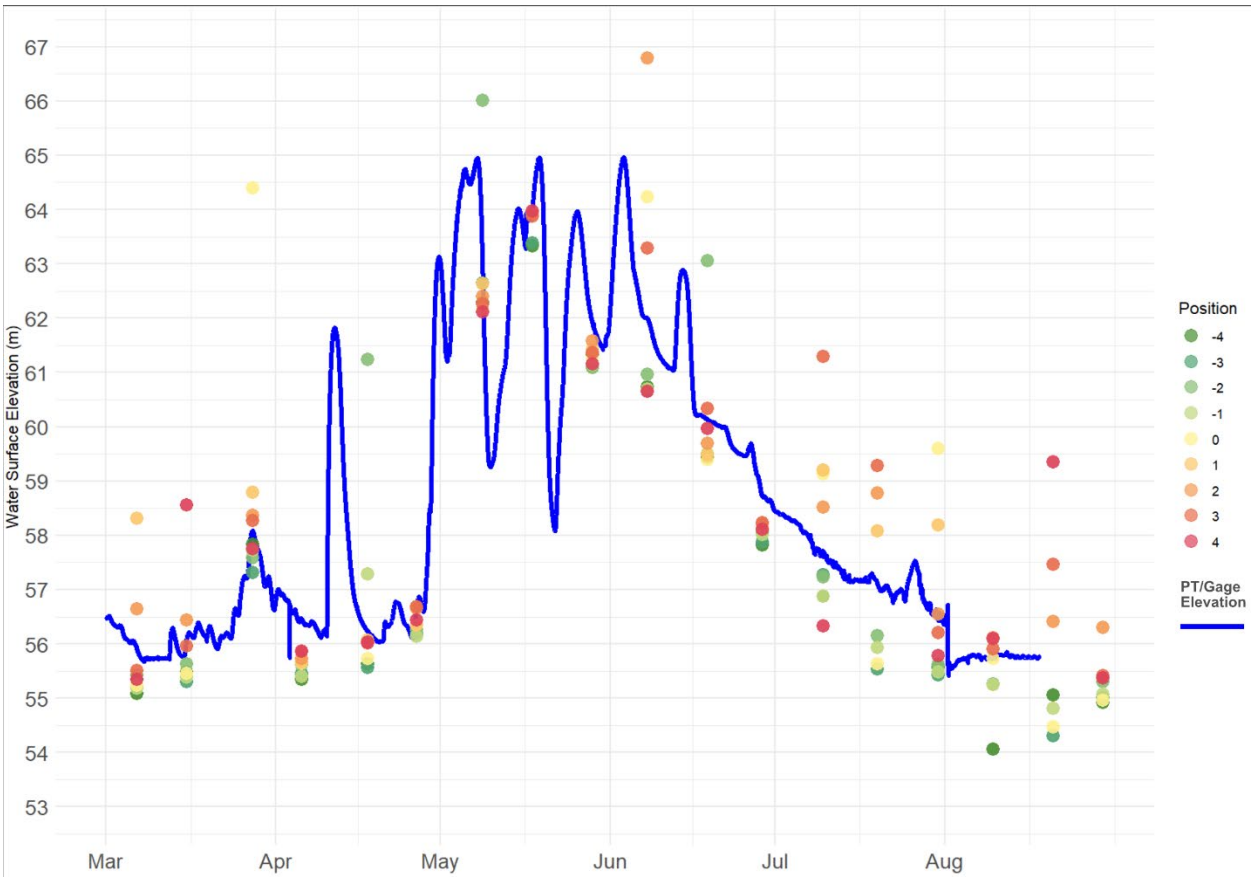

Figure 5.11 **Moore SWOT and pressure transducer elevations. Units are meters.**

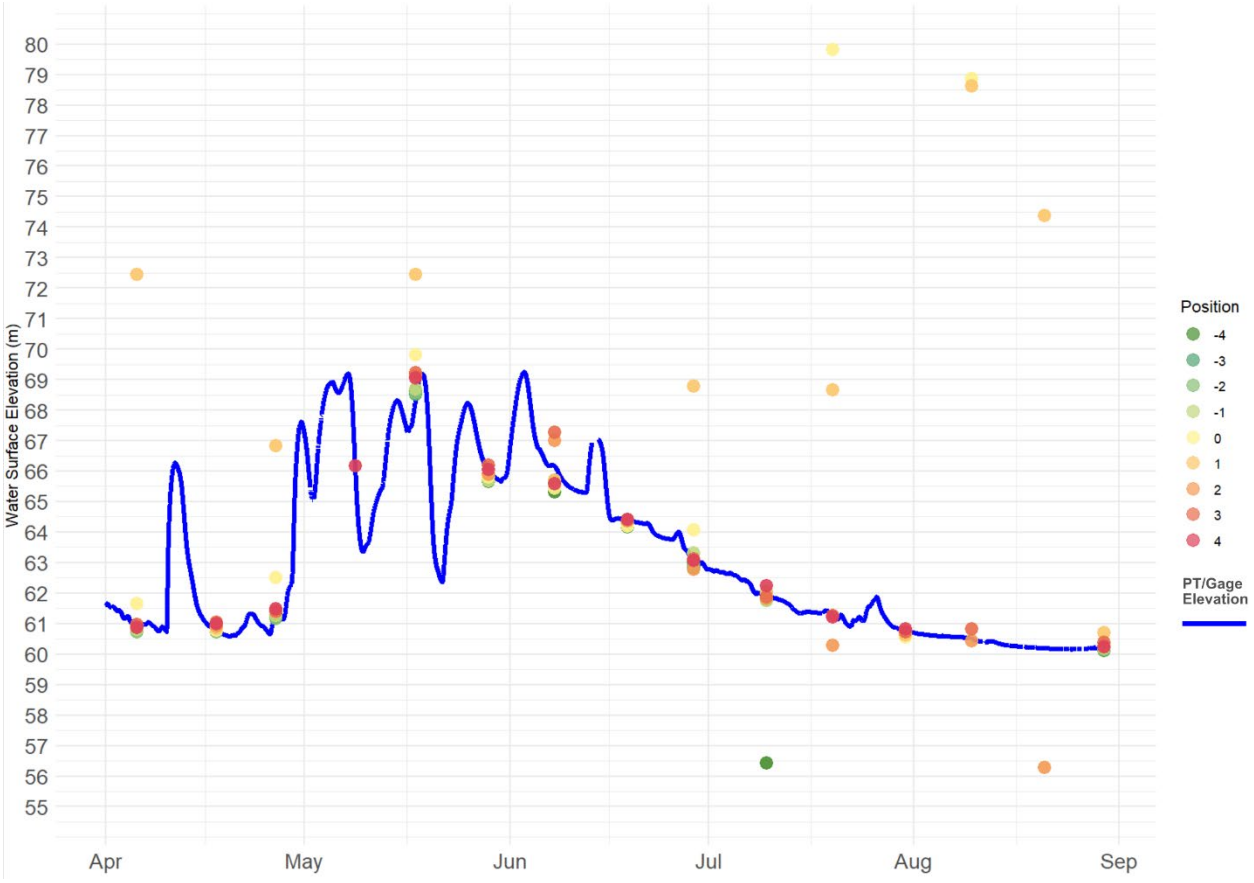

Figure 5.12 Bryan Gage reported river stage and SWOT elevations. Units are meters.

The patterns of error visible in the plots are also site-specific. At the Vaughn site, for instance, SWOT elevation measurements are consistently 0.5 – 1 meter higher than field measurements. Channel morphology may play a role in this case. There is a sharp bend in the river just upstream, and a large island just downstream splits the river into two narrow channels. The coarse resolution of the SWOT sensor relative to the narrow channel widths could potentially result in the misclassification of water pixels. If land pixels were to be classified as water, node-averaged elevations would likely be too high. At the Moore site, elevation values become much more scattered following the period of summer high storm flows. Significant levels of scouring were observed between the April and August field visits, and channel morphology may have been altered in a way that affects the coherence of node measurements.

Another takeaway from the time-series plots is that the SWOT measurements are missing a large degree of temporal variability, due to the 10-day cycle between satellite passes. A major storm pulse in mid-April is absent entirely from SWOT elevations at all four sites. This is to be expected, due to the coarseness of the temporal resolution – yet needs to be considered when assessing the usefulness of such data for water management.

Ultimately, the observed error in reported water surface elevation node elevations may be too large to use for quantifying groundwater-surface water interactions at a fine scale. That will ultimately

depend on how well the other three flow parameters can be estimated, and such assessments will need to wait until SWOT discharge estimates are published in 2025. However, the presence of systematic biases and higher-quality nodes is promising in that more accurate data could be extracted from SWOT data products. The SWOT sensor and processing algorithms are very novel in comparison to many other types of remote sensing data, and estimates are likely to become more refined as the field matures.

Another possibility is the extraction of data from less processed forms of SWOT data – such as the raw radar backscatter signals or the raster datasets used to generate node elevation values. At present, the same processing algorithm is used for averaging node elevations on all rivers globally. It would be feasible to optimize these processing steps for different sized rivers, or under different flow conditions. The development of regional data calibration or incorporation into local models has always been an important component of the SWOT mission, and tools are provided for users to develop their own discharge algorithms (NASA-JPL Confluence, 2024).

In addition to elevation measurements at single locations, the ability of SWOT to instantaneously measure elevations along the entire river at unprecedented vertical accuracy and temporal resolution. The following two charts plot all SWOT elevation measurements in the area of interest from the period of record from November 2023 through September 2024. Measurements flagged as low quality have been filtered out, but some erroneous values do remain. Each SWOT pass was classified as coinciding with low, medium or high flows at the FM485 Hearne gage, and the data points have been colored accordingly. The first chart (Figure 5.13) shows the location of various river features, and the second (Figure 5.14) shows the extent of aquifer outcrops and subcrops.

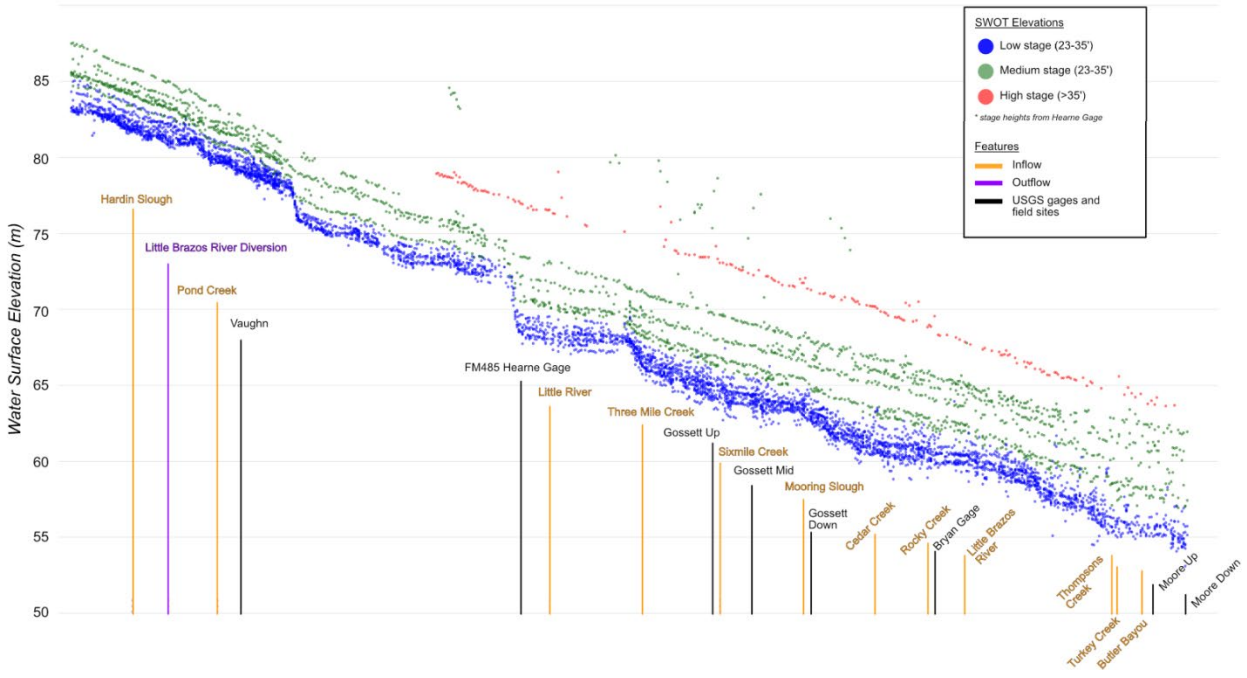

Figure 5.13 **Location of features on the Brazos River and their relation to water surface elevation. Units are meters.**

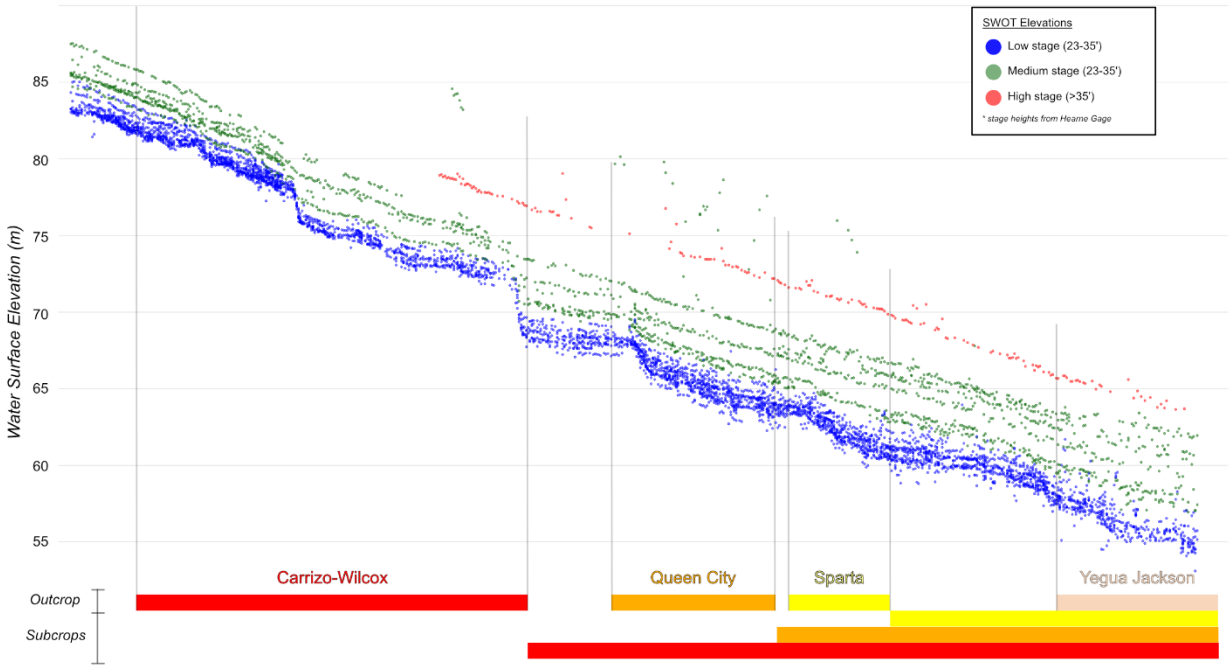

Figure 5.14 **Location of geologic features on the Brazos River, and their relation to water surface elevation. Units are meters.**

Because the slope gradients of water elevation appear relatively stable between measurements, one possibility for increasing temporal resolution of discharge measurements would be to establish a relationship between reported river stage at US Geological Survey gages and individual SWOT nodes. If a node is consistently higher or lower than a gage by a certain amount, continuous gage data could be used to estimate node elevations in between SWOT passes. This could be the topic of further study, but to explore the possibilities, the difference was calculated between each node and the Bryan and Hearne gages for each SWOT pass. At each node, the standard deviation of those deviations was then calculated to see how stable the relationship was between gage and node elevation.

The following plot (Figure 5.15) shows the standard deviation of differences between node elevations and each of the two gages. All nodes in the area of interest are plotted along the x-axis, from upstream on the left to downstream on the right, with the locations of the two gages indicated. The red line shows the standard deviation of difference with the Hearne gage, and the blue line with the Bryan gage. Essentially, the plot shows how well node elevations can be predicted using only river stage at the two gages.

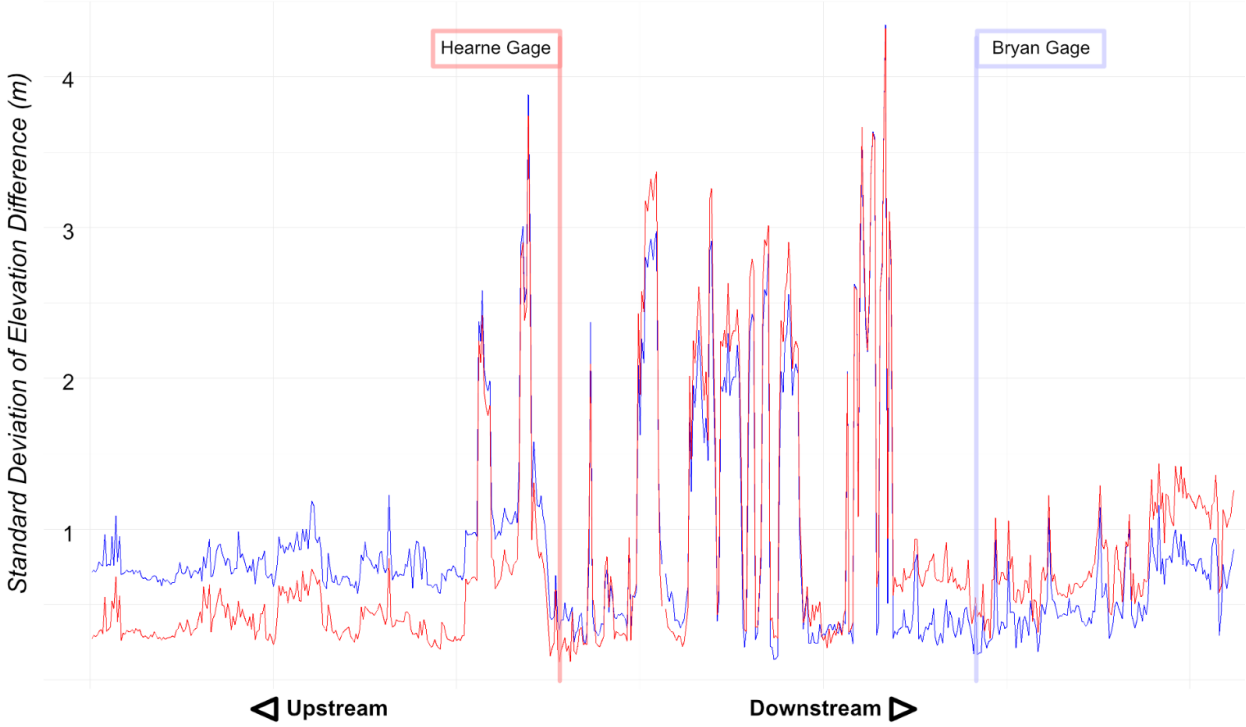

Figure 5.15 **Standard deviation of differences between node elevations and each of the streamgages. Units are meters.**

Within certain regions, nodes do show a relatively consistent relationship to gage heights. For the upstream third of the area of interest, most nodes have less than 0.5 meters of variability with the nearer Hearne gage. The relationship with the Bryan gage is less consistent but still has a standard deviation of less than 1 meter. The middle third shows high levels of variability, apart from a region close to the Hearne gage itself. The downstream third is relatively consistent as well, though more closely tied to the Bryan gage than the one at Hearne. Note that this analysis is assuming a linear relationship between gage and node height, and that a curve based on varying river stage would likely predict node elevations more accurately.

5.3.2 Thermal trends

Trends in surface water temperatures collected by drone were assessed for potential gaining reaches. This analysis was qualitative – due to the noisiness associated with surface temperature data, low sample size, and the confounding effect from time of day. Flights took place over 3-7 hours each, and the effect of increasing surface temperatures throughout the day is particularly difficult to address. Select criteria were used to subjectively assess different reaches for groundwater seepage:

- **Relatively cooler surface water temperatures** – This is the primary consideration and assumes that the cooler groundwater will have some influence on the average surface temperatures in gaining reaches.
- **Consistent trends in both field visits** – If cooling trends are present in data from both spring and summer, it is more likely that they are the result of groundwater plumes, and not the result of noise in the data or other factors. Trends are expected to be more pronounced in the summer dataset when flows are lower, as groundwater would have a greater effect on average temperatures. However, the seasonality of groundwater pumping and flux may reduce or eliminate this effect.
- **Lowering temperatures later in the day –** Because surface temperatures tend to increase throughout the day, temperature trends in the other direction are especially significant. At the same time, increases in shade cover on the river surface beginning in the late afternoon may create confounding cooling effects that are dependent on the presence of shoreline vegetation and channel orientation.

The following charts (Figures 5.16 through 5.18) present measured water surface temperatures at the three field sites from both spring and summer field visits. Temperatures were sampled at every 0.01 mile along the river centerline to reduce the effect of shading, and also adjusted using rolling averages with a window of 0.05 miles to reduce noise in the data. Each site acquisition included between 2-5 flights, and the start times of each flight are indicated below the temperature line to assist in interpreting trends. Extents of potential gaining reaches are indicated, but is it important to keep in mind that these are the result of subjective interpretation and not statistical analysis.

Ultimately, while it was possible to make informed speculations as to the presence of gaining reaches, the data collected did not allow for a rigorous identification – much less quantification – of groundwater flux. Refinement of the data collection methods by synchronizing data collection efforts, and repeated collections, would improve the predictive power of the thermal data. Collecting data in areas where groundwater-surface water interactions are already well studied would lead to a better understanding of other factors influencing water surface temperature, the relationship between temperatures on the surface and deeper in the water column, and the patterns of thermal signatures which indicate gaining reaches.

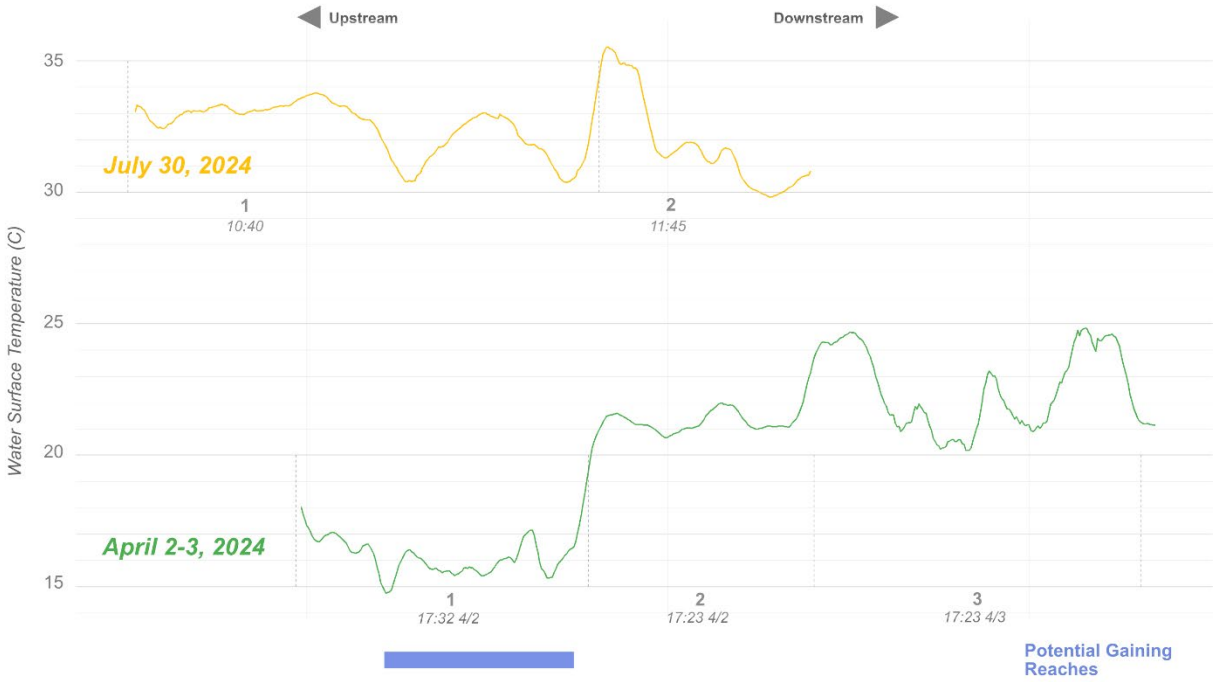

Figure 5.16 **Vaughn site measured water surface temperatures from drone flights.**

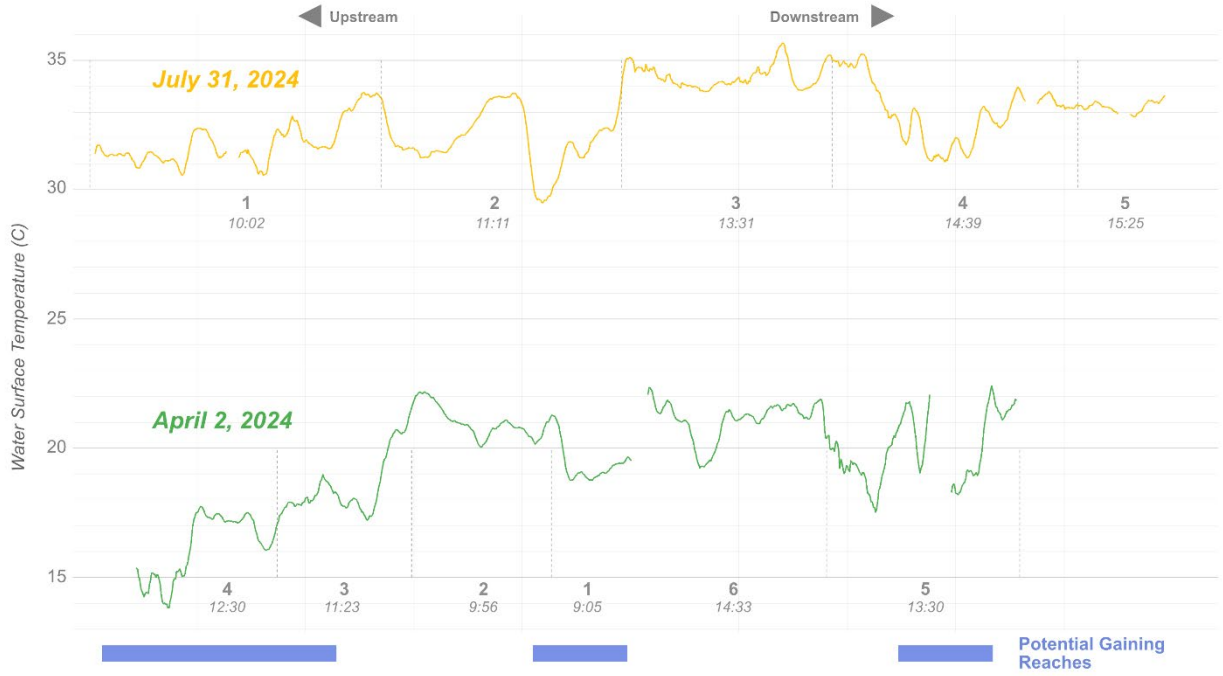

Figure 5.17 **Gossett site measured water surface temperatures from drone flights.**

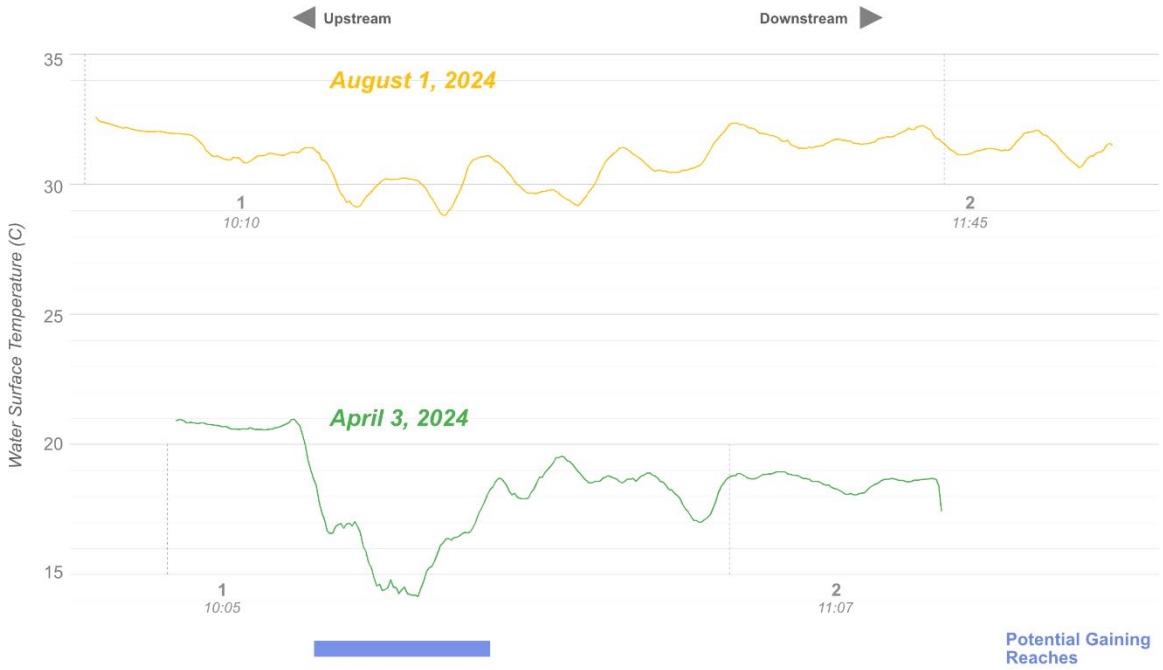

Figure 5.18 Moore site measured water surface temperatures from drone flights.

5.4 Groundwater availability model analysis

A limitation of using an annual time step in the groundwater availability model simulations is that the seasonal effects on surface water–groundwater interaction is ignored. Among the hydrogeologic and climatic variables with known seasonal variations that could affect groundwater-surface water interactions are precipitation, evapotranspiration, river stage, and groundwater pumping. To investigate the potential significance of seasonal changes in hydrogeology on the groundwater-surface water interaction, a series of groundwater availability model simulations were developed and performed to account for seasonal changes in the aforementioned hydrogeologic and climatic variables. Among the first steps to simulate the season change is to reduce the groundwater availability model's time step.

5.4.1 Temporal model refinement

In order to more accurately evaluate interactions using the groundwater availability model, the temporal discretization was refined from annual to quarterly stress periods. Each previously defined annual stress period in the transient simulation was subdivided into four quarterly periods, resulting in a total of 325 stress periods. Among the MODFLOW packages adjusted on a quarterly basis were the WEL, RCH, and RIV packages, while other packages were held constant for each respective year due to their comparatively minor influence on the overall water balance. Figure 5.19 and Figure 5.20 summarize the modeled annual and quarterly water balances, respectively, for the river cells intersecting the Brazos River in the area of interest. The figures demonstrate similar ranges and behavior, indicating that the overall water budget remained consistent between the annual and quarterly models. The quarterly model will serve as the basis for the sensitivity analysis presented later in this section.

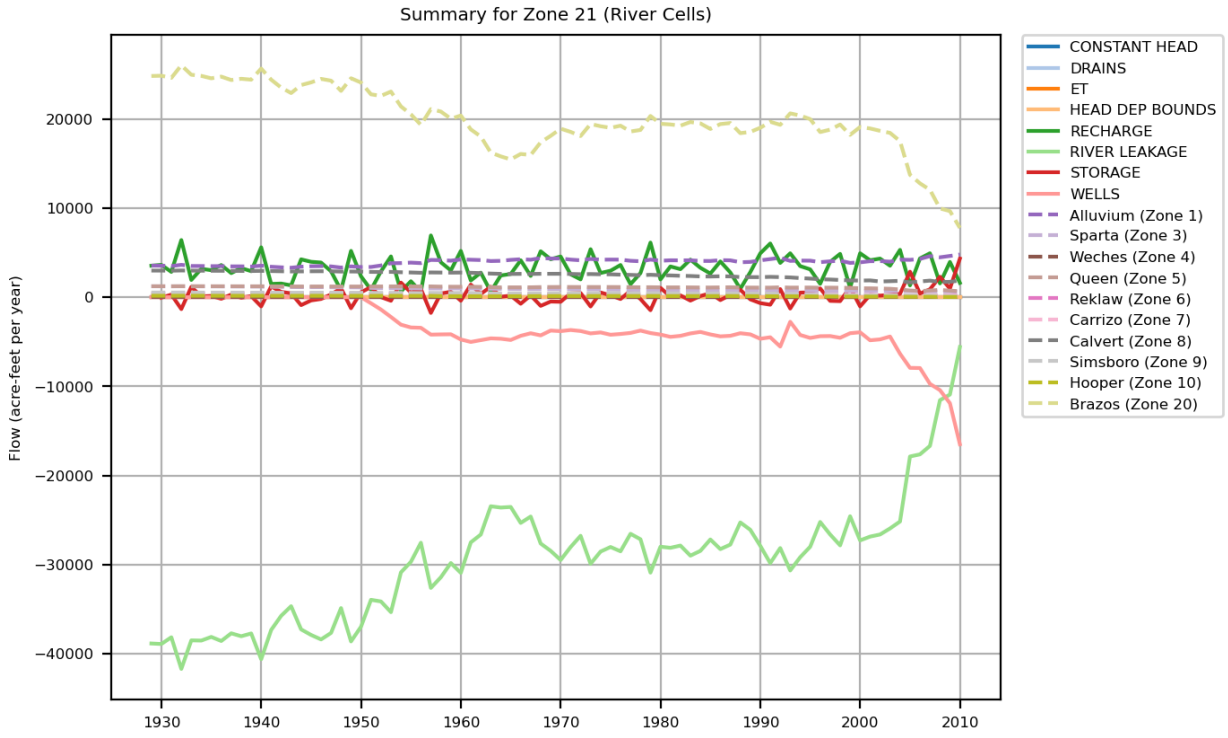

Figure 5.19 **Modeled annual water budget for River Cells in the area of interest.**

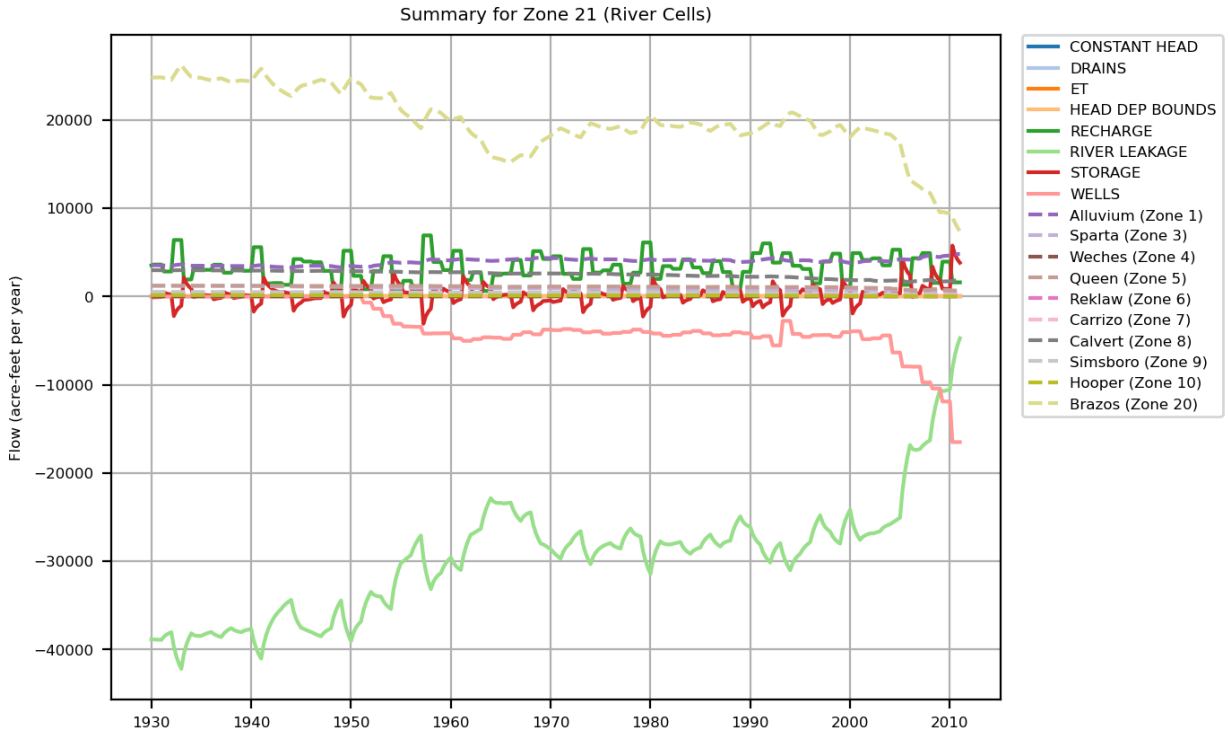

Figure 5.20 **Modeled quarterly water budget for River Cells in the area of interest.**

5.4.2 Seasonality of pumping, recharge, and river stage

The water budget focused in the area of interest, presented in Section 3.1.3, highlights the importance of the WEL, RCH, and RIV packages in the Brazos Alluvium, as they represent pumping, recharge, and the interaction between the river and the surrounding alluvium. This section details how field data described in Chapter 4 were used to enhance the model's fidelity in representing groundwater-surface water exchange.

5.4.2.1 Pumping

Quarterly irrigation deficit fractions were subsequently derived for each year, and the resulting quarterly factors were used to partition estimated annual pumping volumes. As shown in Young and others (2018a) and Ewing and Jigmond (2016), the pumping that occurs in the alluvium primarily supports agricultural uses. As shown in Table 5.18, the quarterly pumping factors derived from OpenET data indicate that most pumping occurs in the third quarter (July–September) at approximately 58%, with smaller contributions in the first and fourth quarters (7% and 5%, respectively) and a moderate portion in the second quarter (30%). These factors are used as parameters in the sensitivity analysis.

Table 5.18 Quarterly pumping factors derived from OpenET data.

Quarter	*Pumping Factor*
Q1 (Jan-Mar)	0.07
Q2 (Apr-Jun)	0.30
Q3 (Jul-Sep)	0.58
Q4 (Oct-Dec)	0.05

To evaluate the irrigation estimates, the total irrigation volume within the area of interest was compared against pumping data reported for the alluvium in the original groundwater availability model WEL package. Figure 5.21 summarizes pumping rates for the period of record with reported pumping in the groundwater availability model (1950-2010). Figure 5.22 presents comparable estimates derived from OpenET between 2016 through 2023. Groundwater availability model-based estimates suggest that most of the pumping within the area of interest occurs from the Brazos Alluvium allowing a direct comparison between the two estimates. OpenET estimates range from about 60,000 to 120,000 acre-feet/year, while the 2010 groundwater availability model estimate reached approximately 70,000 acre-feet/year, supporting the plausibility of remotely sensed data. Figure 5.22 also includes total precipitation for quarter 2 and quarter 3 to assess the temporal variability of total irrigation. Year 2022 had the highest pumping estimates, coinciding with one of the lowest recorded summer precipitation values, while years with low pumping exhibit summer precipitation above 20 inches. This pattern is consistent with the historical data shown previously, where high actual evaporation values align with low precipitation during peak summer months. These comparisons indicate that further exploration of OpenET data could help fill existing information gaps and better characterize seasonal irrigation trends.

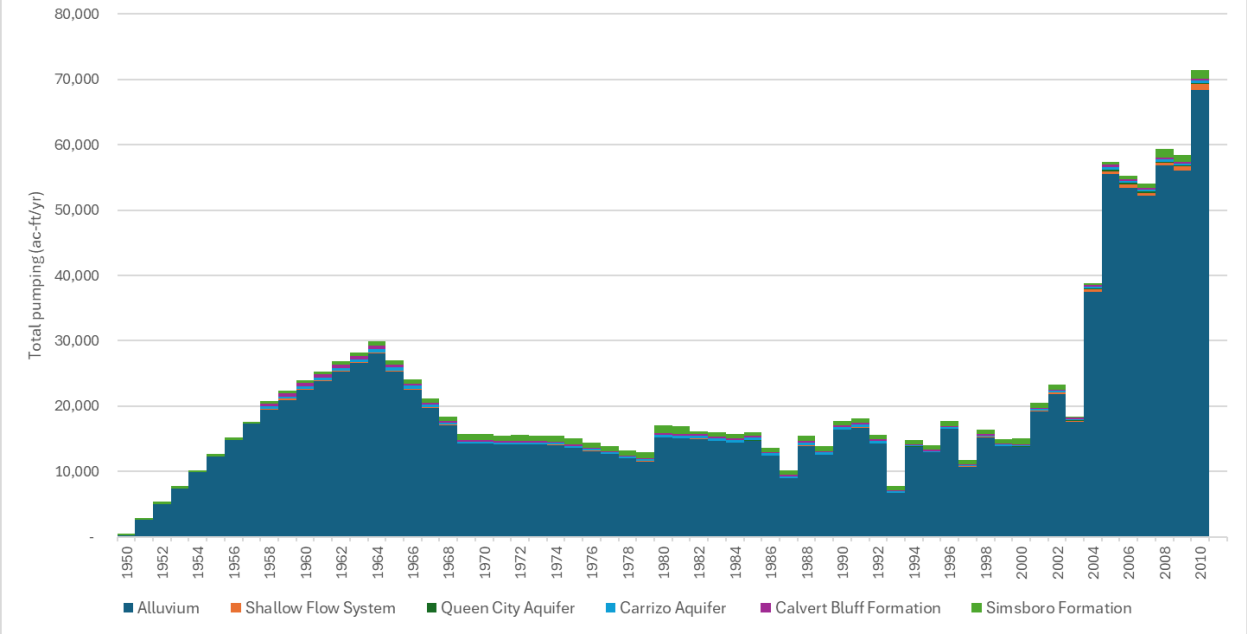

Figure 5.21 **Total Pumping in the area of interest reported in the central portion of the Carrizo-Wilcox Aquifer groundwater availability model. Units are acre-feet per year.**

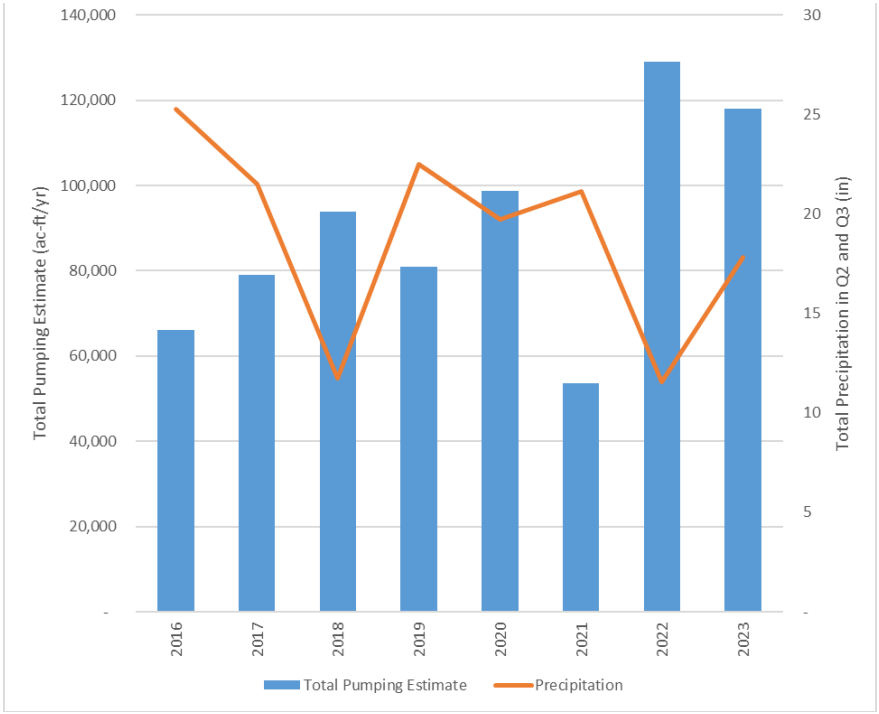

Figure 5.22 **Total Pumping derived from OpenET and Total Precipitation in quarter 2 (Q2) and quarter 3 (Q3) in the area of interest. Units are acre-feet per year.**

5.4.2.2 Recharge

To simplify the original recharge estimation, which was developed for the groundwater availability model by integrating precipitation, observed runoff, and extrapolations from baseflow indices and runoff data, an alternative approach was adopted. In this approach, monthly precipitation data from a centrally located grid node in the long term 1895 to 2025 PRISM dataset (PRISM Climate Group, 2024) within the area of interest was used to determine average monthly precipitation (Figure 5.23). These monthly values were then aggregated by quarter and normalized by mean annual precipitation.

Table 5.19 presents the quarterly results, indicating that quarter 2 (April to June) receives the highest average precipitation (10.91 inches) and therefore has the largest recharge factor (0.30). In contrast, quarter 3 (July to September) has the lowest average precipitation (7.08 inches) and thus the smallest recharge factor (0.20). This reduced recharge in quarter 3 compounds its influence on surface water and groundwater interactions in the alluvium, given that this quarter also corresponds to the highest fraction of observed pumping (as discussed in the previous section). The factors shown in Table 5.19 were incorporated into the sensitivity analysis described in Section 5.4.3.

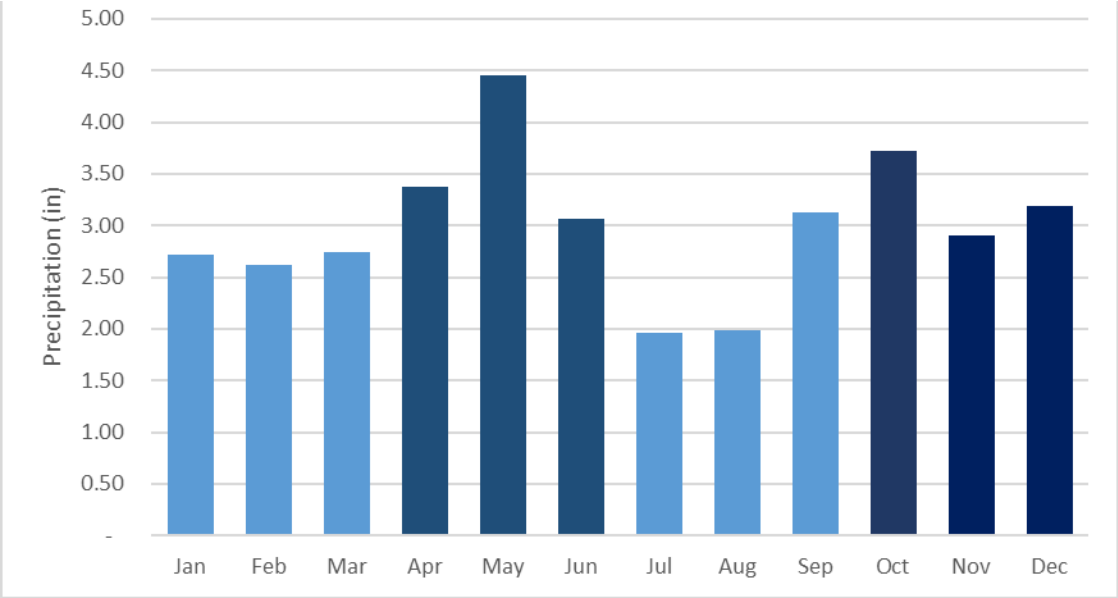

Figure 5.23 **Monthly summary of PRISM precipitation data used for estimating quarterly recharge factors. Units are inches.**

Table 5.19 Quarterly recharge factors derived from PRISM data.

Quarter	*Average precipitation by quarter (inches)*	*RCH factor based on PRISM*
Q1 (Jan-Mar)	8.08	0.23
Q2 (Apr-Jun)	10.91	0.30
Q3 (Jul-Sep)	7.08	0.20
Q4 (Oct-Dec)	9.82	0.27
All Year	35.88	1.00

5.4.2.3 River stage

In the Texas Groundwater Modeling program, characterizing river stage for the RIV package is challenging because it requires continuous estimation across all cells intersecting streams. Often, there is insufficient data to develop depth estimates based on observed river stage measurements. As a result, river stage is typically approximated using an average depth relative to the channel bottom elevation obtained from river bathymetry or available digital elevation model data. For the area of interest and the Brazos River, this assumed depth was 3 feet.

The availability of SWOT data, described in detail in Section 4, offers the potential to estimate river stage using actual surface water elevations, reducing reliance on average depths or hydraulic calculations based on existing cross-sectional data. For the sensitivity analysis described in Section 5.4.3, SWOT data were processed to determine averages of river depth over three-month intervals. SWOT data, available from November 24, 2023, through October 11, 2024, were filtered to include only dates with no more than five percent missing values. Ten dates met this criterion, representing flows ranging between 200 and 22,000 cubic feet per second, as recorded by the US Geological Survey gage on the Brazos River near Highbank, Texas.

Figure 5.24 compares conditions at the 109 RIV cells along the Brazos River in the area of interest with the selected SWOT data. The SWOT estimates were averaged for each corresponding RIV model cell. In the top plot, cell top (cell top) and cell bottom (cell bot) elevations are shown along with the assumed river stage (Stage) and river bottom (Rbot). In the bottom plot, the same values are depicted in black and contrasted with the color-coded SWOT data, where colors represent increasing flow in the Brazos River from low to high. The large drop in the river surface from approximately 245 feet to 225 feet above mean sea level under low-flow conditions occurs where the Little River converges with the Brazos River.

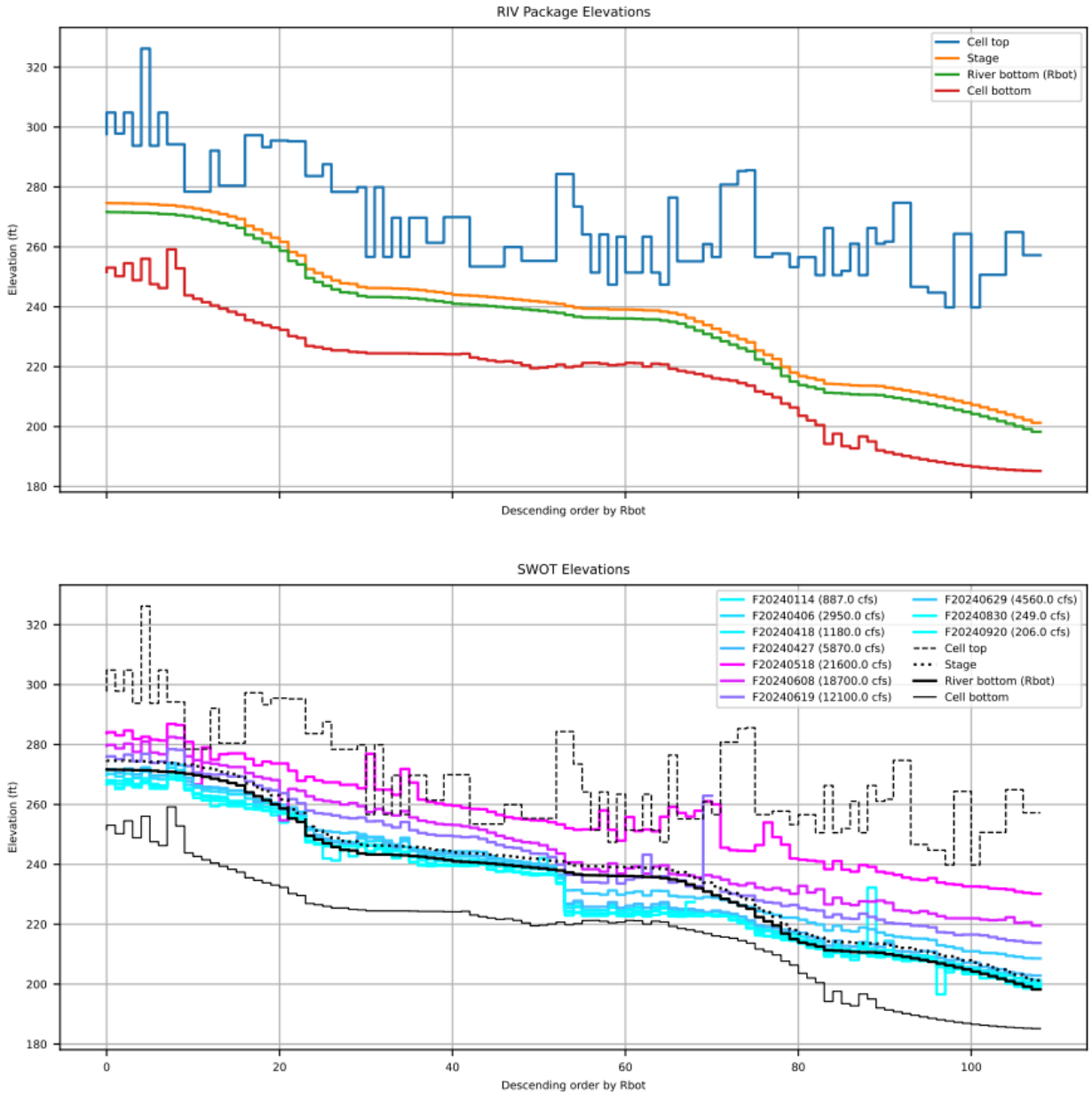

Figure 5.24 **Comparison of RIV Package parameterization and selected SWOT data along Brazos River cells. Units are feet.**

The US Geological Survey gage at the Brazos River near Highbank, Texas, was selected because of its long record of mean daily flow and river stage. Figure 5.25 and Figure 5.26 present a summary of flow and head statistics by quarter using violin plots, which illustrate the full distribution of the dataset, including its probability density. In addition to showing the data's spread, these plots report median, mean, and mode statistics for each quarter, with the mode indicating the most frequently occurring value, often visible as the thickest section of the violin. Quarter 2 is characterized by having the highest statistics, with a mean flow of 4,734 cubic feet per second and

a mean flow stage of 5.25 feet, while quarter 3 represents the lowest mean flow and stage (1,533 cubic feet per second and 3.31 feet). Quarter 1 statistics rank second, while quarter 4 ranks third.

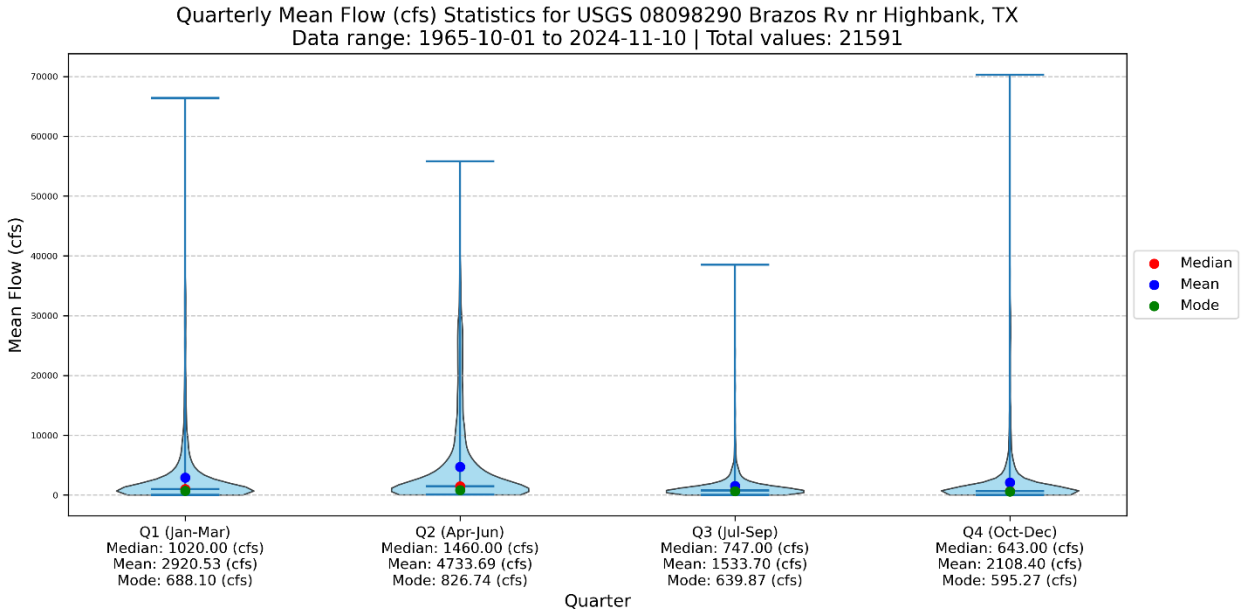

Figure 5.25 Violin plots and quarterly statistics for mean daily flow at US Geological Survey 08098290 Brazos River Near Highbank, Texas. Units are cubic feet per second.

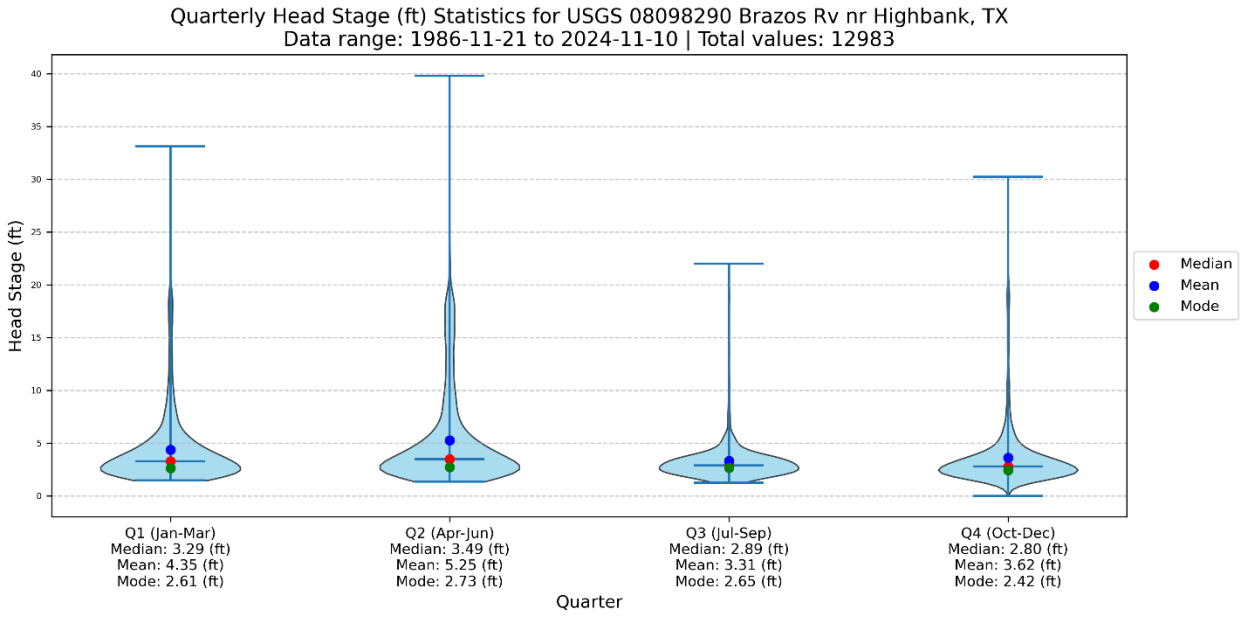

Figure 5.26 Violin plots and quarterly statistics for mean head stage at US Geological Survey 08098290 Brazos River Near Highbank, Texas. Units are feet.

Since an average river depth was assumed to represent conditions in the Brazos River within the area of interest during the groundwater availability model study period, the mean annual flow at Highbank can serve as a proxy for that average depth and be compared against the quarterly

statistics shown in Figure 5.27. This figure includes annual flow estimates near Highbank, the annual mean, and the quarterly means presented in Figure 5.25. Notably, the mean flow in quarter 1 is very close to the annual mean, quarter 3 remains the lowest, and quarter 2 the highest, as also shown in Figure 5.25 and Figure 5.26.

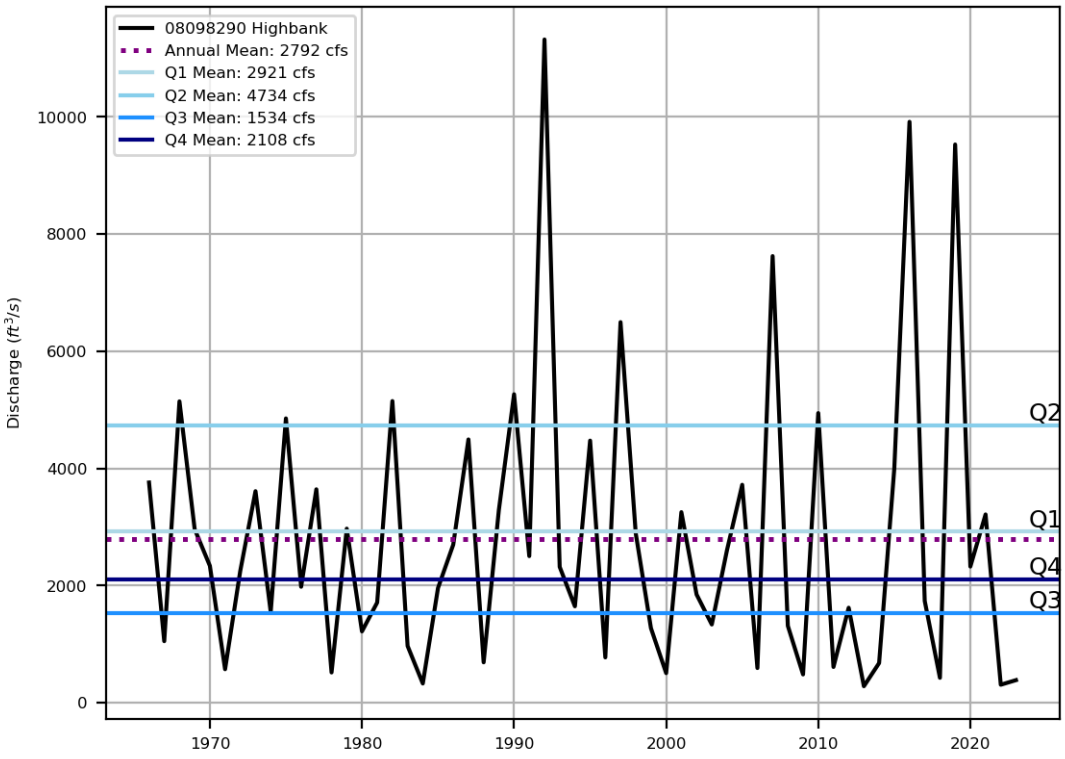

Figure 5.27 **Comparison of annual flow with mean annual flow and mean quarterly flows at US Geological Survey 08098290 Brazos River Near Highbank, Texas. Units are cubic feet per second.**

As of the time this report was prepared, SWOT data do not include river bottom elevations. However, this can be addressed by using the date of the lowest flow as a reference point. In this case, the lowest flow occurred on September 20, 2024 (204 cubic feet per second), and average depths for the other dates were computed relative to this reference date. To further reduce the influence of outliers caused by spikes in the SWOT data, the top and bottom five percent of the differences calculated by averaging SWOT node data for each of the model nodes between the reference data and the other nine dates were also removed. As a result, it was possible to calculate an average difference in flow between September 20, 2024, and the other selected dates, as presented in Figure 5.28. It is anticipated that this rating curve can be refined as methods to identify anomalous SWOT values improve, and as additional dates with similar flow conditions become available.

Linear interpolation between the available dates was then applied to estimate depths corresponding to each of the quarterly statistics and the mean annual flow, as shown in both Figure 5.28 and the Delta to baseline column of Table 5.20. An additional column was calculated by assuming the mean annual flow delta corresponds to the annual flow, and that the annual flow

delta is zero, providing a relative depth measurement shown in the Revised Stage column. Since a multiplier approach compatible with PEST is being used, multiplier factors were calculated for each quarter by assuming that a depth of three feet corresponds to a factor of one. These multipliers were then incorporated into the sensitivity analysis presented in Section 5.4.3.

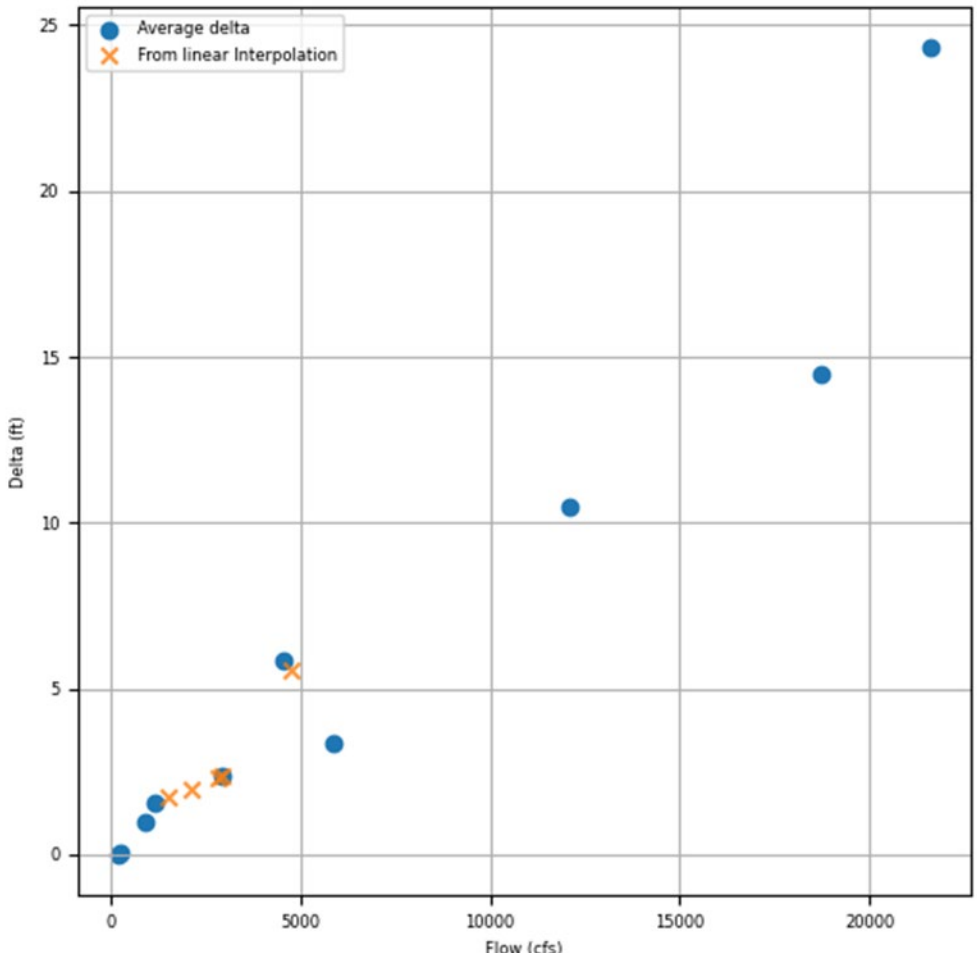

Figure 5.28 **Average reference depth Delta Function along Brazos River against flow conditions on 9/20/2024 versus flow at US Geological Survey 08098290 Brazos River Near Highbank, Texas. Flow units are in cubic feet per second, and Delta units are in feet.**

Table 5.20 **RIV package stage factors derived from SWOT data and flow statistics. Units are cubic feet per second (cfs) and feet (ft).**

Time Period	*Median (cfs)*	*Mean (cfs)*	*Delta to baseline (ft)*	*Delta to Mean Annual (ft)*	*Revised Stage (ft)*	*Delta Multiplier (-)*
Q1 (Jan-Mar)	1020	2921	2.4	0.0	3.05	1.02
Q2 (Apr-Jun)	1460	4734	5.5	3.2	6.23	2.08
Q3 (Jul-Sep)	747	1534	1.7	-0.6	2.42	0.81
Q4 (Oct-Dec)	643	2108	2.0	-0.3	2.68	0.89
Mean Annual	**875**	**2817**	**2.3**	**0.0**	**3.00**	**1.00**

5.4.3 Sensitivity analysis

With the purpose of illustrating how remote sensing can help simulate seasonal variations and calibration of groundwater availability models this section incorporates the quarterly factors for pumping, recharge, and river stage in a sensitivity analysis focused on the representation of the Brazos River in the area of interest. The sensitivity analysis consisted of the twenty-two simulations in Table 5.21. Each simulation involves using 3-month time steps and different assumptions of how quarterly values for pumping, recharge, and river stage will change and how the riverbed conductance will change from a baseline run. For the baseline run the quarterly values for pumping, recharge, and river stage are uniform and thus contain no seasonal differences.

Model cells for comparison and evaluation of field data are shown in Figure 5.29. Three out of the four sites presented in Section 4 are within the area of interest: Vaughn, Gossett 1 and Gossett 2. These cell locations represent the segments of the Brazos River where water levels were collected within the area of interest. The Gossett locations were the main sites for detailed plotting in the following sections, as the combined groundwater- and surface-water-level observations provided the longest time series, and they showed consistency with model results. As indicated earlier in Section 4, the Vaughn Site surface water levels collected during 2024 were affected by high flows causing malfunction during low flow periods. For the water levels and riverbed flow at each cell of interest as well as total riverbed flow in the area of interest are presented to evaluate the sensitivity to the selected parameters.

Table 5.21 Sensitivity analysis parameter matrix.

Run ID	*WEL Factors*				*RCH Factors*				*RIV Factors*				*Riverbed Conductance Multiplier*	*Sensitivity Group*
	Q1	**Q2**	**Q3**	**Q4**	**Q1**	**Q2**	**Q3**	**Q4**	**Q1**	**Q2**	**Q3**	**Q4**		
1	0.25	0.25	0.25	0.25	0.25	0.25	0.25	0.25	1.00	1.00	1.00	1.00	1.00	Baseline
2	0.20	0.26	0.33	0.20	0.25	0.25	0.25	0.25	1.00	1.00	1.00	1.00	1.00	WEL
3	0.16	0.28	0.41	0.15	0.25	0.25	0.25	0.25	1.00	1.00	1.00	1.00	1.00	WEL
4	0.11	0.29	0.50	0.10	0.25	0.25	0.25	0.25	1.00	1.00	1.00	1.00	1.00	WEL
5	0.07	0.30	0.58	0.05	0.25	0.25	0.25	0.25	1.00	1.00	1.00	1.00	1.00	WEL
6	0.25	0.25	0.25	0.25	0.244	0.264	0.237	0.256	1.00	1.00	1.00	1.00	1.00	RCH
7	0.25	0.25	0.25	0.25	0.238	0.277	0.224	0.262	1.00	1.00	1.00	1.00	1.00	RCH
8	0.25	0.25	0.25	0.25	0.231	0.291	0.210	0.268	1.00	1.00	1.00	1.00	1.00	RCH
9	0.25	0.25	0.25	0.25	0.225	0.304	0.197	0.274	1.00	1.00	1.00	1.00	1.00	RCH
10	0.07	0.30	0.58	0.05	0.225	0.304	0.197	0.274	1.00	1.00	1.00	1.00	1.00	RIVBRS
11	0.07	0.30	0.58	0.05	0.225	0.304	0.197	0.274	1.00	1.27	0.95	0.97	1.00	RIVBRS
12	0.07	0.30	0.58	0.05	0.225	0.304	0.197	0.274	1.01	1.54	0.90	0.95	1.00	RIVBRS
13	0.07	0.30	0.58	0.05	0.225	0.304	0.197	0.274	1.01	1.81	0.86	0.92	1.00	RIVBRS
14	0.07	0.30	0.58	0.05	0.225	0.304	0.197	0.274	1.02	2.08	0.81	0.89	1.00	RIVBRS
15	0.25	0.25	0.25	0.25	0.25	0.25	0.25	0.25	1.00	1.00	1.00	1.00	0.10	COND
16	0.25	0.25	0.25	0.25	0.25	0.25	0.25	0.25	1.00	1.00	1.00	1.00	10.00	COND
17	0.25	0.25	0.25	0.25	0.25	0.25	0.25	0.25	1.00	1.27	0.95	0.97	1.00	RIV
18	0.25	0.25	0.25	0.25	0.25	0.25	0.25	0.25	1.01	1.54	0.90	0.95	1.00	RIV
19	0.25	0.25	0.25	0.25	0.25	0.25	0.25	0.25	1.01	1.81	0.86	0.92	1.00	RIV
20	0.25	0.25	0.25	0.25	0.25	0.25	0.25	0.25	1.02	2.08	0.81	0.89	1.00	RIV
21	0.25	0.25	0.25	0.25	0.225	0.304	0.197	0.274	1.02	2.08	0.81	0.89	0.10	CONDBRS
22	0.25	0.25	0.25	0.25	0.225	0.304	0.197	0.274	1.02	2.08	0.81	0.89	10.00	CONDBRS

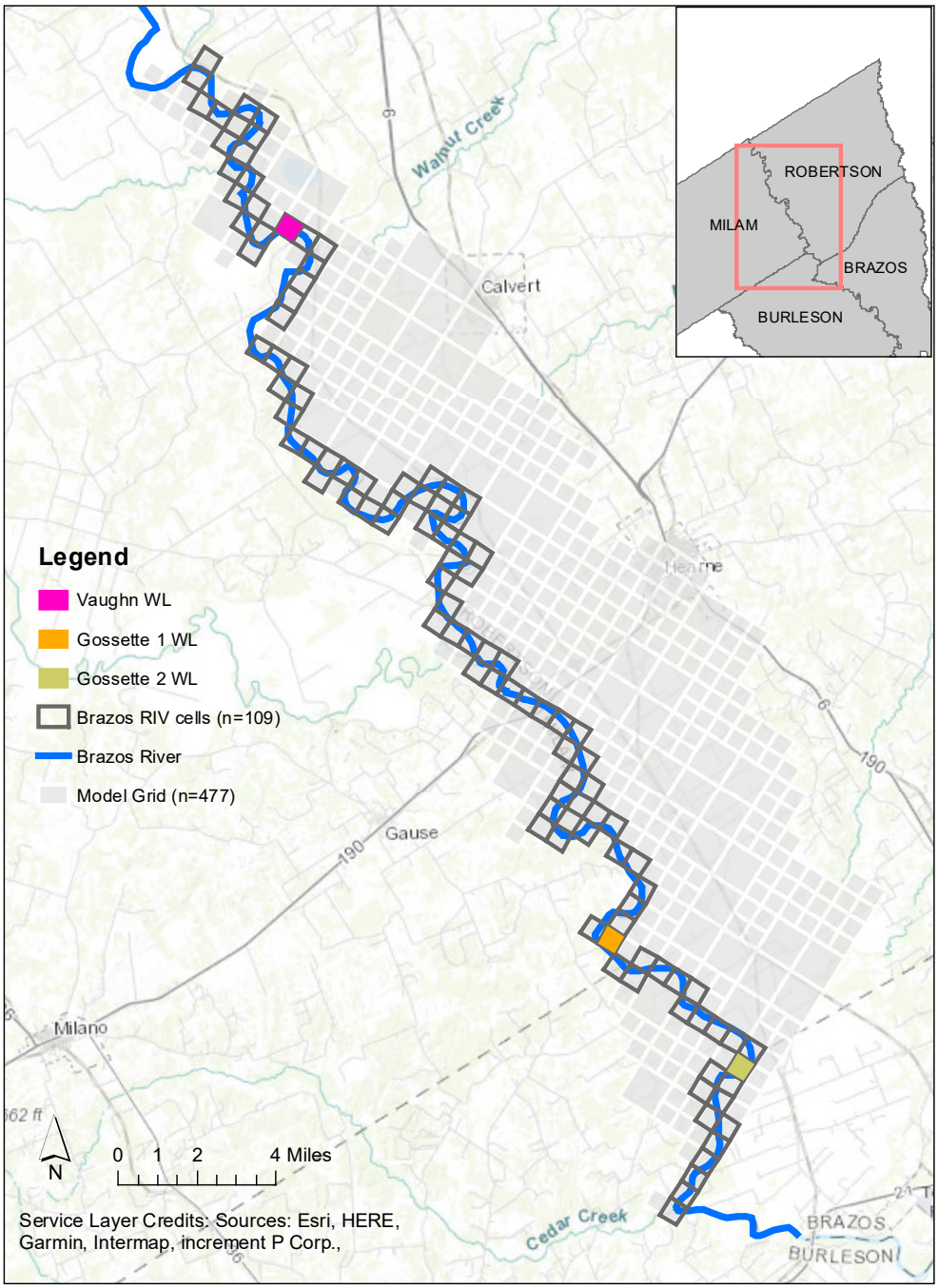

Figure 5.29 Site locations of RIV model cells evaluated with sensitivity analysis.

5.4.3.1 WEL package

Five different simulations were conducted to evaluate the impact of quarterly pumping factors on groundwater heads and riverbed flow. Two of these simulations served as bounding cases: the baseline model simulation, which utilized evenly distributed pumping factors, and a simulation

using pumping factors derived from remote sensing analysis. The other three simulations were defined by linearly interpolating the quarterly pumping factors between these two extremes.

Figure 5.30 and Figure 5.31 provide summaries of simulated groundwater heads and riverbed flow for the model nodes intersecting the Gossett 1 and Gossett 2 sites, respectively. At both locations, simulated groundwater head consistently exceeds the river stage specified in the RIV package, indicating that groundwater contributes to surface water. This is reflected in the negative riverbed flow. Simulated groundwater head responds to the quarterly pumping patterns in adjacent cells, with the highest levels observed during quarter 1 and the lowest during quarter 3. The effects of seasonal pumping manifest earlier at Gossett 1 compared to Gossett 2, suggesting earlier pumping activity in the vicinity of the Gossett 1 site. This observation aligns with the larger range of head fluctuations observed annually at Gossett 1.

Figure 5.32 compares the total river leakage for the 109 model cells intersecting the Brazos River within the area of interest over the entire span of the groundwater availability model simulation. Simulations with quarterly variations in pumping closely resemble the baseline simulation, exhibiting relatively minor fluctuations due to quarterly pumping patterns that intensify as pumping increases. Over the course of the simulation, the total simulated river leakage oscillates around 60 cubic feet per second for the first two decades, then transitions to approximately 45 cubic feet per second between 1960 and 2002. During the final decade of the simulation, contributions to groundwater from river cells decrease sharply to about 10 cubic feet per second. This decrease corresponds with the increased groundwater pumping in the area. For this set of simulations, intra-annual variability increased from zero to about 10 cubic feet per second. Overall, the introduction of groundwater pumping seasonality adds intra-annual variability while maintaining the same annual volume.

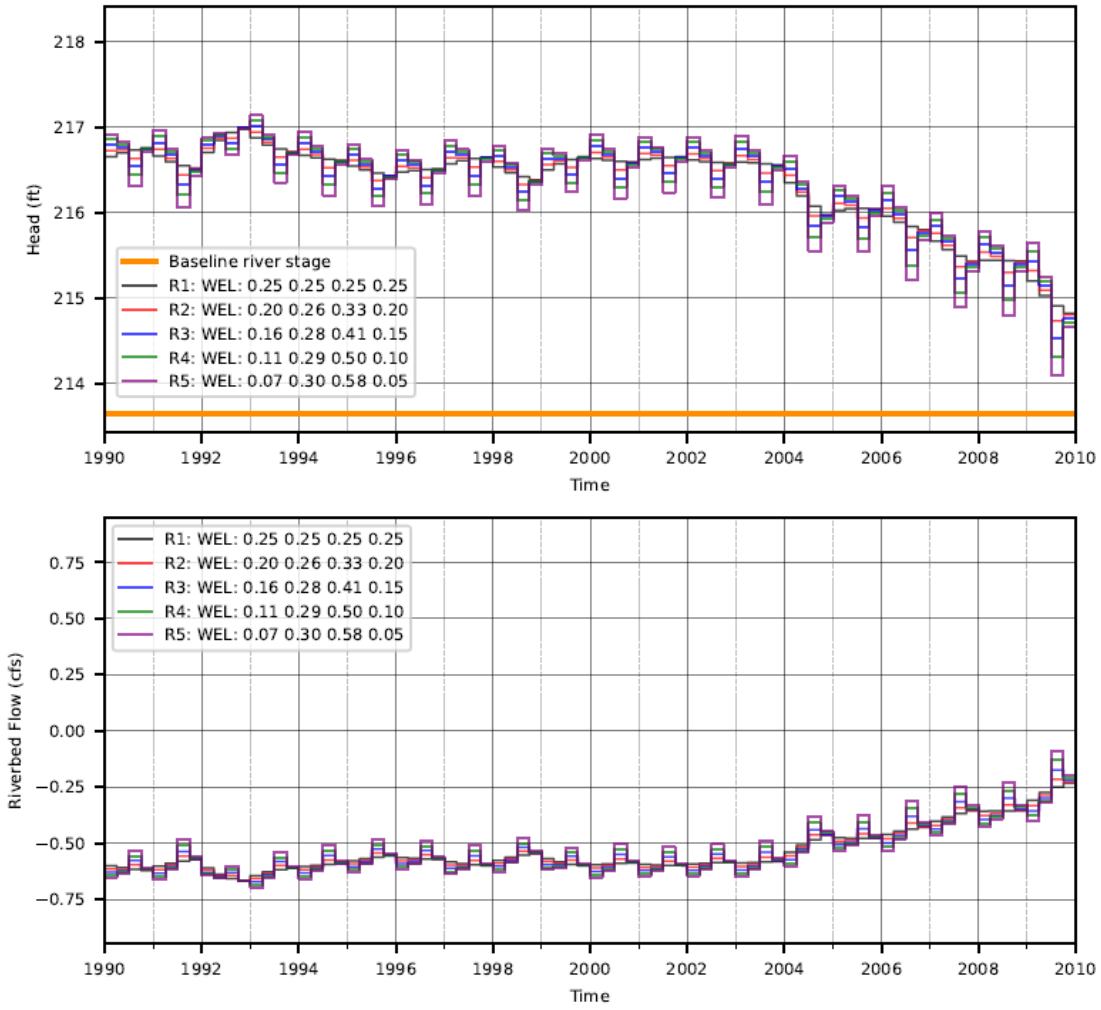

Figure 5.30 **Sensitivity to changes in quarterly pumping factors groundwater head and riverbed flow at Gossett 1 (Model Node 1916). Head units are in feet, and Flow units are cubic feet per second.**

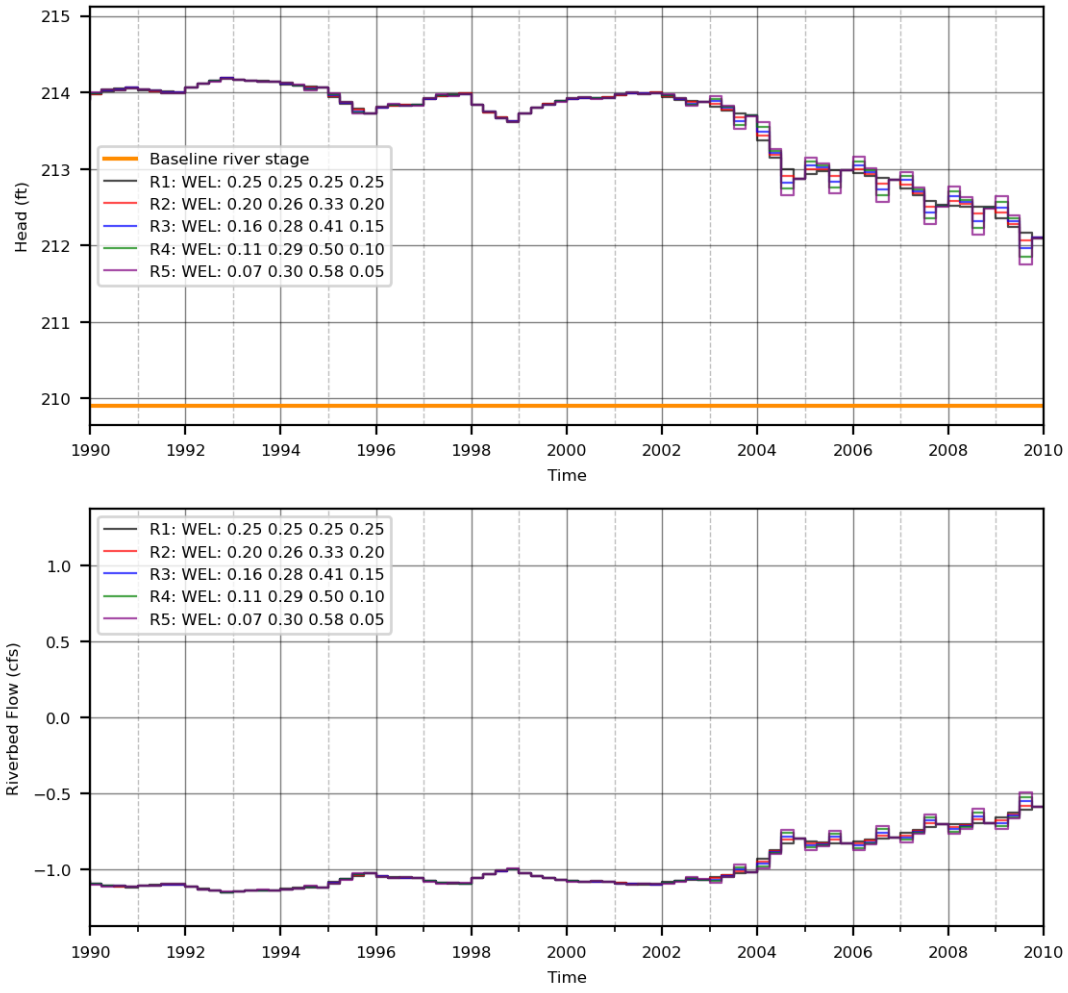

Figure 5.31 **Sensitivity to changes in quarterly pumping groundwater head and riverbed flow at Gossett 2 (Model Node 2204). Head units are in feet, and Flow units are cubic feet per second.**

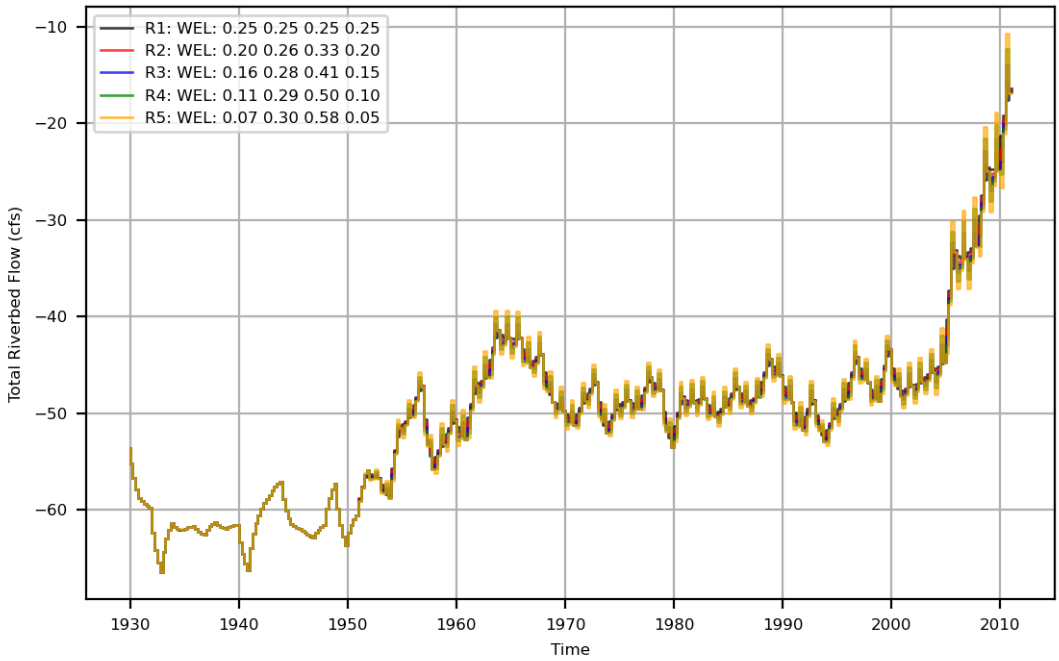

Figure 5.32 **Sensitivity of quarterly pumping factors to total river leakage in the area of interest. Units are cubic feet per second (cfs).**

5.4.3.2 RCH package

Quarterly recharge factors identified in Section 5.4.2.2 were applied to the RCH package throughout the entire groundwater availability model domain. Similar to the approach used for determining quarterly pumping factors, the quarterly recharge factors were specified by interpolating between two bounding cases: uniform recharge conditions and factors derived from precipitation record analyses. Results are presented in terms of groundwater heads and riverbed flow at selected sites, as well as total river leakage from cells intersecting the Brazos River.

As shown in Figure 5.33 and Figure 5.34, the model exhibits minimal sensitivity to quarterly recharge factors at the model node that contains the Gossett 1 site and the entire Brazos River reach within the area of interest. This outcome can be explained by the aquifer characteristics of the Brazos Alluvium, which differ significantly from the properties of underlying layers. The Brazos Alluvium demonstrates a strong dominance of lateral flow due to its high horizontal hydraulic conductivity (K_h), averaging around 322 feet/day, a vertical hydraulic conductivity (K_v) set at one-tenth of K_h, and a relatively high specific yield (S_y) of 0.2. These conditions reduce the influence of quarterly recharge variations on both groundwater heads and river leakage, leading to the minimal sensitivity observed.

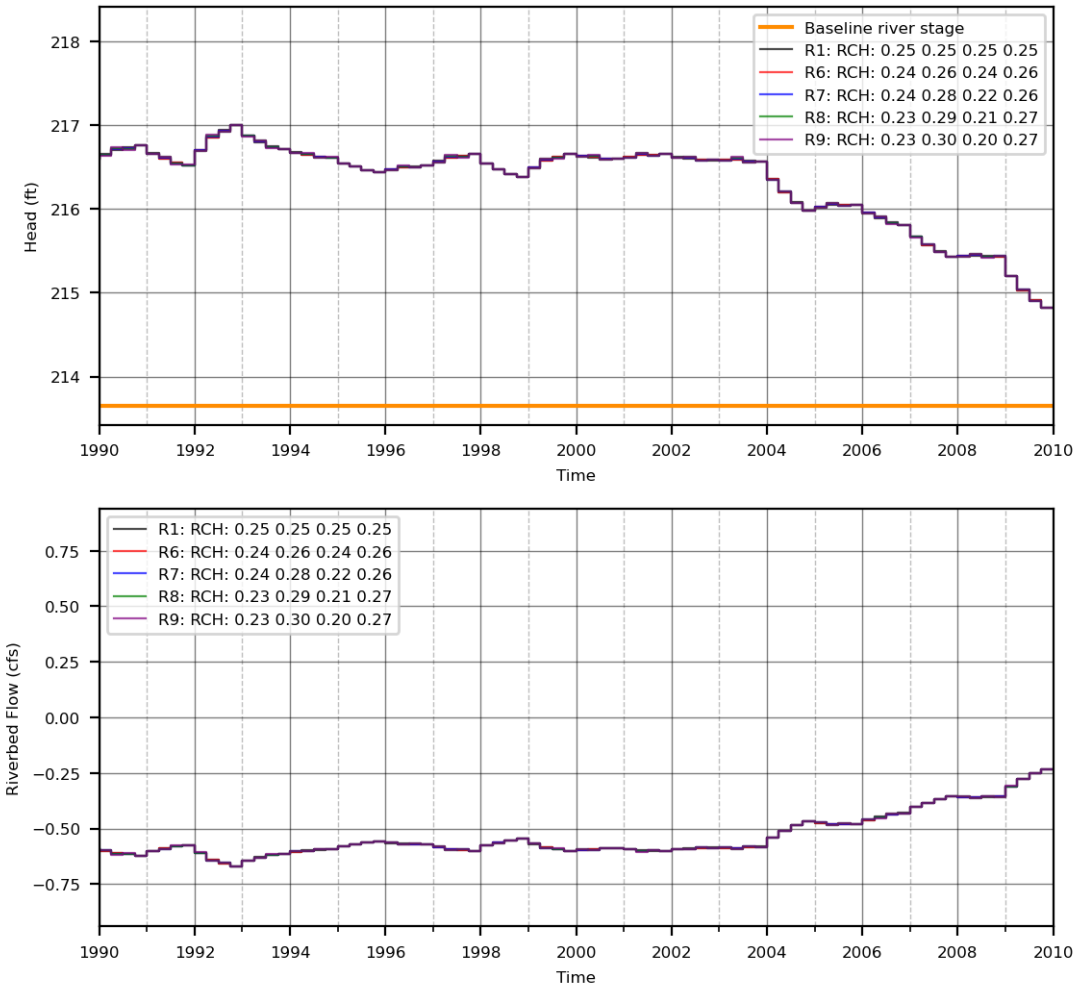

Figure 5.33 **Sensitivity to changes in quarterly recharge factors on groundwater head and riverbed flow at Gossett 1 (Model Node 1916). Head units are in feet, and Flow units are cubic feet per second.**

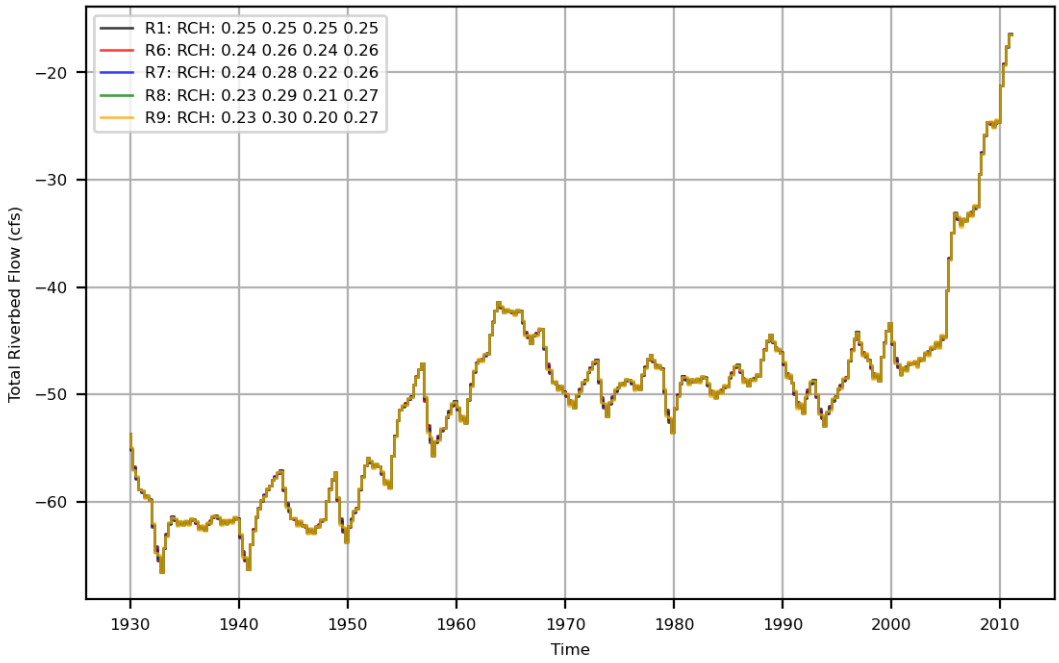

Figure 5.34 **Sensitivity of quarterly recharge factors to total river leakage in the area of interest. Units are cubic feet per second (cfs).**

5.4.3.3 River stage

Quarterly river stage factors identified in Section 5.4.2.3 were applied to the Brazos River cells along the area of interest. Similar to the approach used for determining quarterly pumping and recharge factors, the stage factors were specified by interpolating between two bounding cases: constant river stage conditions and quarterly factors derived from remote sensing analysis and streamflow records. As shown in the previous two sections, the results are presented in terms of groundwater heads and riverbed flow at selected model nodes, as well as total river leakage from cells intersecting the Brazos River.

Results at the model nodes intersecting Vaughn and Gossett 1 sites are presented in Figure 5.35 and Figure 5.36, respectively. Both sites exhibit a quarterly variation of groundwater head consistent with the quarterly variation introduced with the quarterly variation of the stage. The effect of quarterly changes on river stage impacts the magnitude and direction of river leakage. In the case of the Vaughn model node, the quarterly variation reverses the direction of the riverbed leakage during the second quarter for all years shown, while in the Gossett 1 model node reversals of the riverbed leakage only occur in the last three years of the simulation. Note that the corresponding river stage for each simulation is not shown here, only the baseline river stage. Figure 5.37 shows an additional sensitivity to river state while using the best seasonal estimates for pumping and recharge, in this case the intra-annual variability of groundwater head increases and shows more significant low values during quarter 3 where pumping is higher, and river stage is the lowest. The intra-annual variability of the riverbed is slightly smaller than the one seen while the

constant pumping and shows a different ranking of the flows during quarter 3 which emphasizes the need of including pumping to reproduce seasonal behaviors in the area of interest.

Figure 5.38 presents the total river leakage for Brazos River cells in the area of interest. In this case the quarterly variation of stage results in much larger fluctuations of total river leakage flow when compared to the effect of seasonality on pumping and a net reversal of direction of the flow during the last three years of the simulation and an intra-annual variability around 60 cubic feet per second. The seasonal variability of river stage results in a much larger impact on intra-annual variability than the one seen by changing seasonal pumping factors.

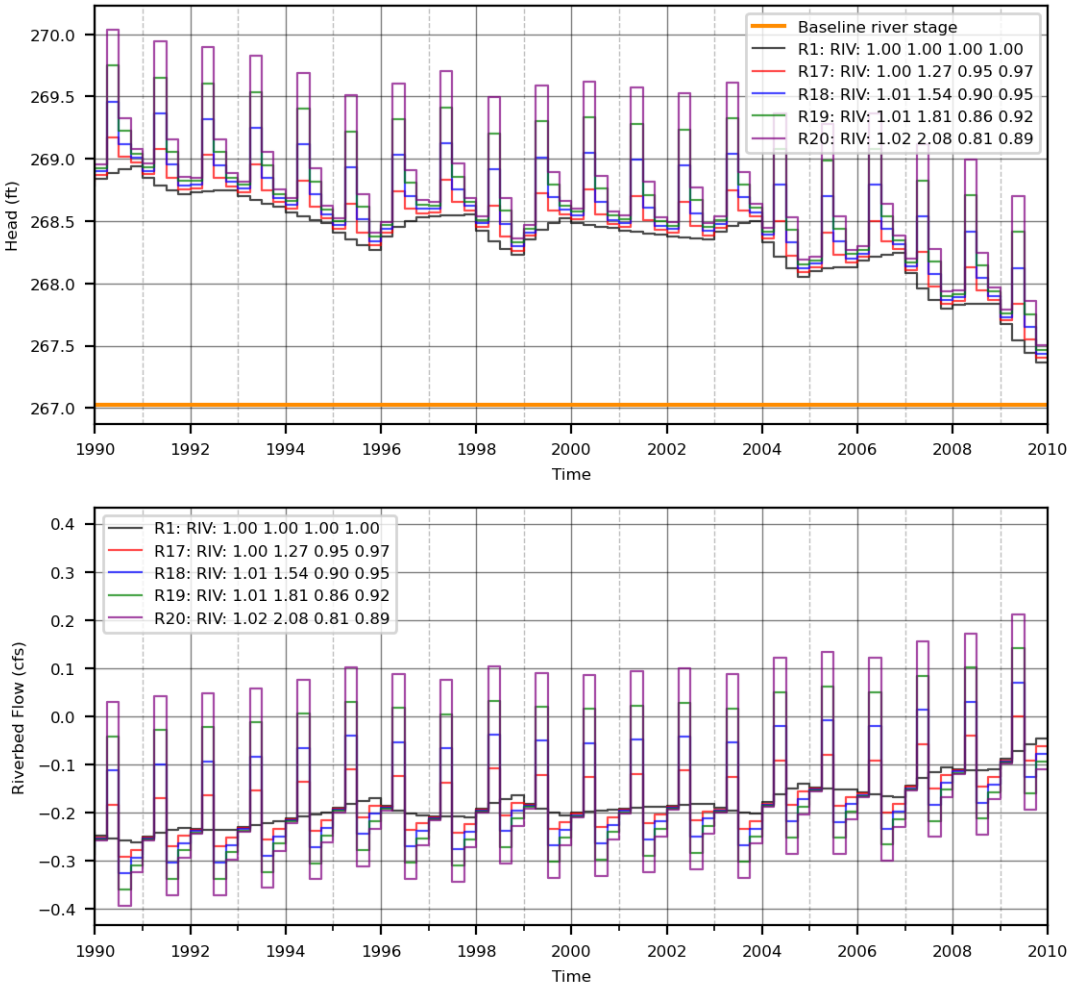

Figure 5.35 **Sensitivity to changes in quarterly river stage factors on groundwater head and riverbed flow at Vaughn (Model Node 556). Head units are in feet, and Flow units are cubic feet per second.**

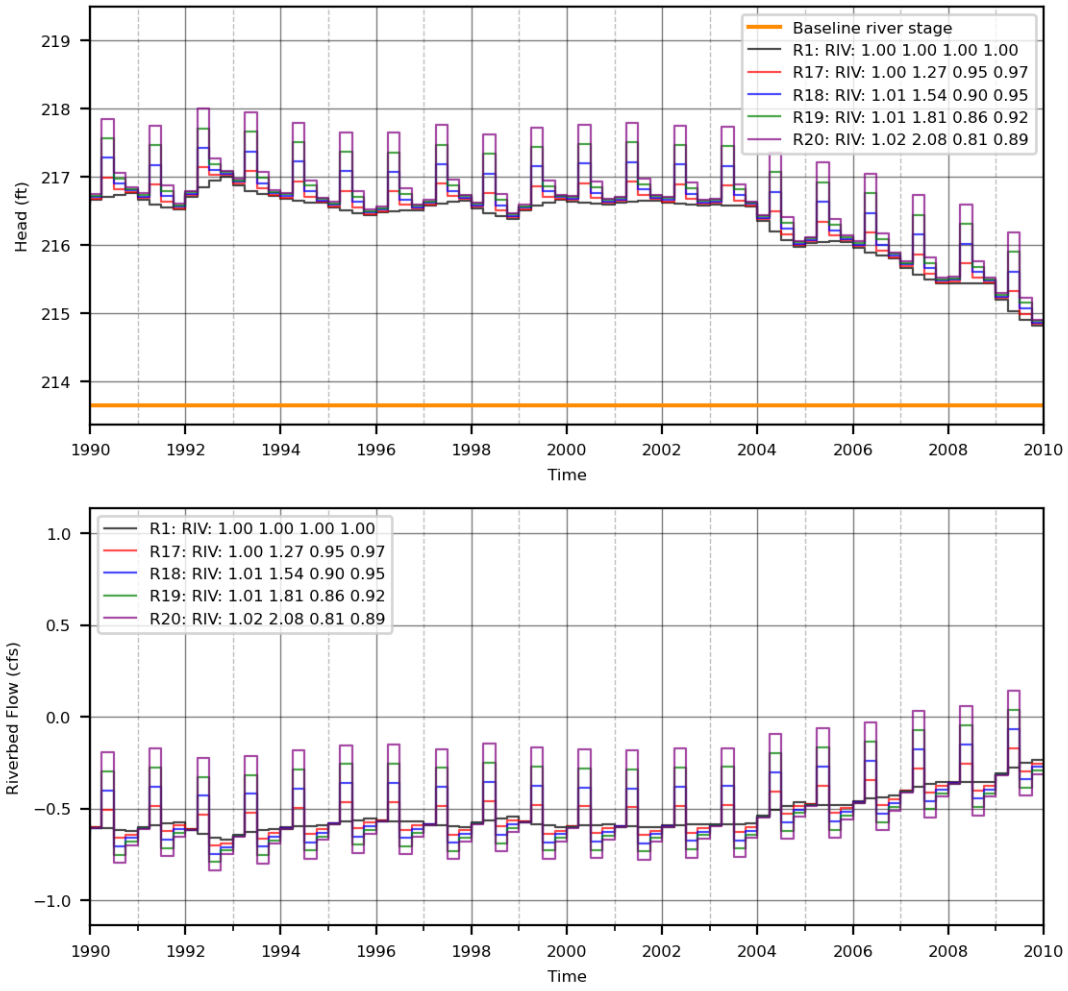

Figure 5.36 **Sensitivity to changes in quarterly river stage factors on groundwater head and riverbed flow at Gossett 1 (Model Node 1916). Head units are in feet, and Flow units are cubic feet per second.**

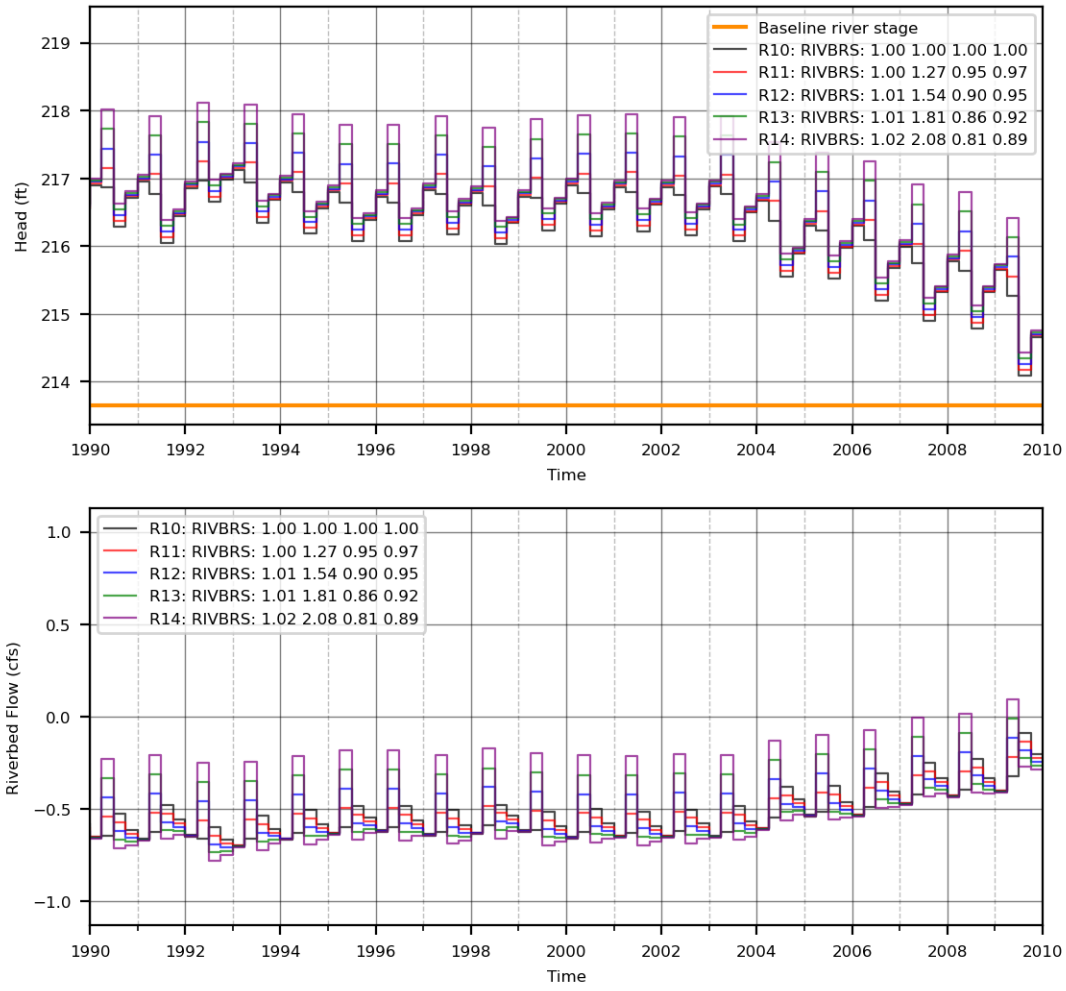

Figure 5.37 **Sensitivity to changes in quarterly river stage factors using seasonal pumping factors on groundwater head and riverbed flow at Gossett 1 (Model Node 1916). Head units are in feet, and Flow units are cubic feet per second.**

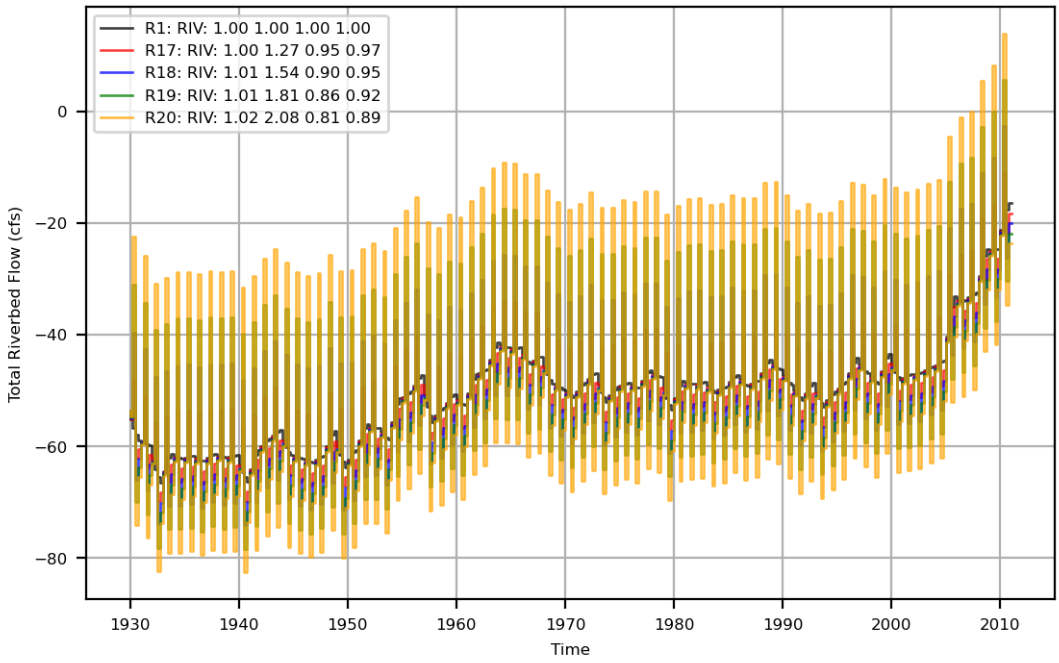

Figure 5.38 **Sensitivity of quarterly river stage factors to total river leakage in the area of interest. Units are cubic feet per second (cfs).**

5.4.3.4 Riverbed conductance

To evaluate the impact of river conductance, the original parameter values for the Brazos River in the area of interest were adjusted by a factor of ten in both the upward and downward directions. Two sets of conditions were considered:

1. Uniform quarterly factors: Pumping, recharge, and river stage were each varied by the same factor for all quarters (analogous to an annual time-step simulation).
2. Variable quarterly Factors: Pumping, recharge, and river stage were modified according to quarterly parameters derived from the seasonality analysis described in Section 5.4.2.

Under the uniform quarterly factors scenario (Figure 5.39), the baseline conductance scenario produces heads that fall between those of the bounding conductance values. From the early 1990s through 2004, the lower conductance factor (0.1) results in substantially higher head values compared to the baseline, while the upper conductance factor (10.0) leads to slightly lower head values than the baseline case. In contrast, under the variable quarterly factors scenario (Figure 5.41), the upper conductance simulation shows much greater fluctuations in water levels compared to both the baseline and lower-bound conductance simulations. This increased variability is tied to the seasonal adjustments of pumping and river stage. With respect to total river leakage (Figure 5.40 and Figure 5.42), both scenarios display a similar central tendency for each conductance value. However, the variable quarterly factors introduce a far greater degree of intra-annual variability in the fluxes. This outcome underscores the importance of incorporating seasonal variations in river seasonal changes in pumping when developing groundwater availability models that may be used to help evaluate groundwater-surface water interactions.

The elements presented in this sensitivity analysis illustrate the significant effect that seasonality has on: 1) the magnitude and direction of the exchange between the Brazos River and the Brazos River Alluvium; and 2) the variables that are used by the MODFLOW River Package to predict groundwater-surface water interaction. The incorporation of seasonality and any temporal discretization must be guided by an understanding of the main drivers in the area of investigation. The results from the sensitivity analysis suggest that inset models with refined grid spacing and smaller time steps than the groundwater availability model may be useful for understanding seasonal impacts for years where extreme values in the river stage and pumping occur. Selected timed periods for investigation should contain sufficient extreme conditions to capture the key aspects of the system.

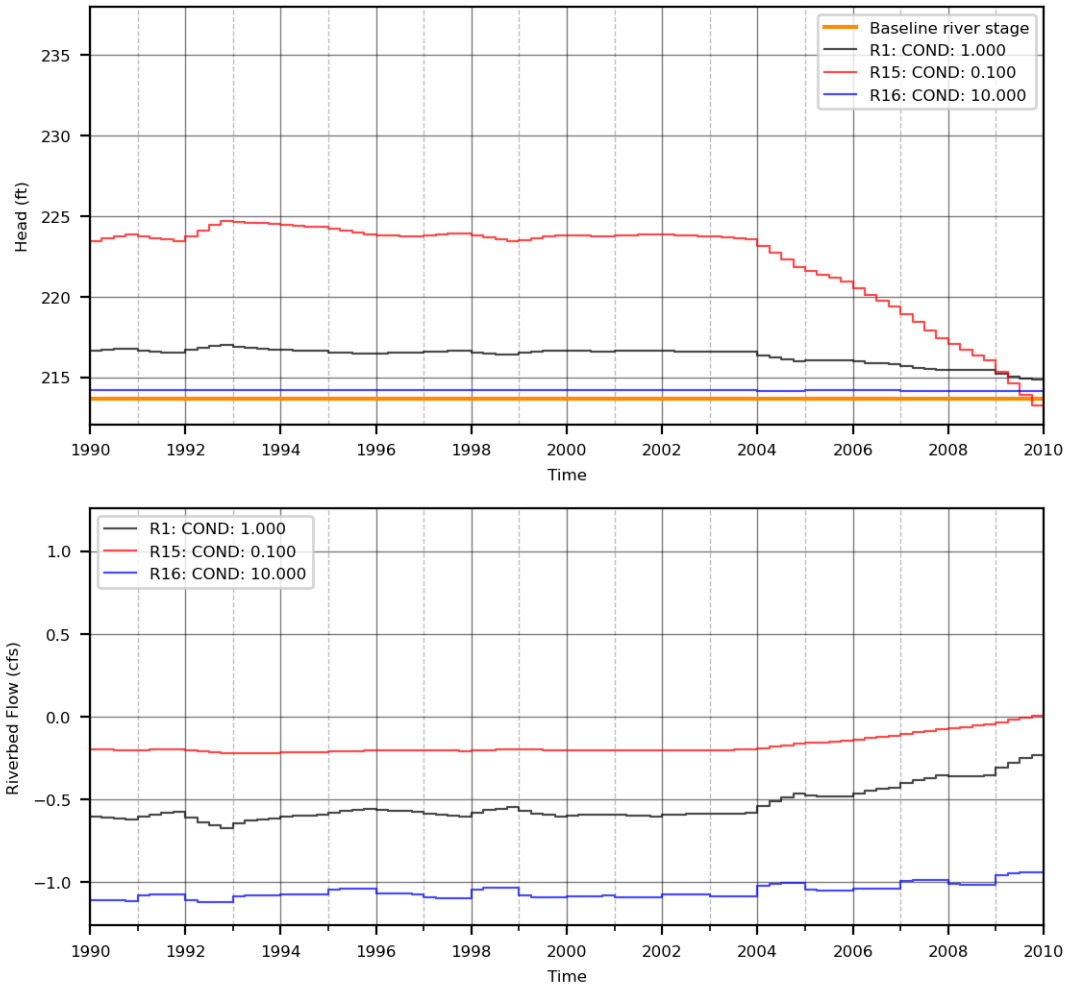

Figure 5.39 **Sensitivity to changes in conductance factors on groundwater head and riverbed flow at Gossett 1 using mean annual parameters (Model Node 1916). Head units are feet, and Flow units are cubic feet per second.**

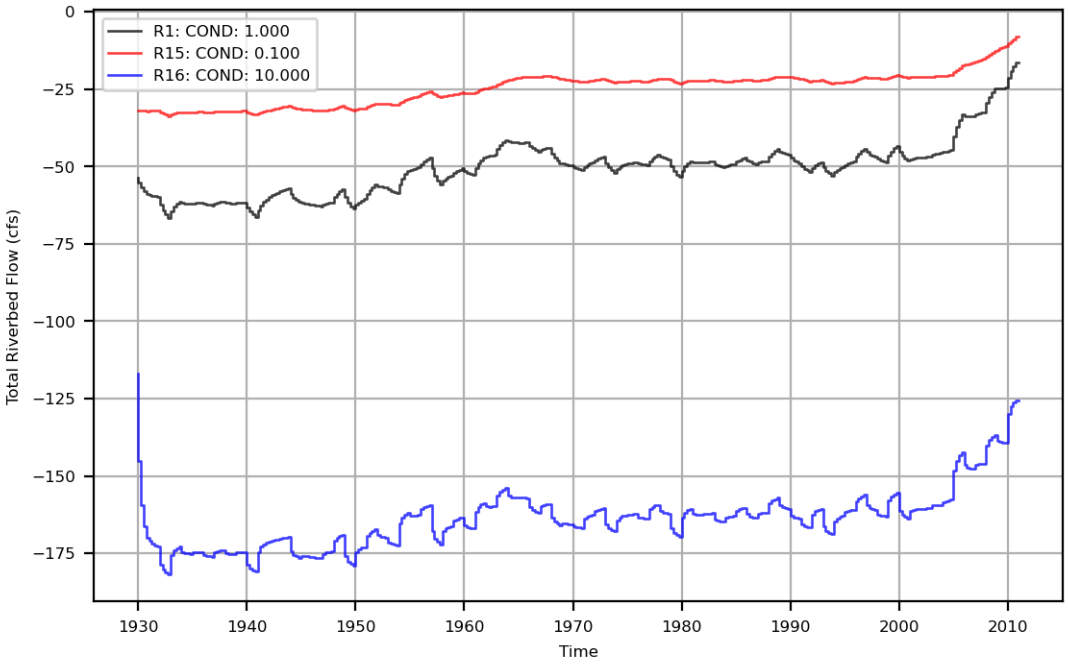

Figure 5.40 **Sensitivity of conductance factor to total river leakage in the area of interest using mean annual parameters. Units are cubic feet per second (cfs).**

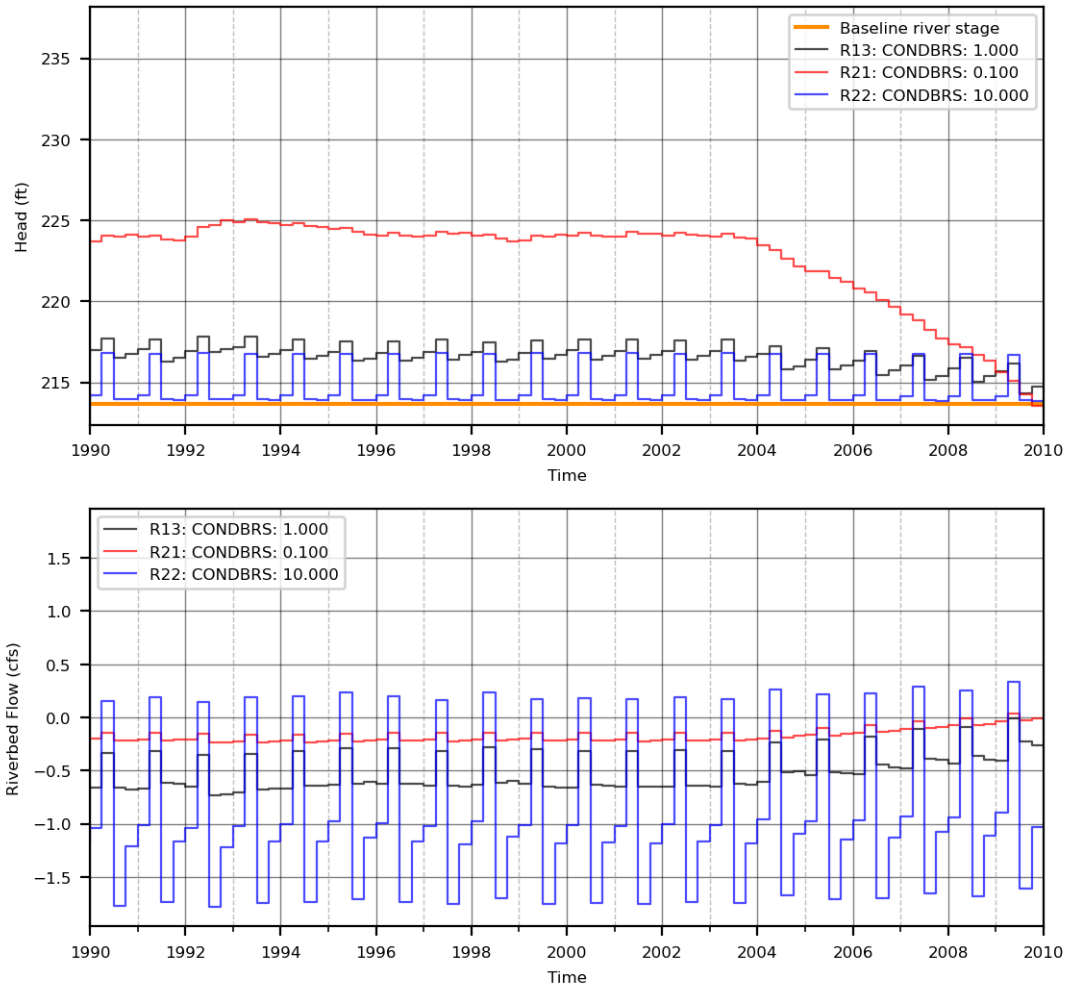

Figure 5.41 **Sensitivity to changes in conductance factors on groundwater head and riverbed flow at Gossett 1 Model Cell 1916 using estimated quarterly factors from remote sensing and climate data for WEL, RCH and RIV packages (Model Node 1916). Head units are feet, and Flow units are cubic feet per second.**

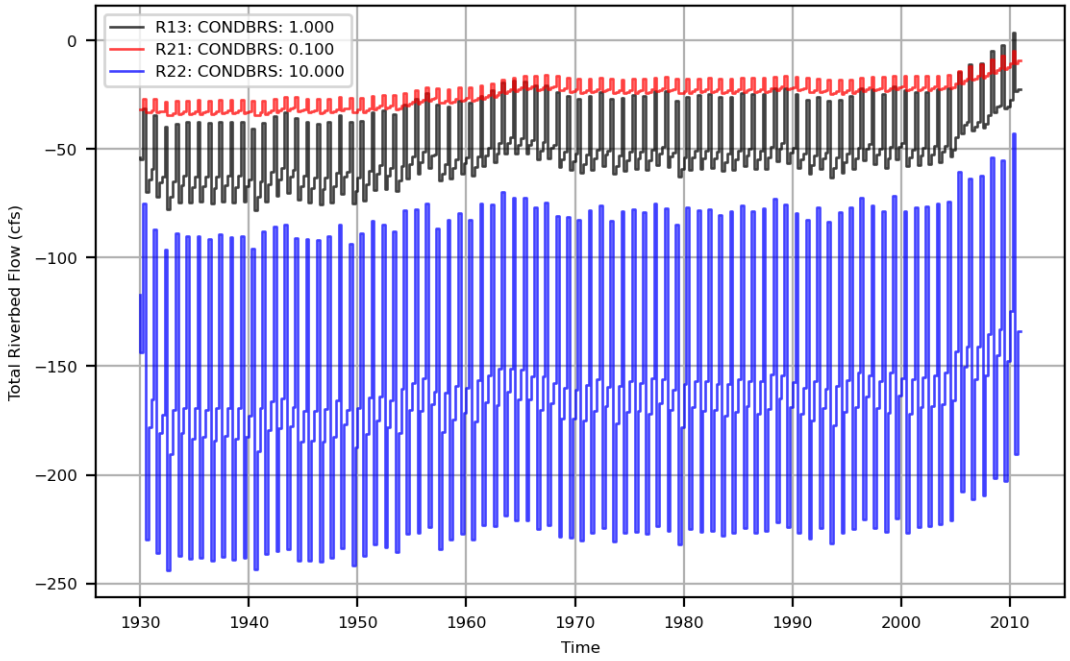

Figure 5.42 **Sensitivity of conductance factor to total river leakage in the area of interest using estimated quarterly factors from remote sensing and climate data for WEL, RCH and RIV packages. Units are cubic feet per second (cfs).**

5.5 Groundwater availability model calibration approach using remote sensing data

To properly calibrate a model so that it provides useful predictions of groundwater-surface water interactions requires several types of information. This information includes the following items:

1. Equations that provide credible predictions of groundwater-surface water interactions measured based on the properties/parameters of the river and aquifer system that can be measured and appropriately quantified.
2. Water budget analysis of the selected areas of interest to evaluate the magnitude of groundwater-surface water interactions and the level of temporal and spatial detail required to understand seasonal variability and evaluate the assumptions in Item 1.
3. Reliable measurements of the flow rates between rivers and groundwater along known river reaches at a scale and accuracy consistent with Item 2.
4. Field methods for measuring river and aquifer properties/parameters in Item 3 that determine groundwater-surface water interactions from the equation associated with Item 1.
5. Measurements of the river and aquifer properties/parameters when measurements of groundwater-surface water interaction were made as part of Item 4.
6. Estimates of how the river and aquifer properties/parameters would change over time as a result of intra-annual and inter-annual changes caused by anthropogenic factors such as pumping and natural conditions such as precipitation.

Item 1 is outside of the scope of the study as these equations are a part of the MODFLOW suite of codes used by the TWDB to develop the groundwater availability models. For the groundwater availability model used in this study, these equations are embedded in the MODFLOW River Package discussed in Section 3.1.2. Section 3.3 presented a detailed analysis of the water budget to address Item 2. The water budget analysis was also used to compare and evaluate the results of the sensitivity analysis. Within the last two decades, the development and calibration of the groundwater availability models have relied on river gain-loss studies to address Item 4. This study did not successfully demonstrate a remote sensing method to replace the river gain-loss studies. However, this study did successfully demonstrate several innovative remote sensing methods that can improve in gathering of data to satisfy Items 4 through 6.

A limitation of the remote sensing data is that it is only available in recent years. For instance, the SWOT data only became available for the area of interest in 2023 and OpenET is only available since 2016. Given this limitation, a sensible approach to improving the calibration of the groundwater availability model is to use the remote sensing data to 1) augment the data collection during future gain-loss studies for river stage and groundwater pumping; and 2) develop seasonal factors to help estimate the seasonal and yearly changes in the model parameters and variables used to estimate groundwater-surface water interactions.

6. Discussion and Recommendations

There is increasing use of remote sensing in the management and monitoring of water resources globally and in Texas. Sensors are deployed on satellites, by both government agencies such as the National Aeronautics and Space Administration and private entities, but also on airplanes and drones. By providing valuable data on the distribution, quality, and dynamics of water bodies – both surface water and groundwater – the promise of more accurate and higher temporal and spatial resolution remote sensing data in the future is extremely promising for water resources managers. The groundwater availability model program at the TWDB regularly improves the groundwater availability models it develops and manages, incorporating additional complexity of groundwater-surface water interactions require increased intra-annual resolution. Remote sensing can be a cost-effective method to help incorporate information about seasonal cycles.

This research effort was focused specifically on remote sensing tools and products for the identification and quantification of groundwater-surface water interaction. While the technology is promising, and this report shows which approaches and sensors are most useful, it is obvious that the interaction between the Brazos River and the Brazos River Alluvium Aquifer is highly complex. The aquifer is not uniform in its physical characteristics, with water-bearing alluvial sediments up to seven miles wide, stretching for some 350 miles from north of Waco to the Gulf Coast. The Quaternary alluvial sediments consist of clay, silt, sand, and gravel, each of which has very different hydraulic properties. The saturated thickness of the alluvium can be as much as 85 feet. The electromagnetic survey that will likely be sponsored by the TWDB in the near future promises to provide a better understanding of the heterogeneity and hydraulic properties of the Brazos River Alluvium Aquifer in the near future. Revised gain-loss for corresponding reaches addresses all significant inputs and output terms in the gain-loss equation are also needed. This will help refine the groundwater availability model by improving the understanding of heterogeneity and addressing the challenges of integrating finer resolution data at the regional scale, potentially by defining models that focus on selected portions of the aquifer and supporting better geostatistical representations of its alluvial deposits.

6.1 Fieldwork

The flow in the lower Brazos River is highly variable – the river experienced flows between 128 and over 52,000 cubic feet per second during the study, with the corresponding water surface elevation fluctuating by some 25 feet. Field work was a challenge with the river inaccessible by boat for most of the project duration. The river is very dynamic and during the summer of 2024 high flows scoured out some of the team's equipment and buried other sites under several feet of sediment. The river itself looks very different now, after the summer floods, compared to what it looked like when the equipment was installed and flow measurements were taken. Beyond river access, this is another reason US Geological Survey streamgages are usually located at or near bridges, where equipment can be safely secured. In fact, the US Geological Survey is moving towards the use of radar sensors attached to these bridges for estimating water surface elevation and surface water velocity so that they can keep their equipment completely out of the water. Scientists building on the work presented in this report should consider installing radar-based water surface elevation sensors to *all* of the bridges crossing the river and tributaries and leaving them deployed for at least three years

or periods with sufficient hydrologic variability. Aqua Strategies also recommends more extensive monitoring of groundwater levels, particularly in wells near the river.

6.2 Remote sensing

Recent developments in satellite- and drone-based remote sensing technology have led to rapid improvement in the spatial and temporal resolution of available data. Satellite constellations like the Surface Water Ocean Topography mission and Planet Scope provide regular (i.e. daily to bi-weekly), precise water surface elevations and optical imagery, respectively, while drones offer controlled timing of data collection and a wide variety of sensor types. Furthermore, advances in data processing techniques allow for existing remote sensing datasets to be leveraged in new ways.

This study has evaluated a variety of satellite- and drone-based remote sensing data to assess their applicability to quantifying groundwater-surface water interactions and specifically whether remote sensing data can be incorporated into existing groundwater availability models, along with direct measurements of water flux through thermal signatures and stream discharge variation. Table 6.1 below lists evaluated data products, recommended uses of the data, and any additional comments.

In sum, both satellite- and drone-based remote sensing products demonstrate significant potential for improving the understanding and measurement of groundwater-surface-water interactions. Remote sensing data can be incorporated into existing groundwater availability models in three ways which are actionable now using existing public data and scalable throughout the state without need for additional field efforts:

- Defining RIV cells in the groundwater availability models based on observed surface water occurrence in optical satellite imagery
- Estimating pumping seasonality based on precipitation, crop type, and actual evapotranspiration
- Estimating hydraulic heads for large rivers and lakes to define hydraulic gradients between groundwater and surface water, improving the representation of groundwater-surface water interactions.

In terms of directly measuring volumes or the influence of groundwater-surface water flux, new remote sensing data products show a great deal of promise, but the analyses herein indicate systemic bias and error require further study to calibrate them for local conditions.

Table 6.1 Summary of satellite data products evaluated.

Data Product	Uses	Comments
Landsat Collection 2 DSWE	Modeling water occurrence for RIV cells	Few days with cloud-free imagery; water extents less accurate than Sentinel 2 due to lower spatial resolution. https://www.usgs.gov/landsat-missions/landsat-collection-2-level-3-dynamic-surface-water-extent-science-product
Sentinel 2 Level-2A	Modeling water occurrence for RIV cells	Few days with cloud-free imagery, although more than Landsat; water extents quite accurate when using a calibrated Modified Normalized Difference Water Index threshold but few overlaps with Surface Water Ocean Topography makes data fusion challenging. https://docs.sentinel-hub.com/api/latest/data/sentinel-2-l2a/
OpenET	Determining pumping seasonality (estimating actual evapotranspiration)	Only monthly average data available in raster format. Of the several evapotranspiration models, eeMETRIC is most appropriate for this use case and region. https://developers.google.com/earth-engine/datasets/catalog/OpenET_EEMETRIC_CONUS_GRIDMET_MONTHLY_v2_0
US Department of Agriculture Cropland Data Layer	Determining pumping seasonality (filtering areas with irrigated agriculture)	Updated on an annual basis, data is available at a 10-m resolution starting in 2024. Earlier data is at a 30-m resolution.
gridMET	Determining pumping seasonality (estimating precipitation volume)	Daily data at a 4-km spatial resolution. https://developers.google.com/earth-engine/datasets/catalog/IDAHO_EPSCOR_GRIDMET
Surface Water Ocean Topography Mission	Estimating discharge (measuring water surface elevations)	Water surface elevations are relatively accurate, but channel width values are inaccurate unless averaged over a long (>10km) reach. Elevations use the EGM2008 geoid
PlanetScope	Validating surface water extents	Commercial imagery must be purchased; highest resolution available on a regular basis, so useful for validating other datasets; more cloud-free imagery than Landsat or Sentinel because of daily acquisitions, but majority of days are still cloudy; cannot use Modified Normalized Difference Water Index because of lack of Short Wave Infrared band

6.2.1 Use of remote sensing data in existing groundwater availability models

Use of Water Occurrence to Improve RIV Cell Locations

In groundwater availability models, RIV cells are assigned to model cells that intersect a river's surface water. In many cases these assignments are inaccurate because they are based on older maps and do not account for the variability in surface water extents. A Google Earth Engine script was developed for this study which iterates over thousands of satellite images, classifying the presence or absence of surface water and calculating the percentage of the time surface water is present at each pixel. Versions of the script were developed for both Landsat (30-m x 30-m) and Sentinel 2 (10-m x 10-m) data. These scripts provide an automated, empirical method for assigning RIV cells which are easy to implement and improve the spatial parameterization of the groundwater availability model. They could also be modified to provide annual or decadal models of water occurrence from 1972 (start of the Landsat program) to the present, to account for lateral shifts in the river. The same scripts can be used with any input region, allowing it to be quickly scalable to other river basins. In combination with grid refinement of the RIV cells, this application should improve the ability of a groundwater availability model to model groundwater-surface water interactions.

Use of OpenET to Estimate Groundwater Pumping Seasonality

Groundwater pumping from the Brazos River Alluvium due to agriculture can be estimated from the crop demand determined from actual evapotranspiration that is balanced by precipitation, surface water diversions and groundwater pumping. OpenET provides an accurate estimate of monthly actual evapotranspiration on a 30-m x 30-m spatial scale and daily estimates of precipitation at a 4-km scale are available from gridMET. Both these datasets can be retrieved from Google Earth Engine and in combination with the US Department of Agriculture Cropland Data Layer, it is possible to approximate the seasonality of groundwater pumping in each location. Because groundwater pumping for irrigation is the largest influence on groundwater-surface water flux along most reaches of the Brazos River, this data on seasonality provides a basis for how to refine groundwater pumping in the groundwater availability model from an annual to monthly or semi-annual time step.

As for water occurrence and the RIV cells, all three datasets for estimating pumping seasonality are public and freely available. The workflow is also conducive to automated scripting and could be applied in other reaches and basins with significant groundwater pumping. In this study, Google Earth Engine scripts were used to batch download OpenET and gridMET data, and to average actual evapotranspiration values for each month within agricultural fields. Much of the intermediate processing and calculations were done manually but could be automated as well. However, the process would need to be modified in areas with more surface water diversions for irrigation to account for those additional inputs to irrigation.

Use of Surface Water Ocean Topography (SWOT) water surface elevations to characterize river stage

In the MODFLOW RIV package, river stage is a required variable for the simulation of flow between river and aquifer. Stage has been difficult to estimate due to insufficient data – stage must be continuously estimated across all RIV cells, and gages are generally spaced widely apart. As a result, stage is typically estimated by assuming an average depth, which is added to any available data on river bottom elevations.

Because Surface Water Ocean Topography regularly measures water surface elevations at a high spatial resolution (~ 50 m grid, averaged to nodes every 200 m), it allows for empirical observations of river stage in ungaged reaches. Furthermore, the regular return interval (1-2 weeks) provides numerous samples per quarter. River stage seasonality can thus be characterized by quarter. These estimations could be further refined with further calibration and quality control of Surface Water Ocean Topography elevation data.

6.2.2 Direct measurement of groundwater – surface water flux

The potential spatial and temporal resolution of remote sensing data is orders of magnitude higher than the groundwater availability model cells (1 square mile) and time-steps (annual) and therefore offer much more detail into groundwater-surface water patterns in space and time. The two primary remote sensing methods assessed herein were (1) using variations in remotely sensed discharge estimates from Surface Water Ocean Topography satellite data to quantify gain and loss and (2) detecting the thermal signatures of groundwater seepage with drone-mounted sensors to identify gaining reaches.

Satellite Remotely Sensed Discharge

Satellite-based estimation of river discharge is the purpose of the recent Surface Water Ocean Topography mission, which began publishing preliminary data at the end of 2023. Although no discharge estimates have yet been published, reported water surface elevations from Surface Water Ocean Topography show an unprecedented accuracy when compared to existing satellite-based altimeters (Normandin and others, 2024). However, there are two main limitations to the use of Surface Water Ocean Topography data in understanding groundwater-surface water interactions:

1) Error in water surface elevation measurements – Although the Surface Water Ocean Topography Ka-band radar can measure elevations more accurately than previous satellite-based altimeters, analysis from the current study has shown that the observed error is still generally 20 cm or greater. This magnitude of error is too high to estimate discharge at the level of precision necessary to quantify groundwater-surface water flux.

2) Coarse spatial resolution in discharge estimations – Surface Water Ocean Topography estimates discharge at the scale of 10 km reaches, because the horizontal resolution of the sensor requires averaging over this length to approximate the actual width. To quantify groundwater-surface water flux, the scale of discharge estimations would need to be significantly finer, thus requiring another method of determining channel width and cross-sectional area.

The analysis herein showed that much of this error was systemic, meaning that Surface Water Ocean Topography elevations showed a consistent bias when compared to field observations, rather than random error due measurement limitations of the sensor. Although field sites showed root mean square errors of 20-50 cm, 70-95% of that error was systematic. These consistent biases indicate that Surface Water Ocean Topography data can likely be made more accurate through local calibration. Whether the error can be reduced enough to measure groundwater flux is unclear and requires further study.

Calculations of river discharge rely on values for slope, channel geometry, and roughness. The principal innovation of Surface Water Ocean Topography is the ability to precisely measure water surface elevations and therefore derive slope. To improve Surface Water Ocean Topography estimates of channel geometry or roughness will require synthesis with other datasets to characterize discharge variations at a fine scale. Optical satellites like Planet Scope and Sentinel-2 showed better results at channel width measurements, but are of limited use in humid, cloudy regions like the study area. Furthermore, the fly-over times of Surface Water Ocean Topography and other satellites may be offset by 10-20 hours in some cases, during which discharge may have changed significantly.

Ultimately, high resolution bathymetric data in combination with remote sensing data will likely be necessary to estimate discharge at the scale needed for quantifying groundwater flux. If channel bathymetry is mapped (for example, using green LiDAR or side-scanning sonar), this terrain surface can be "filled in" up to the level of Surface Water Ocean Topography water surface elevations in desktop geographic information system software. If the bathymetric surface is up to date, the resulting surface water extents will show accurate channel widths and cross-sectional areas. These models would provide higher resolution than optical satellite imagery, and therefore better represent the actual wetted extent. This is especially true where bankline vegetation obscures the wetted edge from optical satellites. A further advantage is that both slope and channel geometry would be calculated using the same set of Surface Water Ocean Topography elevations, rather than elevations and water extents from different times in the day.

More details on a data fusion approach to remotely sensed discharge are provided in Section 6.4.

Thermal Signatures

The relatively cool water temperature of groundwater can indicate the presence of seepage and gaining reaches and to some degree its magnitude, but methods for quantifying volumes of flux are not well established. Interpretation of drone collected thermal data was difficult due to a low signal to noise ratio and the increase of surface temperatures due to diurnal effects throughout the drone flights. Several reaches of ¼ to ½ mile showed cooler temperatures than upstream or downstream in both spring and summer datasets, however it is difficult to say with confidence that this represents seepage into the channel.

If future thermal data collection is conducted, it is recommended that water temperatures also be collected deeper in the water column with a boat-mounted sensor, which is less subject to the influence of glare, sun angle and shading. Additionally, the effect of diurnal temperature cycles should be controlled by continuously measuring temperatures at one or more static points throughout the data collection process.

6.3 Improving groundwater modeling

The groundwater availability model analysis presented in previous sections demonstrates the potential of remote sensing methods in groundwater availability models. By incorporating quarterly factors for pumping, recharge, and river stage derived from remote sensing and hydroclimatic data, the analysis demonstrates how these variables influence groundwater heads and riverbed flows at intra-annual scales. The study shows that variations in pumping and river stage introduce significant intra-annual and seasonal variability, highlighting the necessity of incorporating such

temporal changes to improve model simulation and calibration. Remote sensing can provide data that enhances the representation of seasonal behaviors and informs the estimation of model parameters.

Remote sensing offers consistent, spatially extensive datasets that can supplement limited field measurements, such as groundwater pumping or surface water elevation, in areas where observational data may be sparse or temporally inconsistent. This approach not only enhances the development of groundwater availability models but also establishes a framework for leveraging remote sensing as a cost-effective, scalable, solution to improve the integration and synthesis of hydrological data, facilitating an integrated understanding of hydrologic systems where groundwater availability models represent the groundwater component.

Increasing the temporal resolution in the groundwater availability model can be paired with finer spatial discretization as local information becomes available, taking advantage of MODFLOW 6's capabilities to support multiple models with local grid refinement (Langevin and others, 2024). These refined models can be applied over shorter periods that exhibit large variability in surface water–groundwater flow conditions, enabling detailed evaluations of changes in groundwater-surface water flow while reducing computational burdens. The effectiveness of these models can be further enhanced by continued expansion and standardization of river gain-loss datasets, such as those presented by Slade and others (2002).

As discussed in Section 5.5, proper groundwater availability model calibration to predict groundwater-surface water interactions requires the definition of underlying flow equations, robust data on aquifer and river properties, a detailed water budget analysis, and reliable measurements of flow rates between rivers and groundwater. Although remote sensing does not yet replace conventional river gain-loss studies (Items 4 through 6 in Section 5.5), it can significantly augment them by supplying seasonal factors, up-to-date river stage data, and enhanced pumping estimates, thereby allowing for a more precise representation of dynamic aquifer and river properties over time and improving the calibration and predictive capabilities of future groundwater availability models. Using OpenET to inform seasonality, SWOT data to refine assumptions about rivers and lakes, and Sentinel/Landsat with Google Earth Engine to inform RIV cell assignment are all scalable, rapid, ways that remote sensing can improve the Groundwater Modeling program right now.

6.4 Recommended path forward

Aqua Strategies recommends two parallel strategies to improve the capability of the groundwater availability models to model GW-SW interactions.

6.4.1 Develop 1D hydraulic model

A 1-dimensional hydraulic model can be built for the entire stretch of river that encompasses the Brazos River Alluvium Aquifer. This model would need detailed bathymetry at many cross-sections (perhaps 50-100), with between-the-banks topography collected via LiDAR flown at low elevation, or using a photogrammetry approach (see limitations discussed in a previous section). The calibrated hydraulic model would produce river water surface elevations (and thus slope) for the entire model domain, for a full range of Brazos River flows. Aside from a few known physical features in the river, the substrate (and thus the roughness factor) is pretty uniform, and thus

calibration of the model should be fairly straightforward. This calibrated model could be used to validate the SWOT data for surface water elevation, slope, extent, and ultimately the flow. Unexpected variations in water surface elevation in the future, identified by SWOT and/or the streamgages, could thus be translated into river losses (groundwater recharge), or river gains (groundwater discharge).

This 1D hydraulic model would also have lots of applications, such as providing a better understanding of flow attenuation and losses from reservoir releases for water supply contracts and monitoring the impacts of the proposed Allens Creek Reservoir on channel morphology and mesohabitat for aquatic organisms. The model and associated data would also help identify the river reaches where most of the groundwater-surface water interaction is occurring. Combined with the expansion of river gain-loss datasets, by fielding additional flow gages at tributaries and intermediate locations for 5-10 years to monitor a range of hydrologic conditions to facilitate validation of hydraulic models. A compelling next step would be to bring the results of this hydraulic modeling into a daily surface water availability model. For example, there is a daily RiverWare model for the lower Brazos that would benefit tremendously from the results of this proposed study.

At the same time, Aqua Strategies recommends improving the water budget for the groundwater availability model through the use of the hydraulic model (and the data feeding it), as well as the remote sensing data discussed in this report, and the RiverWare model, if it too is enhanced. Improved groundwater level monitoring data, and better estimates of evapotranspiration, groundwater recharge, and irrigation rates could ultimately lead to the calibration of a spatially and temporally refined version of the central portion of the Carrizo-Wilcox Aquifer groundwater availability model that incorporates and identifies better estimates of groundwater-surface water interaction.

6.4.2 Surface Water Ocean Topography elevation calibration and bathymetry/water elevation data fusion

Aqua Strategies recommends investigating methods to calibrate and improve Surface Water Ocean Topography discharge predictions. The Surface Water Ocean Topography elevation and discharge estimates are produced globally, and therefore the default algorithms make no use of other data products or field calibration apart from existing stream gages. There is therefore significant potential for refinement of the estimations through calibration and data fusion.

Calibration of Water Surface Elevation

When time-series of Surface Water Ocean Topography-reported elevations were compared to data from the pressure transducers and United States Geological Survey gages, the majority of error appeared to be due to systemic bias which ranged from 70-95% of the total error. Consequently, calibration of Surface Water Ocean Topography elevation estimates using field collected surface water elevations during flyover periods should be able to reduce the systemic error observed and ideally arrive at measured elevations with < 10 cm of error. A calibration curve or correction factor can be developed from either temporary pressure transducers installed at regular intervals in the study reach, or through field efforts scheduled to coincide with Surface Water Ocean Topography passes (which occur every 1-2 weeks).

Additionally, it was observed in the analyses that certain Surface Water Ocean Topography nodes tended to have more accurate elevations than others. Elevations are averaged at the nodes, which are spaced every 200 m along the centerline of the river. Nodes near sharp meanders or narrow sections tended to have less accurate elevation values, likely because land pixels were being factored into the average. A desktop analysis of consistently erroneous nodes would allow these to be filtered out, improving the quality of the elevation dataset.

Bathymetry/Surface Water Ocean Topography Data Fusion

The coarse (50-100 m) horizontal resolution of the Surface Water Ocean Topography sensor is likely the largest contributor to uncertainty in discharge estimations, and this is particularly true in rivers like the Brazos that are on the narrower end of what Surface Water Ocean Topography measures. Unlike the elevation measurements, uncertainty in channel width is primarily due to limitations in the sensor. If accurate bathymetry models are available, they provide highly accurate values of channel width and cross-sectional area at specific river elevations. and will significantly reduce total uncertainty of the discharge variables, allowing discharge to be estimated on a much finer scale – although the actual resolution merging Surface Water Ocean Topography and bathymetry data would need to be empirically determined.

There are several methods for collecting bathymetry by drone, although most methods using typical optical sensors are limited by depth and turbidity. Photogrammetry is possible with clear and shallow water, and the United States Geological Survey has developed a machine learning toolkit to derive bathymetry from multispectral imagery (USGS 2021). Recent developments in side-scanning sonar and “uncrewed surface vessels” have made affordable and efficient collection of bathymetry data possible, in the case that drone-based acquisitions are not viable. In addition to bathymetric data, temporary pressure transducers could be used to calibrate Surface Water Ocean Topography elevations at regular intervals, and channel roughness could be characterized using a combination of field and remote sensing methods.

7. References

Ahmad, S. K., Hossain, F., Eldardiry, H., & Pavelsky, T. M. (2019). A fusion approach for water area classification using visible, near infrared and synthetic aperture radar for South Asian conditions. IEEE Transactions on Geoscience and Remote Sensing, 58(4), 2471-2480.

Ablian, M., Legeais, J. F., Prandi, P., Marcos, M., Fenoglio-Marc, L., Dieng, H. B., ... & Cazenave, A. (2017). Satellite altimetry-based sea level at global and regional scales. In Integrative study of the mean sea level and its components (pp. 9-33). Cham: Springer International Publishing.

Binley, Andrew. 2023. *R2 Version 4.11 Manual*. Lancaster University.

Birkinshaw, S. J., Moore, P., Kilsby, C. G., O'donnell, G. M., Hardy, A. J., & Berry, P. A. M. (2014). Daily discharge estimation at ungauged river sites using remote sensing. Hydrological Processes, 28(3), 1043-1054.

Blanchy, Guillaume, Sina Saneiyan, and James Boyd. 2020. "ResIPy, an Intuitive Open Source Software for Complex Geoelectrical Inversion/Modeling." *Computers & Geosciences* 104423.

Cooley, S. W., Ryan, J. C., & Smith, L. C. (2021). Human alteration of global surface water storage variability. Nature, 591(7848), 78-81.

Cronin, J. G., and C. A. Wilson. 1967. *Ground water in the flood-plain alluvium of the Brazos River, Whitney Dam to vicinity of Richmond, Texas*. Report 41, Texas Water Development Board.

Driscoll, F. G. 1986. *Groundwater and Wells, Second Edition*. Johnson Filtration System Inc.

Duan, J. G., Engel, F. L., & Cadogan, A. (2023). Discharge estimation using video recordings from small unoccupied aircraft systems. Journal of Hydraulic Engineering, 149(11), 04023048.

Durand, M., Gleason, C. J., Pavelsky, T. M., Frasson, R. P. M., Turmon, M., David, C. H., Altenau, E. H., Tebaldi, N., & Larnier, K. (2023). A Framework for Estimating Global River Discharge From the Surface Water and Ocean Topography Satellite Mission. Water Resources Research, 59(4).

Ewing, J., and M. Jigmond, 2016. Final Numerical Model Report for the Brazos River Alluvium Aquifer Groundwater Availability Model, unnumbered report, INTERA Incorporated. August 2016

Fu, L.L., Pavelsky, T., Cretaux, J.F., Morrow, R., Farrar, J.T., Vaze, P., Sengenes, P., Vinogradova-Shiffer, N., Sylvestre-Baron, A., Picot, N. and Dibarboure, G., 2024. The surface water and ocean topography mission: A breakthrough in radar remote sensing of the ocean and land surface water. *Geophysical Research Letters*, *51*(4), p.e2023GL107652.

Fulton, J. W., Anderson, I. E., Chiu, C. L., Sommer, W., Adams, J. D., Moramarco, T., ... & Pulli, J. J. (2020). QCam: SUAS-based Doppler radar for measuring river discharge. Remote Sensing, 12(20), 3317.

Gejadze, I., Malaterre, P. O., Oubanas, H., & Shutyaev, V. (2022). A new robust discharge estimation method applied in the context of SWOT satellite data processing. Journal of Hydrology, 610, 127909.

Ghysels, G., Mutua, S., Veliz, G.B. and Huysmans, M., 2019. A modified approach for modelling river–aquifer interaction of gaining rivers in MODFLOW, including riverbed heterogeneity and river bank seepage. *Hydrogeology Journal*, *27*(5), pp.1851-1863.

Gleason, C. J., & Durand, M. T. (2020). Remote sensing of river discharge: A review and a framing for the discipline. Remote Sensing, 12(7), 1107.

Google Earth Engine. (2024). OpenET Ensemble Monthly Evapotranspiration v2.0. https://developers.google.com/earth-engine/datasets/catalog/OpenET_ENSEMBLE_CONUS_GRIDMET_MONTHLY_v2_0

Hendrickx, J. M., Allen, R. G., Brower, A., Byrd, A. R., Hong, S. H., Ogden, F. L., ... & Wilson, J. L. (2016). Benchmarking optical/thermal satellite imagery for estimating evapotranspiration and soil moisture in decision support tools. JAWRA Journal of the American Water Resources Association, 52(1), 89-119.

Huang, C., Chen, Y., Zhang, S., & Wu, J. (2018). Detecting, extracting, and monitoring surface water from space using optical sensors: A review. Reviews of Geophysics, 56(2), 333-360.

Kelley, V.A., Deeds, N.E., Fryar, D.G., and Nicot, J-P, 2004, Groundwater availability models for the Queen City and Sparta aquifers, unnumbered report, INTERA Incorporated. October 2004

Kinzel, P. J., & Legleiter, C. J. (2019). sUAS-based remote sensing of river discharge using thermal particle image velocimetry and bathymetric lidar. Remote Sensing, 11(19), 2317.

Koparan, C., Koc, A. B., Sawyer, C., & Privette, C. (2020). Temperature profiling of waterbodies with a UAV-integrated sensor subsystem. Drones, 4(3), 35.

Langevin, C.D., Hughes, J.D., Provost, A.M., Russcher, M.J. and Panday, S., 2024. MODFLOW as a Configurable Multi-Model Hydrologic Simulator. *Groundwater*, *62*(1), pp.111-123.

Legleiter, C. J., & Harrison, L. R. (2024). Evaluating the potential for efficient, UAS-based reach-scale mapping of river channel bathymetry from multispectral images. Frontiers in Remote Sensing, 5, 1305991.

Liu, C., Liu, J., Hu, Y., Wang, H., & Zheng, C. (2016). Airborne thermal remote sensing for estimation of groundwater discharge to a river. Groundwater, 54(3), 363-373.

McDonald, M.G., and Harbaugh, A.W., 1988. A modular three-dimensional finite-difference ground-water flow model. *Techniques of Water-Resources Investigations of the United States Geological Survey*.

Mukherjee, R., Policelli, F., Wang, R., Arellano-Thompson, E., Tellman, B., Sharma, P., ... & Giezendanner, J. (2024). A globally sampled high-resolution hand-labeled validation dataset for evaluating surface water extent maps. Earth System Science Data, 16(9), 4311-4323.

Nair, A. S., Verma, K., Karmakar, S., Ghosh, S., & Indu, J. (2022). Exploring the potential of SWOT mission for reservoir monitoring in Mahanadi basin. Advances in Space Research, 69(3), 1481-1493.

National Aeronautics and Space Administration. (2024). https://www.earthdata.nasa.gov/

Neeck, S. P., Lindstrom, E. J., Vaze, P. V., & Fu, L. L. (2012, November). Surface water and ocean topography (SWOT) mission. In Sensors, systems, and next-generation satellites XVI (Vol. 8533, pp. 111-120). SPIE.

Normandin, C., Frappart, F., Baghdadi, N., Bourrel, L., Peña Luque, S., Ygorra, B., ... & Wigneron, J. P. (2024). First results of the surface water ocean topography (SWOT) observations to rivers elevation profiles in the Cuvette Centrale of the Congo Basin. Frontiers in Remote Sensing, 5, 1466695.

O'Rourke, David. 2006. "Conjunctive Use of the Brazos River Alluvium Aquifer." In *Aquifers of the Gulf Coast of Texas*, by Robert E. Mace, Sarah C. Davidson, Edward S. Angle and William F. Mullican. Texas Water Development Board.

Panday, Sorab, Christian D. Langevin, Richard G. Niswonger, Motomu Ibaraki, and Joseph D. Hughes. *MODFLOW–USG version 1: An unstructured grid version of MODFLOW for simulating groundwater flow and tightly coupled processes using a control volume finite-difference formulation*. No. 6-A45. US Geological Survey, 2013.

Paris, A., Dias de Paiva, R., Santos da Silva, J., Medeiros Moreira, D., Calmant, S., Garambois, P. A., ... & Seyler, F. (2016). Stage-discharge rating curves based on satellite altimetry and modeled discharge in the Amazon basin. Water Resources Research, 52(5), 3787-3814.

Pettorelli, N., Schulte to Bühne, H., Tulloch, A., Dubois, G., Macinnis-Ng, C., Queirós, A. M., ... & Nicholson, E. (2018). Satellite remote sensing of ecosystem functions: opportunities, challenges and way forward. Remote Sensing in Ecology and Conservation, 4(2), 71-93.

Planet Labs PBC. (2024). PlanetScope Monitoring. https://www.planet.com/products/satellite-monitoring/

PRISM Climate Group, 2024. PRISM 4-km resolution monthly precipitation dataset, 1895–2022. Oregon State University, http://prism.oregonstate.edu. Accessed November 27 2024.

Shah, Sachin, and Natalie Houston. 2007. *Geologic and Hydrogeologic Information for a Geodatabase for the Brazos River Alluvium Aquifer, Bosque County to Fort Bend County, Texas*. Open File Report, United States Geological Survey.

Shah, Sachin, Natalie Houston, and Christopher Braun. 2007. *Hydrogeologic Characterization of the Brazos River Alluvium Aquifer, Bosque County to Fort Bend County, Texas*. Scientific Investigations Map 2989, United States Geological Survey.

SkyWatch. (2024). https://skywatch.com/

Slade Jr, R.M., Bentley, J.T. and Michaud, D., 2002. *Results of streamflow gain-loss studies in Texas, with emphasis on gains from and losses to major and minor aquifers, Texas, 2000* (No. 2002-68). US Geological Survey.

NASA-JPL Confluence. (2024). swoT-Confluence. GitHub. https://github.com/swoT-Confluence/

Texas Water Development Board (TWDB). (2024). Submitted Drillers Reports Database [Data set]. Retrieved December 27, 2024, from https://www.twdb.texas.gov/groundwater/data/GWDBDownload.zip

Turco, M.J., East, J.W., and Milburn, M.S., 2007, Base flow (1966–2005) and streamflow gain and loss (2006) of the Brazos River, McLennan County to Fort Bend County, Texas: U.S. Geological Survey Scientific Investigations Report 2007–5286, 27 p.

Volk, J. M., Huntington, J. L., Melton, F. S., Allen, R., Anderson, M., Fisher, J. B., ... & Yang, Y. (2024). Assessing the accuracy of OpenET satellite-based evapotranspiration data to support water resource and land management applications. Nature Water, 2(2), 193-205.

Young, S., M. Jigmond, T. Jones, and T. Ewing. 2018a. Groundwater Availability Model for Central Portion of the Sparta, Queen City, and Carrizo-Wilcox Aquifer, prepared for the TWDB, unnumbered report, INTERA Incorporated. September 2018

Young, S., Mace, R.E. and Rubinstein, C., 2018b. Surface water-groundwater interaction issues in Texas. Texas Water Journal, 9(1), pp.129-149. Available from: https://doi.org/10.21423/twj.v9i1.7084.

Young, S., and R. Kushnereit. 2020. GMA 12 Update to the Groundwater Availability Model for the Central Portion of the Sparta, Queen City, and Carrizo-Wilcox, Aquifers prepared for Groundwater Management Area 12, INTERA Incorporated. September 2020

Attachment A – Draft final report comments and responses

The following provides the comments received from the TWDB on the draft final report and our responses to those comments.

General comments to be addressed

1. Per contract Exhibit A, Page 10 of 33, Section III, subsection D - All final reports must be sealed by a professional geoscientist or professional engineer licensed to practice in Texas. Please provide the proper Texas professional license seal(s) for the final report.
    - *Done*.

2. Per contract Exhibit A, Page 10 of 33, Section III, Tabel 3.1 Contract Deliverables, and subsection E – A File Geodatabase with all datasets used for the study with the capability to be used to fully reproduce the investigation, including remote sensing data and stream gage, stream reach and/or other ground truthing datasets fully documented with metadata is expected as part of the deliverables. All draft and final file geodatabases must contain all relevant source data, including metadata that documents the content, data structure, source(s), date(s), quality, and other characteristics of the data within the geodatabases. Metadata must be created using the Federal Geographic Data Committee (FGDC) metadata editor within ESRI's ArcCatalog. TWDB-provided schemas include some basic metadata, which must be extended by the Contractor's project manager to completely document all source and derivative data. No geodatabase(s) was/were submitted. Please provide the deliverable geodatabase(s) for all the geospatial, remote sensing data (satellite and drone imagery), and the field data discussed in Section 4 of the report used to characterize and calibrate the groundwater model in this research project. Additionally, please provide all the calibrated MODFLOW datasets with R and Python programming scripts and documentation to properly run the groundwater model.
    - *Done*.

3. The only acronym allowed in TWDB reports is TWDB after the first use where it is spelled out. Please spell out all other acronyms including units. Acronyms in formulas are okay as long as they are spelled out beneath with a "*where*" statement.
    - *Fixed throughout*.

4. When referring to the central portion of the Carrizo-Wilcox Aquifer groundwater availability model, only the words Carrizo, Wilcox, and Aquifer should be capitalized.
    - *Fixed throughout*.

5. When referring to "groundwater-surface water interactions", be consistent in the order of groundwater and surface water in that phrase. We suggest using "groundwater-surface water", not "surface water-groundwater".
    - *Fixed throughout*.

6. All figure and table captions must end with a period (“.”).
    - *Fixed throughout.*

7. Figure and table captions should be left aligned with tabbed indentation.
    - *Fixed throughout.*

8. Tables and figures should be centered.
    - *Fixed throughout.*

9. For all tables and figures: only first word, proper names, and aquifer names should be capitalized.
    - *Fixed throughout.*

10. Please ensure that either all tables are all on one page or that the row on the second page also has a header (using the Split Table function in Microsoft Word).
    - *Done.*

11. Please left-align all paragraph text. Starting in section 3.1, text becomes justified in places.
    - *Fixed throughout.*

12. Citations (commas between authors and date; three or more authors listed as “and others”).
    - *Fixed throughout.*

13. Please make sure all in-text citations are added to the References section.
    - *Done. Some citations replaced, others added , and one or two deleted.*

14. There are 3-4 USGS gages referred to in the document (Hearne, Highbank, Cameron, and Bryan gages) but their locations are not included on any maps. Please add these gages to either a new map or an existing map.
    - *Done.*

15. If referring to more than one county as “counties” don’t capitalize “counties”.
    - *Fixed throughout.*

16. Suggest starting each of the 7 main sections on a new page following a page break to improve readability.
    - *Fixed throughout.*

17. Gain/loss is referred to as “gain-loss”, “gain-lost”, “gain/loss”, etc throughout the document. Please be consistent.
    - *Fixed throughout.*

18. Suggest adding a figure showing an example of the SWOT water surface elevation nodes for one of the sites.
    - *Example included later in the report*.

19. There are a few figures (e.g. Page 23, Figure 3.4) in the text that have bookmarks/hyperlinks to the figures. Please either remove these or hyperlink all figures and tables within the document.
    - *Hyperlinks removed*.

20. Both the Central Carrizo-Wilcox Aquifer GAM and the Brazos River Alluvium Aquifer GAM are included in the report's text. The GAM analysis described in Sections 3 and 5.4 was done using the Central Carrizo-Wilcox GAM. Some of the report's recommendations suggest that the Brazos River Alluvium Aquifer GAM can be improved by this analysis. Please ensure that the correct model is being referred to. Also, please note that the Brazos River Alluvium Aquifer GAM already has monthly stress periods and one of recommendations was to use a similar type of analysis from this report to improve temporal resolution of GAMs.
    - *Clarified. Modeling was done using the Carrizo-Wilcox GAM*.

21. Please correct the spelling issues throughout the document.
    - *Fixed*.

22. Please ensure that final report passes Adobe PDF Accessibility checks.
    - *Fixed*.

Specific comments to be addressed

1. Executive Summary, Key Findings, Item 1, Bullet 2: change to "This report documents an approach for improving the Brazos River Alluvium Aquifer GAM using the remote sensing data collected."
    - *Clarified*.

2. Executive Summary, Key Findings, Item 5, Bullet 2: add period (".") at the end of the bullet.
    - *Added*.

3. Executive Summary, Page 2, last paragraph, first sentence: change "Brazos alluvium" to "Brazos River alluvium".
    - *Changed*.

4. List of Tables in Table of Contents section is required.
    - *Inserted*.

5. List of Figures in Table of Contents section is required.
    - *Inserted*.

6. Project Background, Page 6, Paragraph 1, Sentence 3: change “the MODFLOW” to “MODFLOW”.
    - *Changed*.

7. Project Background, Page 7, Figure 1.1: What does the callout of “Travel Time ~7 days” mean? Explanation should be added to the text or figure caption.
    - *Reference to 7 days removed*.

8. Project Background, Page 7, Paragraph 2, Sentence 1: remove comma in “…Jon Boat and cameras, to identify…”.
    - *Removed*.

9. Project Background, Page 7, Paragraph 4, Sentence 2: remove extra spaces between words in “…of the river for the reach selected…”.
    - *Removed*.

10. Project Background, Page 8, Figure 1.2: Text is very difficult to read. Can you export this image at a higher resolution and make sure it fills the entire page with the exception of space for the caption?
    - *Image fixed*.

11. Section 1, Page 8: Please add page number.
    - *Fixed*.

12. Section 2, Page 9, Paragraph 1, Sentence 1: change “Remote sensing (remote sensing)…” to “Remote sensing…”.
    - *Changed*.

13. Section 2.1, Page 9, Paragraph 2, Sentence 2: capitalize the first letter in “Remote…”.
    - *Fixed*.

14. Section 2.1, Page 10, Figure 2-1: Please remove “(Sremote sensing)” from the caption.
    - *Removed*.

15. Section 2.2, Page 11, third bullet: add space in “and/orsurface water”.
    - *Added*.

16. Section 2.2, Page 11, Paragraph 1: Please avoid using footnotes.
    - *Removed*.

17. Section 2.2, Page 11: Please insert a page break after Table 2.1 so the heading “Planet Scope Imagery” starts on the next page.
    - *Fixed*.

18. Section 2.2, Pages 12 and 13, all paragraphs: Please cite a web link reference for each of the satellite products (platforms) discussed in this section.
    - *Referenced*.

19. Section 2.4, Page 15, Paragraph 3, last sentence: Change "In cloudy regions like the study area" to "On cloudy days".
    - *Changed*.

20. Section 2.6, Page 18, First paragraph, first sentence: Add oxford comma between the words "radar" and "and".
    - *Added*.

21. Section 2.6, Page 18, Second paragraph, last sentence: Add oxford comma between the words "Sentinel-2" and "and".
    - *Added*.

22. Section 2.7, Page 19, Paragraph 1: Please consider removing one blank line before equation "*Normalized Difference Water Index (NDWI) = (Green + NIR) / (Green – NIR)*".
    - *Removed*.

23. Section 3, Page 20, Second paragraph, third sentence: Remove duplicate "image velocimetry" text.
    - *Removed*.

24. Section 3, Page 20, Second paragraph, second to last sentence: I am not sure what "GAM shallow aquifer model domain" means here. Is this referring to areas where the model layers themselves are thin, where they outcrop, or both?
    - *Text clarified*.

25. Section 3.1, Page 20, only paragraph, last sentence: Authors needed in model citation.
    - *Added*.

26. Section 3.1.1, Page 20, First paragraph, first sentence: name of model should be "central portion of the Sparta, Queen City, and Carrizo-Wilcox aquifers" and citation for 2020 model needs to be "Young and Kushnereit, 2020".
    - *Fixed*.

27. Section 3.1.1, Page 21, first set of bullets: verbs need to be in past tense.
    - *Fixed*.

28. Section 3.1.1, Page 21, last paragraph, fourth sentence: Brazos River Alluvium occurs in Layer 1.
    - *Fixed*.

29. Section 3.1.1, Page 21, last paragraph, last sentence: add “where” between “and” and “recharge”.
    - *Added*.

30. Section 3.2, Page 22, last paragraph, last sentence: Equation 2 is referred to but there are no labels or numbers for any other equation throughout the document. Please either remove the equation 2 number or label equations throughout the document for consistency.
    - *Fixed*.

31. Section 3.2, Page 23, first paragraph, second sentence: why were initial locations of river cells from Kelley and others (2004) used, and not river cells from Young and others (2018a) or Young and Kushnereit (2020)?
    - *Fixed reference*.

32. Figure 3.4, Page 27: please insert a new version of this figure without the cursor.
    - *Fixed*.

33. Figure 3.5, Page 28: please insert a new version of this figure without the cursor.
    - *Fixed*.

34. Figure 3.5, Page 28: This figure is 4.8a in Young and others (2018a) and not 5.7.
    - *Fixed*.

35. Figure 3.6, Page 29: needs a legend item to specify what the blue cells mean. It would also be better if the Brazos River RIV cells were shown in the legend as a box rather than a gray line.
    - *Figure replaced*.

36. Section 3.3, Page 30, first paragraph, second to last sentence: Add oxford comma between “streams” and “and”.
    - *Added*.

37. Section 3.3, Page 31, only sentence on page (sentence directly beneath Figure 3.9): Figure number is missing.
    - *Fixed*.

38. Figure 3.11, Page 33: Legend item missing for gray lines.
    - *Legend item added*.

39. Figure 3.11, Page 33: Please spell out legend items (e.g., “Cell bottom” instead of “cell_bot”).
    - *Revised figure inserted*.

40. Figure 3.11, Page 33: What does the line for Stage represent? And how does that differ from Rbot? Some explanation of the Stage line is needed in the text. Section 5.4.2.3 has a good description of what it is, but I think a short sentence explanation would be good before this figure.
    - *Description included.*

41. Section 3.3, Page 33, first paragraph, second sentence: Add text to specify that sentence is walking the reader downstream.
    - *Added.*

42. Section 3.3, Page 33, first paragraph, third sentence. "from about 5,000 ft/day": where about does this low occur?
    - *Fixed.*

43. Figure 3.12, Page 34: Please spell out all abbreviations (e.g., "Conductance" instead of "Cond").
    - *Image replaced.*

44. Figure 3.13, Page 35: Please spell out legend items (e.g., "Cell bottom" instead of "cell_bot").
    - *Done.*

45. Figure 3.14, Page 36: Please spell out legend items (e.g., "Cell bottom" instead of "cell_bot").
    - *Done.*

46. Figure 3.14, Page 36: Please move upper left legend box on lower plot to not overlap with graph.
    - *Done.*

47. Section 4, Page 38, first paragraph, first sentence: Remove comma after "November".
    - *Removed.*

48. Section 4, Page 38, first paragraph, first sentence: Add oxford comma after "rate".
    - *Added.*

49. Section 4, Page 38, second paragraph, first sentence: The USGS gage 08108700 referred to is the Bryan gage at SH 21 that is downstream of all the sites except Moore site. The sentence states the gage is upstream of all the sites. Please revise to add more clarity.
    - *Text fixed.*

50. Section 4, Page 38, third paragraph, fourth sentence: Change "month" to "period".
    - *Changed.*

51. Section 4, Page 38, fourth paragraph, last sentence: This sentence should be parenthetical to the previous sentence.
    - *Fixed*.

52. Section 4, Page 38, Figure 4.1: Please include the USGS Gage name and ID in the figure caption.
    - *Done*.

53. Section 4, Page 38, Figure 4.1: The 2 drone flight time periods don't match the 2 drone flight time periods in Figures 5.16 – 5.18.
    - *Figure 4.1 fixed*.

54. Section 4, Page 39, second paragraph, first sentence: Add parenthesis and remove comma after "Day".
    - *Fixed*.

55. Section 4.1.1, Page 40, last paragraph, second to last sentence: Collection is misspelled as "colection".
    - *Fixed*.

56. Section 4.1.1, Page 41, first paragraph, first sentence: add location and owner in clause separated by commas. Vaughn and surface water are misspelled.
    - *Fixed*.

57. Section 4.1.1, Page 41, first paragraph, first sentence: Suggest removing the full well owner name for privacy reasons.
    - *Removed*.

58. Section 4.1.1, Page 41, first paragraph, last sentence: "about" and "basis" are misspelled.
    - *Fixed*.

59. Section 4.1.1, Page 41, Paragraph 1: Please add comma between Calvert and TX and between Mumford and TX and College Station and TX.
    - *Added*.

60. Section 4.1.4, Page 43, section after formula: TWDB Database citation needs date accessed and well as specification of database. Needs to be added to the References section.
    - *Citation inserted*.

61. Section 4.1.6, Page 43, first paragraph, first sentence: what is the “middle Brazos River”? Middle of the river channel?
    - *Fixed*.

62. Section 4.2, Page 45, fist paragraph, last sentence: Space needed between “and” and “channel”.
    - *Added*.

63. Section 4.2.1.1, Page 46, first paragraph, first sentence: The drone data collection dates of March/April 2024 and July/August 2024 don’t match the dates in Figure 4.1 of January 2024 and March/April 2024.
    - *Fixed in Figure 4.1*.

64. Section 4.2.1.1, Page 46, first paragraph, eighth sentence: This sentence should be parenthetical to the previous sentence.
    - *Fixed*.

65. Section 4.2.2.1, Page 48, first paragraph, fourth sentence: change “satellites” to “satellite”.
    - *Changed*.

66. Section 4.2.2.2, Page 50, third paragraph, first sentence: Add space between “gage” and “data”.
    - *Added*.

67. Section 4.2.2.2, Page 50, last paragraph, first sentence: Add oxford comma between “Landsat” and “and”.
    - *Added*.

68. Section 4.2.2, Page 51, fourth paragraph, second sentence: It is stated that observations with a 2 or 3 quality indicator were excluded. However, on page 50, first paragraph it is stated that the range in quality indicators was 0 – 2. Should the range be 0 – 3?
    - *Fixed. Was a typo*.

69. Section 4.2.2.2, Page 51, fourth paragraph, last sentence: Add period (“.”) at end of sentence.
    - *Added*.

70. Section 4.2.2.2, Page 53, second paragraph, fourth sentence: is there a reason why 80% was chosen?
    - *Approach described*.

71. Section 4.2.2, Page 53, third paragraph, last sentence: Please change “the resulting estimated of irrigation deficit for each month.” to “the resulting estimated irrigation deficit for each month.”.
    - *Changed*.

72. Section 5.1, Page 56, first paragraph, second sentence: change “aquifer in focus” to “Brazos River Alluvium Aquifer”.
    - *Changed*.

73. Section 5.1, Page 56, first paragraph: change fill behind citations to “No fill”.
    - *Changed*.

74. Section 5.1, Page 58, first paragraph: change fill behind citations to “No fill”.
    - *Changed*.

75. Table 5.1, Page 58: columns need to be adjusted so that they line up with table header.
    - *Fixed*.

76. Table 5.2, Page 59: Please add the total acres for each of the 4 sites used to derive the ft/day GW-SW fluxes shown in the table. We are unable to verify the average acre-ft/yr values in the table without this information.
    - *Info added*.

77. Table 5.2, Page 59: Caption needs description of unit abbreviations.
    - *Added*.

78. Table 5.3, Page 60: Caption needs description of unit abbreviations.
    - *Added*.

79. Section 5.2.1, Page 60, first paragraph, third sentence: add space between “water” and “exchange”.
    - *Added*.

80. Section 5.2.2, Page 62, first paragraph, first sentence: split into two sentences for clarity.
    - *Changed*.

81. Section 5.2.1, Page 63, second paragraph, second sentence: I believe April 2023 should be April 2024 if it is referring to the month of full transducer deployment. Please verify that April 2023 is not supposed to be April 2024.
    - *Fixed*.

82. Section 5.2.2, Page 63, second paragraph, third sentence: add commas to separate “as well as” clause.
    - *Added*.

83. Section 5.2.2, Page 63, second paragraph, third sentence: what uncertainties are being referred to here?
    - *Rephrased*.

84. Section 5.2.2, Page 63, second paragraph, third sentence: split into two sentences for clarity.
    - *Changed*.

85. Section 5.2.2, Page 64, first paragraph, second sentence: is text supposed to say “3rd quarter”?
    - *Yes*.

86. Section 5.2.2, Page 64, Table 5.4: Should the units for all columns be “acre-ft/d” and not “ft/d”? Gains – 21,206 af/day*365 days = 7,740,190 af/yr.
    - *Units corrected*.

87. Section 5.2.2, Page 65, first paragraph, first sentence: add space between “water” and “exchange”.
    - *Added*.

88. Figure 5.8, Page 65, caption: should “green colored circles” just be “colored circles” since the color scale goes from blue to yellow?
    - *Text changed to “colored circles”*.

89. Section 5.3.1.1, Page 66, HLS-DSWx paragraph: add oxford comma between “data” and “and”.
    - *Added*.

90. Section 5.3.1.1, Page 68, last paragraph: Last few sentences should be placed in Table caption. Table 5.9 citation can be moved to parenthesis at end of sentence.
    - *Changed*.

91. Section 5.3.1.2, Page 71, first paragraph, last sentence: last sentence should be moved to table caption.
    - *Changed*.

92. Section 5.3.1.2, Page 72, second paragraph: Table 5.16 citation can be moved to parenthesis at end of sentence.
    - *Changed*.

93. Section 5.3.1.2, Page 72, third paragraph: Table 5.17 citation can be moved to parenthesis at end of sentence.
    - *Changed*.

94. Figures 5.9 through 5.12, Pages 73-76: legend item needed for blue pressure transducer line.
    - *Images updated*.

95. Section 5.3.1.2, Page 76, first paragraph, third sentence: Split into two sentences.
    - *Changed*.

96. Figures 5.16 through 5.18, Pages 81-82: could these be combined into one figure?
    - *We feel that adding names to the captions is enough. It doesn't make sense to combine them, because the reaches are not continuous. The reaches represented include a couple miles upstream and downstream of each site, but there's still many miles in between them. Also, in order for the figures to still display readable information, the figure and page would probably need to be 11x17 landscape format, which is a little awkward given the rest of the document. Furthermore, combining them does not provide any additional interpretive value*.

97. Figures 5.16 through 5.18, Pages 81-82: Please add the site names to the figure captions.
    - *Done*.

98. Section 5.4.2, Page 84, third paragraph, sixth sentence: The reference to the precipitation quarters 1 and 2 in the text does not match the quarters presented in Figure 5.22.
    - *Done*.

99. Section 5.4.2, Page 86, second paragraph, last sentence: The Sensitivity Analysis section is referred to as "Section 5.2.3", but the reference should be changed to "Section 5.4.3".
    - *Fixed*.

100. Section 5.4.2, Page 87, second paragraph, second sentence: The Sensitivity Analysis section is referred to as "Section 5.2.3", but the reference should be changed to "Section 5.4.3".
    - *Fixed*.

101. Figure 5.24, Page 88: Please spell out legend items (e.g., "Cell bottom" instead of "cell_bot").
    - *Done*.

102. Figure 5.24, Page 88: Please move or re-arrange upper right legend box in lower plot to not overlap with graph.
    - *Done*.

103. Section 5.4.2, Page 88, last paragraph, last sentence: The last sentence should be updated to say Q1 statistics rank second.
    - *Fixed*.

104. Table 5.21, Page 92: Add horizonal borders between factors and bottom border below header to improve readability.
    - *Added*.

105. Section 5.4.3, Page 92, second paragraph, fourth sentence: where is the detailed plot mentioned here?
    - *Clarified*.

106. Section 5.4.3, Page 93, Figure 5.29: Please correct figure legend showing line symbols for polygon symbols.
    - *Done*.

107. Figure 5.30, Page 95: Please move or re-arrange upper right legend box to not overlap with graph.
    - *Done*.

108. Section 5.4.3.2, Page 97, first paragraph, first sentence: Section number needs to be identified. I believe it should be Section 5.4.2.2?
    - *Correct. Fixed*.

109. Section 5.4.3.3, Page 99, first paragraph, first sentence: Section number needs to be identified. I believe it should be Section 5.4.2.3?
    - *Correct. Fixed*.

110. Section 5.4.3, Page 99, last paragraph, fourth sentence: It is indicated that there is reversal of flow at the Vaughn site for the second and third quarters. However, looking at Figure 5.35 reversal of flow (>0 cfs) only occurs in the second quarter.
    - *Clarified*.

111. Section 5.4.3, Page 101, Figure 5.36: Please add the Gossett site number to caption.
    - *Site number added*.

112. Section 5.4.3, Page 103: Please change the reference to “Section 5.2.2” to “Section 5.4.2”.
    - *Changed*.

113. Section 5.5, Page 107, first paragraph, first sentence: remove commas.
    - *Removed*.

114. Section 5.5, Page 108: The reference to “Section 3.2” should be changed to “Section 3.3”.
    - *Changed*.

115. Section 6, Page 108, first paragraph, third sentence: this sentence seems like it should be two (or more) sentences. The way it is currently written needs to be revised.
    - *Fixed*.

116. Section 6, Page 108, second paragraph, second sentence: add full name of aquifer for clarity.
    - *Added*.

117. Section 6.1, Page 109, first paragraph, third sentence: Please replace “summer of 2025” with either “summer of 2024”.
    - *Replaced*.

118. Section 6.3, Page 111, third paragraph, first sentence: The Langevin and others reference shows 2023 as the year of publication but the reference list shows 2024.
    - *Fixed*.

119. References, Page 113: Please change 20224 to 2024 for the PRISM reference.
    - *Fixed*.